MINISTÉRIO DA EDUCAÇÃO
UNIVERSIDADE FEDERAL DO RIO GRANDE DO SUL
PROGRAMA DE PÓS-GRADUAÇÃO EM ENGENHARIA MECÂNICA

STUDY OF PROGRESS VARIABLE DEFINITION OF FLAMELET-BASED MODELS USING OPTIMIZATION ALGORITHM

por

Lisandro Candiani Maders

Dissertação para obtenção do Título de
Mestre em Engenharia

Porto Alegre, Julho de 2018

STUDY OF PROGRESS VARIABLE DEFINITION OF FLAMELET-BASED MODELS USING OPTIMIZATION ALGORITHM

por

Lisandro Candiani Maders
Engenheiro Mecânico

Dissertação submetida ao Corpo Docente do Programa de Pós-Graduação em Engenharia Mecânica, PROMEC, da Escola de Engenharia da Universidade Federal do Rio Grande do Sul, como parte dos requisitos necessários para a obtenção do Título de

Mestre em Engenharia

Área de Concentração: Fenômenos de Transporte

Orientador: Prof. Dr. Fernando Marcelo Pereira

Aprovada por:

Prof. Dr. Amir Antônio Martins Oliveira Filho ..... POSMEC / UFSC

Prof. Dr. Felipe Roman Centeno ..... PROMEC / UFRGS

Prof. Dr. Cirilo Seppi Bresolin ..... PROMEC / UFRGS

Prof. Dr. Jakson Manfredini Vassoler
Coordenador do PROMEC

Porto Alegre, 6 de Julho de 2018

AGRADECIMENTOS

Dedico esta página para agradecer às pessoas que, direta ou indiretamente, estiveram envolvidas nesta caminhada.

Ao Conselho Nacional de Desenvolvimento Científico e Tecnológico (CNPq) pelo suporte financeiro para a elaboração desta dissertação.

Ao André, Cristian, Isaias e Lucho, pela parceria e amizade construída nestes anos. Vocês possuem páginas especiais neste livro escrito por Saramago. Ao Leonardo Donatti, pela grande ajuda nesta fase final da dissertação. Ao Guilherme Garber, por ser um amigo impecável diariamente. Ao Leonardo Zimmer, pelo auxílio com a técnica FGM. Aos demais colegas do Laboratório de Combustão e do GESTE, por todos os momentos compartilhados que tornaram nossa rotina mais divertida.

Aos meus pais, Jorge Raul Maders Filho e Elisa Candiani Maders. Quanto mais o tempo passa, mais fácil fica perceber que boa parte dos frutos que eu colho hoje vêm de sementes plantadas por vocês. Obrigado.

Por fim, ao meu orientador Fernando Marcelo Pereira, que se tornou para mim uma referência profissional. Tenho muito a agradecer pela orientação neste trabalho, por estar disponível sempre que necessário e por ser responsável por boa parte de minha evolução profissional nos últimos anos.

RESUMO

A definição da variável de progresso em técnicas de redução baseadas nos modelos de flamelets é geralmente escolhida arbitrariamente ou baseada na experiência do usuário. No entanto, quando sistemas complexos de combustão são objeto de interesse, tais escolhas podem se tornar nada triviais. No presente trabalho, um método automático para otimizar a definição da variável de progresso é implementado e acoplado com a técnica Flamelet-Generated Manifold (FGM). Esta implementação é baseada em algorítmos de otimização cuja função objetivo a ser minimizada é o requerimento de monotonicidade da variável de progresso. Para avaliar a viabilidade da variável de progresso, não somente o requerimento de monotonicidade foi levado em conta, mas também a representativadade da solução da chama em simulações CFD uni e bi-dimensionais. Faltam trabalhos na literatura nos quais uma variável de progresso otimizada é avaliada em simulações multidimensionais e que discutam o fato do requerimento de monotonicidade não garantir necessariamente uma boa solução. Portanto, neste trabalho, diferentes composições de combustíveis são simuladas em chamas difusivas uni-dimensionais e em queimadores co-flow utilizando tanto a técnica FGM com a variável de progresso otimizada quanto mecanismos detalhados de cinética química. Os resultados mostram que, apesar de uma tendência de bons resultados quando existe monotonicidade da variável de progresso, algumas definições monotônicas apresentaram resultados ruins. Também foi observado uma tendência de bons resultados nas chamas multidimensionais quando as chamas unidimensionais apresentam bons resultados. Notou-se ainda que, quando houve uma boa concordância nas simulações unidimensionais para taxas de deformação correspondentes às regiões que são acessadas no manifold, as simulações multidimensionais tenderam a apresentar bons resultados. A minimização dos gradientes das variáveis do manifold também foi utilizada como função objetivo mas não foram encontradas melhorias nos resultados em termos de representatividade da solução.

Palavras-chave: Variável de Progresso; Otimização; FGM;

ABSTRACT

The definition of the progress variable in flamelet-based dimension reduction techniques is generally chosen arbitrarily or based on the experience of the user. When complex combustion systems are the problems of interest, such choices can become a non-trivial task. In the present work, an automated method to optimize the progress variable definition is implemented and coupled to the Flamelet-Generated Manifold (FGM) technique. The automated choice implemented is based on an optimization algorithm whose objective function to be minimized is the requirement of monotonicity of the progress variable. In order to evaluate the feasibility of the progress variable, not only the requirement of monotonicity is analyzed, but also the representativeness of the flame solution in one-dimensional and two-dimensional CFD simulations. There is a lack of studies in the literature in which an optimized progress variable definition is analyzed for a multidimensional solution and that discusses the fact that the monotonicity requirement does not necessarily guarantees an accurate solution. Therefore, in the present work, different fuel compositions are simulated in one-dimensional diffusion flamelets and in two-dimensional co-flow burners using both FGM with the optimized progress variable and detailed mechanisms. The results show that, even though a tendency of good multidimensional results exists when the progress variable is monotonic, some monotonic definitions presented bad results. Also it was observed a tendency of finding good multidimensional results when there are accurate one-dimensional solutions. It was still noticed that, when there was a good agreement of one-dimensional results for strain rate values corresponding to the regions accessed in the manifold, the multidimensional solution tended to be accurate. The minimization of the gradients of the variables of the manifold is also used as an objective function but no improvements were found in terms of representativeness of the results.

Keywords: Progress Variable; Optimization; FGM.

INDEX

LIST OF FIGURES

LIST OF TABLES

LIST OF SYMBOLS

a	Strain rate, 1/s
A	Pre-exponential factor, various units
b	Temperature coefficient, -
c_p	Specific heat capacity at constant pressure of the mixture, J/(kg K)
$c_{p,i}$	Specific heat capacity at constant pressure of species i, J/(kg K)
$\mathcal{D}_{i,j}$	Ordinary binary diffusion coefficients of species i into species j, m^2/s
$\mathcal{D}_{i,M}$	Mixture-averaged diffusion coefficient, m^2/s
$D_{s,i}$	Soot diffusion coefficient of particle class i^{th}, m^2/s
E_a	Activation energy, J/mol
$\vec{g}$	Gravitational acceleration, m/s^2
h	Total specific enthalpy of the mixture, J/kg
h_i	Specific enthalpy of species i, J/kg
h_i^0	Specific enthalpy of formation of species i, J/kg
$\hat{I}$	Identity tensor, -
k	Reaction rate constant coefficient, various units
K	Stretch rate, 1/s
K_c	Equilibrium constant
Le_i	Lewis number of species i, -
M	Mass, kg
MW_i	Molecular weight of species i, kg/kmol
MW	Molecular weight of the mixture, kg/kmol
$\mathcal{M}_i$	Species i, -
N_s	Number of species, -
p	Pressure of the mixture, N/m
p_i	Partial pressure of species i, N/m
p_0	Ambient pressure, N/m
P_i	Partial pressure of species i, atm
$\dot{q_R}$	Radiation heat source term, W/m^3

$\vec{q}$	Heat flux vector, W/m^2
R_u	Universal gas constant, J/(mol K)
t	Time, s
T	Temperature, K
T^{ref}	Reference temperature, K
$\vec{v}$	Flow velocity vector, m/s
V	Volume, m^3
v_C	Volume of carbon atom, m^3
$\vec{V_c}$	Diffusion velocity correction
v_i	Volume of section i , m^3
$\vec{V_i}$	Molecular diffusion velocity vector of species i, m/s
x	Cartesian coordinate, m
X_i	Molar fraction of species i, -
$\mathcal{Y}$	Progress variable, kmol/kg
Y_i	Mass fraction of species i, -
Z	Mixture fraction, -
Z_j	Element mass fraction of element j, -
Z_t	Transported mixture fraction, -

Greek Symbols

α_i	Weight factor of species i, kmol/kg
β	Collision frequency facto, 1/s
ρ	Mixture density, kg/m^3
ρ_i	The partial density of species i, kg/m^3
$\vec{\tau}$	Stress tensor, N/m^2
$\dot{\omega}_i$	Reaction source term of the species i, kg/(m^3 s)
$\bar{\dot{\omega}}_i$	Molar reaction rate of the species i, mol/(m^3 s)
μ	Dynamic viscosity, kg/ (m s)
μ_i	Dynamic viscosity of species i, kg/(m s)
ν	Stoichiometric oxidizer-to-fuel ratio, kg/kg
$\nu_{i,j}$	Stoichiometric number of moles of species i participating in the reaction j, -
λ	Thermal conductivity coefficient, W/(m K)

λ_i	Thermal conductivity coefficient of species i, W/(m K)
χ	Scalar dissipation rate, s^{-1}
	Massa específica

Sub-Indexes

f	Forward reaction
r	Backward reaction

1 THESIS CONTEXT

According to MME, 2017, the burn of petrol derivatives, natural gas, ethanol, coal, wood, and agro-industrial residues represent more than 80% of the energy consumed in Brazil. The combustion processes have great impact in industrial, transport and energy production sectors. Thus, it is essential to use fuels efficiently, which requires the development of tools for reaching a deep understanding of the underlying processes in flames. Among the different types of flames, the laminar non-premixed flames are the object of many fundamental researches aiming to better understand physical and chemical phenomena for complex reacting flows [Cao et al., 2015, Xuan and Blanquart, 2013, Verhoeven, 2011, Smooke et al., 2005, Santoro et al., 1987]. Although simplified analytic solutions for laminar non-premixed co-flow flames are available, the recurrent concern about increasing efficiency of combustion processes and reduction in pollutant emissions demands more sophisticated models. Among them, is worthy to highlight the usage of numerical simulations using detailed chemical kinetic. Detailed kinetic for hydrocarbons oxidation describes the chemical process through elementary reactions. In this way, hundreds of reactions and dozens of chemical species are necessary to model a combustion process. In addition, the system of non-linear differential equations to be solved is stiff and strongly coupled, making the problem computationally demanding even for laminar flames.

Global kinetic mechanisms are an alternative to reduce the computational time and are commonly employed to solve practical problems. Since they describe the chemical kinetic through only few reactions, their use is restricted to conditions for which their rates and constants were adjusted. Despite of being computationally efficient, their solutions present deviations when compared with more detailed mechanisms. Besides that, the post-processing of global mechanisms is limited to the species that comprise the reactions considered. For instance, the 1-step mechanism presented by de Lange, 1992 considers that the oxidation of the hydrocarbon produces only water and carbon-dioxide. Therefore, considering methane as fuel, the only species able to be post-processed are CH_4, O_2, N_2, H_2O and CO_2. Hence, global mechanisms do not allow the study of pollutants formation or the role of the radical pool on the flame behavior, for instance. For such reasons, their use for solving practical combustion problems are losing space and more advanced models for solving complex chemical kinetic have been developed, like chemical kinetic reduction

techniques and flamelet approaches.

The idea of using a conserved scalar to map the thermochemical state of a flame, which is the basis of flamelet models, is commonly used for diffusion flames with the introduction of the mixture fraction as the conserved scalar [Burke and Schumann, 1928]. However, writing the flame structure as function of the mixture fraction is only accurate when the assumption of infinitely fast chemistry is valid. The mixture fraction is a parameter which defines the mixture level in a certain point coming from reactants. Under the infinitely fast chemistry assumption, the chemical kinetics can be decoupled from the flow field being possible to write the flame structure as function of the mixture fraction only. To account for non-equilibrium effects, the Steady Laminar Diffusion Flamelet - SLDF model [Peters, 1984] introduced a second control variable, which is the stoichiometric scalar dissipation rate. In general, the scalar dissipation rate at stoichiometric mixture fraction describes the departure from chemical equilibrium condition [Pitsch et al., 2000]. After the SLDF model, a series of improved models were developed based on the flamelet approaches, like the Flamelet Progress Variable - FPV [Pierce and Moin, 2004], Flame Prolongation of ILDM (Intrinsic Low-Dimensional Manifold) - FPI [Gicquel et al., 2000] and the Flamelet Generated Manifold - FGM [Van Oijen and de Goey, 2000].

Such methods project the high-dimensional thermochemical space onto a low-dimensional lookup table, which is often called a manifold. In this approach, the entire thermochemical space is pre-computed and parametrized in terms of a reduced set of scalar variables that are conveniently solved in a combustion simulation and that properly map the physics of the flame. In most cases, the manifold is computed using both conserved and reactive scalars, being the latter often referred to as reaction progress variables. In general terms, the chemical composition of cold state and fully-reacted mixture is determined from conserved quantities, such as mixture fraction Z or equivalence ratio ϕ, while the progress of combustion between unburned and burned states is described by the reactive progress variables [Ihme et al., 2012].

In the case of the FGM technique, which is the flamelet model used in the present work, a set of one-dimensional flamelets for different conditions (strain rates, enthalpy, etc.) is simulated using a detailed chemical kinetic mechanism. This information is used to represent a multidimensional flame by parameterizing such thermochemical data in terms of controlling variables. Different types of flame require different controlling

variables. An adiabatic laminar diffusion flame, for instance, requires a minimum of two controlling variables, which is the mixture fraction, to track the mixture level coming from reactants, and the progress variable, to track the progress of combustion. If heat loss by radiation is modelled, then enthalpy becomes an additional controlling variable. In case of modelling turbulent flames, the variances of the controlling variables increase the dimension of the manifold as well. The accuracy of the FGM technique improves with the number of controlling variables used, however, the increase in the manifold dimension also increases the computational time. The reduction in the computational time of such flamelet techniques relies on the solution of only the conservation equations for the controlling variables instead of solving all the stiff differential equations of the direct chemistry integration approach. Then, the multidimensional simulation results on fields of the controlling variables, which are used as input data in the retrieval of the information in the look-up table. As result, the entire thermochemical space of the flame is reconstructed containing information from a detailed chemical kinetic mechanism, which is pre-solved in the flamelets, but with a computational time hundreds of times faster in some cases [Van Oijen and de Goey, 2000].

Other methods, like the FPV and FPI, were developed alongside FGM and rely all on the same assumptions. They differ slightly in their implementation process mainly in the construction of the manifold. However, one of the main difficulties of all these techniques is the progress variable definition, which has significant impact on the accuracy of results but usually is chosen based on experience or trial and error approach.

Automated choice of progress variable definition

In the emergence of combustion models based on lookup tables, the definition of the progress variable is often based on the experience and intuition of the user, being conventionally chosen using the mass fraction of major species such as CO_2, H_2O, CO and H_2. As reference, the Table 1.1 shows expressions that have been used as progress variables in applications of hydrocarbon combustion, mostly for non-premixed flames, since it is the object of study in the present work. Most of them has the mass fractions of the species being multiplied by a coefficient, often defined as being the inverse of the molar mass of the species (omitted from the table).

When dealing with simple hydrocarbons like methane, a standard definition which

Table 1.1 – Different progress variable definitions used in the literature and their respective applications.

$\mathcal{Y}$ definition	Application	Reference
$(Y_{CO_2} + Y_{H_2O} + Y_{H2})/(Y^{eq}_{CO_2} + Y^{eq}_{H_2O} + Y^{eq}_{H2})$	1D, premixed, CH_4/air, laminar	Van Oijen and De Goey, 2002
$Y_{CO_2} + Y_{CO}$	1D, premixed, CH_4/air, laminar	Fiorina et al., 2003
$Y_{CO_2} + Y_{H_2O}$	LES, non-premixed, CH_4	Pierce and Moin, 2004
$Y_{CO_2} + Y_{H_2O} + Y_{CO} + Y_{H_2}$	LES, Sandias flames D and E, CH_4/air	Ihme and Pitsch, 2008
$Y_{CO_2} + Y_{CO} + Y_{CH_2O}$	RANS, Diesel (n-heptane)	Bekdemir et al., 2011
$Y_{CO_2} + Y_{CO} + Y_{HO_2}$	RANS, Diesel (n-heptane)	Egüz et al., 2013
$Y_{CO_2} + Y_{H_2O} + 0.9Y_{CO}$	Laminar, non-premixed, C_2H_4, gas-phase	Zimmer, 2016
$0.9Y_{CO_2} + Y_{H_2O} + 0.9Y_{CO} + Y_{H_2} + Y_{C_2H_2}$	Laminar, non-premixed, C_2H_4, soot modelling	Zimmer, 2016
$Y_{CO_2} + Y_{H_2O} + Y_{H_2}$	Laminar, non-premixed, CH_4	Verhoeven et al., 2012
$Y_{CO_2} + Y_{H_2O} + Y_{H_2}$	Laminar, non-premixed, CH_4	Hoerlle, 2015
$Y_{CO_2} + Y_{H_2O} + Y_{CO}$	Laminar, non-premixed, CH_4/CO_2	Hoerlle et al., 2017

proved to give good results for non-premixed laminar flames is a linear combination of CO_2, H_2O and H_2 [Verhoeven et al., 2012, Hoerlle, 2015]. However, when more complex hydrocarbons, different combustion stages or diluted mixtures are the subject of interest, such standard definition can yield inaccurate results and different definitions are required. Hoerlle et al., 2017, for instance, discussed the capabilities of different progress variable definitions in reproducing the composition space when diluting CO_2 in methane flames. It was found that the standard definition used for pure methane diffusion flames, comprised of a linear combination of CO_2, H_2O, and H_2, did not provide accurate results when adding CO_2 into the fuel mixture, leading to bad predictions for the CO species mass fraction profiles. A successful alternative was the replacement of H_2 species by CO in the previous progress variable definition. Even though such alternative provided good results when dealing to CH_4 diluted up to 40% CO_2, it was based on the authors' experience on the FGM technique, and finding a good progress variable for more complex chemical systems could become a non-trivial task even for experienced users.

For ethylene flames, frequently used in soot studies, the standard definition for pure methane produces unsuitable results. Zimmer, 2016, comparing an FGM with a detailed model, found a good definition for the progress variable when dealing only with the gas-phase under unity Lewis number assumption. However, such definition was found by a trial and error approach. Also, when preferential diffusion effects were considered or soot was present in the flame, it was not possible to find a feasible progress variable definition which provided accurate results.

Another recent example of issues in the progress variable definition is presented by Göktolga et al., 2017, who proposed a multistage FGM method to solve Moderate or

Intense Low-oxygen Dilution (MILD) combustion systems. Such type of problem presents clearly distinct stages of combustion: pre-ignition, oxidation and post-ignition. It is not possible to describe the combustion process uniquely and accurately through only one progress variable. Therefore, more progress variables are defined in the multistage FGM method, however, without an addition to the dimension of the manifold. This is done by creating different manifolds for each stage of combustion and defining a threshold for choosing from which manifold to retrieve the information in the multidimensional simulation. Such approach is very promising since it can deal with combustion systems which may contain different stages of combustion without increasing the manifold dimension. The problem now is that two definitions of the progress variable have to be used.

Both examples above reinforce the importance of establishing a methodology for the progress variable definition. Ihme et al., 2012 suggested that there is no general expression for it, and that it is dependent on the particular flame configuration. Therefore, it is worth investigating a general methodology for choosing the progress variable definition. In this scenario, new methodologies for choosing the reaction progress variable are important requirements for the improvement of chemical kinetic reduction techniques based on lookup tables. Recent studies arose in the literature proposing automated methodologies for such task. Most of them rely on optimization techniques, in which an objective function is chosen such that it provides a suitable progress variable. What is a suitable progress variable is discussed in Chapter 4 of this thesis.

Different objective functions were analyzed on such investigations. Ihme et al., 2012, for instance, found progress variables for methane and n-heptane/hydrogen flames based on a cost function which minimizes the non-monotonicity of the progress variable. The monotonicity requirement means that the progress variable uniquely identifies each point in the thermochemical state space. It was found that using the optimization algorithm yields better values of the cost function, which means more monotonic progress variables were found with the algorithm. Unfortunately, the database they analyzed was limited to simple one-dimensional diffusion flames and partially premixed flames, and they did not apply their optimized definitions to a multidimensional problem, as also observed by Chen et al., 2015. The author's group experience from the present work with the FGM technique shows that finding a monotonic progress variable is necessary, but not enough. There is no guarantee that a representative solution will be found with some progress

variable only due to its monotonicity. This will be shown later in the results of Chapter 5 and 6.

Another example is Niu et al., 2013, and Prufert et al., 2015, in which the gradients of the chemical species in relation to the progress variable became the parameter to be minimized. The difference between both studies is that in the former, the monotonicity of the progress variable is a constraint to the optimization problem. In the later, the monotonicity enters directly in the objective function as a penalty factor. The main advantage of it is that, depending on the constraint applied in the first case, no definitions might be found depending on the fuel being analyzed. In the last one, the algorithm will find the most monotonic definition as possible, and it will always find a solution. Again, minimizing the gradients of the look-up table implies in a better application of the flamelet technique, leading to an easier interpolation and less discretization needed of the manifold, but not necessarily in accurate results. Similarly to Ihme et al., 2012, they only applied their method on the one-dimensional flames and perfectly mixed canonical problems. An extension to multidimensional CFD applications needs to be performed in order to guarantee the representativeness of their optimized progress variable definitions.

A different methodology of finding a suitable progress variable definition for flamelet models is based on a Principal Component Analysis (PCA) of species mass fractions in the composition space. It is analogous to the eigenvalue analysis of the ILDM method. Since it is based on a rigorous mathematical formulation applied on the detailed chemical kinetic mechanisms, it is possible that the resultant definition is representative in multidimensional flames. Najafi-Yazdi et al., 2012, provided a rigorous mathematical formulation for flamelet-based models and got the minimum number of linearly independent progress variable definition based on PCA. However, there is no verification of their results with a flow solver. Up to present, it is rare a multidimensional CFD simulation of a combustion field based on an optimized progress variable definition. One example is the work of Chen et al., 2015, which performed such analysis by using PCA to find an optimized progress variable definition and compared it to a DNS solver, finally solving a CFD simulation using a flamelet model with an optimized progress variable. Lift-off flames are simulated and better results were found in comparison to conventional progress variable definitions. Ihme et al., 2012, also suggested that a time-scale analysis to automatically identify the candidate species in the definition of the progress variable could be used as guidance. A

prior analysis of the chemical kinetic mechanism should be performed through computation singular perturbation (CSP), eliminating species which are exhausted in fast reaction modes [Lam, 1993, Lam and Goussis, 1994]. It is possible that coupling such methodologies to the flamelet models can become an alternative for finding representative progress variable definitions.

1.1 Objectives

In the context addressed above, it is remarkable the absence of works in the literature which perform a CFD simulation using a flamelet-based method with an optimized progress variable. The only work so far which does it is Chen et al., 2015 study, which simulates a premixed flame. The present work aims to apply an optimization algorithm coupled to the FGM technique to find a feasible progress variable to be applied on the solution of non-premixed laminar flames. The objectives of the present work can hence be divided in the following items:

- Coupling of an optimization algorithm to the FGM technique using the genetic algorithm toolbox from MATLAB®[MathWorks, 2012];
- Testing the optimized progress variables in a CFD solver (ANSYS Fluent®v16.1) for different flames;
- Evaluation of the representativeness of the optimized definitions in 1D and 2D simulations;

1.2 Outline

The Chapter 1 referred to the thesis context in the literature, presenting the most recent studies on the subject of the progress variable definition applied to flamelet-models. Chapter 2 presents the mathematical formulation of laminar diffusion flames, including the conservation equations and the conserved scalar formulation, important to the understanding of flamelet models. Chapter 3 discusses the FGM technique, the flamelet equations, details of the manifold construction and hence the multidimensional equations solved. Chapter 4 addresses the discussion about the automation of progress variable definition. The concept of a feasible progress variable is assessed and different optimization

formulations are presented. Also, a discussion about the representativeness of the progress variable definition is addressed. Finally, Chapters 5 and 6 present one-dimensional and two-dimensional results for different flames employing the optimized progress variable found. The accuracy of different definitions obtained with the optimization algorithm implemented is evaluated comparing them to conventional ones and to detailed mechanisms. Chapter 7 brings a final conclusion about the present study.

2 MATHEMATICAL FORMULATION OF LAMINAR NONPREMIXED FLAMES

This section will present the conservation equations that describe the physics of non-premixed laminar flames. The equations are expressed in their three-dimensional form and the assumptions considered are described along their presentation. It is important to state that the following equations represent general non-premixed laminar flames, while in chapter 3, one-dimensional equations for non-premixed laminar flamelets, which were used to construct the look-up table, are presented. In the sequence, the conserved scalar formulation for diffusion flames is presented, since it is the basis for the flamelet modelling approach, which will be discussed in the next sections. Then, detailed chemical kinetic modelling is described. Lastly, different simplified models to describe the combustion process are briefly presented in the following sequence: infinitely fast chemistry assumption, flamelet-based models and the ILDM method.

2.1 Conservation equations

The total mass conservation equation is given by

$$\frac{\partial \rho}{\partial t} + \vec{\nabla} \cdot (\rho \vec{u}) = 0, \tag{2.1}$$

where ρ is the mixture density and $\vec{u}$ is the flow velocity vector. In the limit of low-Mach number, the pressure is assumed constant $p \cong p_o$ and density is then only a function of temperature T and composition. Also, for sufficiently low pressure, the ideal gas equation of state can be assumed valid:

$$\rho \cong \frac{p_0 MW_{mixt}}{R_u T}, \tag{2.2}$$

being p_0 the atmospheric pressure, MW_{mixt} the mixture molar mass and R_u the universal gas constant.

The momentum balance is represented by the Navier-Stokes equation in the compressible form

$$\rho \left(\frac{\partial \vec{u}}{\partial t} + \left(\vec{u} \cdot \vec{\nabla} \right) \vec{u} \right) = -\vec{\nabla} p + \rho \vec{g} + \vec{\nabla} \cdot \hat{\tau}, \tag{2.3}$$

where p is the static pressure and $\vec{g}$ represents the gravitational acceleration. In this equation, the term in parenthesis in the L.H.S. represents the material derivative of the velocity field, i.e., the acceleration of one fluid particle that moves in this field. The R.H.S. of the equation is the summation of the forces (per unit volume) that act on the fluid particle, with the first two terms being the pressure and body forces, respectively, while the remaining terms represent viscous forces. Assuming the Stokes hypothesis for a Newtonian fluid, the viscous stress tensor $\hat{\tau}$ is given by

$$\hat{\tau} = \mu \left[\vec{\nabla}\vec{u} + (\vec{\nabla}\vec{u})^T \right] - \frac{2}{3}\mu(\vec{\nabla}.\vec{u})\hat{I}, \tag{2.4}$$

where μ is the dynamic viscosity, $\hat{I}$ is the identity tensor, $\vec{\nabla}\vec{u}$ is the velocity gradient tensor with components $(\partial/\partial x_i)v_j$, $(\vec{\nabla}\vec{u})^T$ is the transpose of the velocity gradient tensor with components $(\partial/\partial x_j)v_i$ and $(\vec{\nabla}.\vec{u})$ is the divergent of the velocity vector. This term accounts for diffusion of linear momentum.

The balance equation of the chemical species i in terms of mass fraction (Y_i), is given by

$$\frac{\partial(\rho Y_i)}{\partial t} + \vec{\nabla} \cdot (\rho \vec{u} Y_i) = -\vec{\nabla} \cdot \vec{J}_i + \dot{w}_i, \tag{2.5}$$

where the L.H.S terms represent the rate of change of the species i mass fraction for a fluid particle that moves with the flow velocity. The R.H.S terms represent the divergent of the diffusive flux $\vec{J}_i$ of species i, and the source term $\dot{w}_i$ of production or consumption of species i. The Equation 2.5 is solved for $N_s - 1$ species, being N_s the total number of species. The mass fraction of the inert species N_2 is given by

$$Y_{N_2} = 1 - \sum_{i=1}^{N_s - 1} Y_i. \tag{2.6}$$

The diffusive flux $\vec{J}_i$, modelled by Fick's Law, is given by

$$\vec{J}_i = -\rho D_{i,m} \vec{\nabla} Y_i, \tag{2.7}$$

where $D_{i,m}$ is the binary diffusion coefficient of species i in the mixture.

The energy conservation equation is expressed through its enthalpy formulation by

$$\frac{\partial(\rho h)}{\partial t} + \vec{\nabla}.(\rho\vec{u}h) = \vec{\nabla}.\left(\frac{\lambda}{C_p}\vec{\nabla}h\right) - \vec{\nabla}.\left[\sum_{i=1}^{N_s}\left(1 - \frac{1}{Le_i}\right)\frac{\lambda}{C_p}h_i\vec{\nabla}Y_i\right] + S_h \tag{2.8}$$

where the L.H.S. represent the rate of change of mixture enthalpy for a fluid particle that moves with the flow velocity. The R.H.S comprises the heat flux terms, being the first term the heat flux due to conduction heat transfer in the presence of a temperature gradient. The second term is the transfer of heat through mass diffusion due to the different heat contents of the various species. The term λ is the thermal conductivity and h the sensible enthalpy. The term S_h in the R.H.S of the equation is the energy source term, defined by

$$S_h = -\sum_i h_i^0 MW_i w_i, \tag{2.9}$$

where h_i^0 is the enthalpy of formation of species i, MW_i is the molar mass of species i and w_i is the volumetric rate of production/destruction of species i. The energy equation considered in Equation 2.8 neglected pressure variations under the assumption of low-Mach number. The Dufour and Soret effects and radiation heat losses were also neglected. The mixture specific heat is described as a weighted average of specific heats of species,

$$C_p = \sum_{i=1}^{N_s} Y_i \cdot C_{p,i}. \tag{2.10}$$

2.2 Transport properties

Assuming unity Lewis number significantly simplifies the diffusion terms calculation through relating species mass and thermal diffusivities. The Lewis number is defined as

$$Le_i = \frac{\lambda}{\rho C_p D_{i,m}}. \tag{2.11}$$

For the calculation of λ and ν, it is assumed the approximation proposed by Smooke and Giovangigli, 1991 for combustion of methane and air to reduce the computational time. This approximation considers that the mixture dynamic viscosity and thermal conductivity are both functions of the temperature and the specific heat at constant pressure of the mixture according to

$$\frac{\mu}{C_p} = 1,67 \times 10^{-8} \left(\frac{T}{298}\right)^{0,51}, \tag{2.12}$$

$$\frac{\lambda}{C_p} = 2,58 \times 10^{-5} \left(\frac{T}{298}\right)^{0,69} \tag{2.13}$$

2.3 Conserved sand composition. Also, for sufficiently low pressure, the ideal gas equation of state can be assumed valid:calar formulation

One of the main issues when solving chemically reacting flows is the presence of the reaction source term $\dot{w}_i$. Although its modelling approach is already well established, $\dot{w}_i$ is extremely nonlinear and results in stiff differential equations to be solved. However, under the assumptions of unity Lewis number and infinitely fast reactions it is possible to show that the concentration of the involved species and the system enthalpy are related through stoichiometry such that, with a proper combination of variables, the chemical reactions cancel out in the conservation equation. This combined quantity is called a conserved scalar or coupling function, and the result is that the flame variables can be described as functions of the conserved scalar only [Law, 2006].

There are different formulations for such approach which use different conserved scalars or coupling functions. Under some assumptions, all different conserved scalars are linearly related so that the choice is arbitrary. Under other circumstances, such as non-equal diffusivity effects, number and uniformity of the reactants feed and the complexity of the chemical mechanism considered, there may be one formulation that is more convenient than others [Bilger, 1980; Law, 2006]. The mixture fraction formulation is another derivative of the coupling functions formulation and therefore is also subjected to the assumption of unity Lewis number. It is the most applied formulation for non-premixed flames and it is used as conserved scalar in the flamelets models. For this reason, its formulation will be discussed in the section 2.5.

The mixture fraction Z is a very convenient quantity for nonpremixed combustion since it quantifies the fuel-air ratio of the mixture with values varying from null to unity. Since the result of the mixture fraction formulation is the solution of the differential equation for Z, it is convenient to have such normalization rather than values from null to infinite, such as the equivalence ratio ϕ in premixed combustion. The physical meaning of

Z is very similar to ϕ, in which both quantify the fuel-air ratio in the mixture. Considering two uniform streams (that could be pure fuel and pure oxidizer), the Z value represents the state of mixing at a certain point, relating the mass which came from stream S_1 to the one which came from stream S_2. Different ways of presenting Z are possible, as presented in Peters, 2000, such as

$$Z = \frac{\dot{m}_1}{\dot{m}_1 + \dot{m}_2}, \tag{2.14}$$

and

$$Z = \frac{Z_C/(mW_C) + Z_H/(nW_H) + 2(Y_{O_2,2} - Z_O)/(\mu_{O_2}W_{O_2})}{Z_{C,1}/(mW_C) + Z_{H,1}/(nW_H) + 2Y_{O_2,2}/(\mu_{O_2}W_{O_2})}. \tag{2.15}$$

In the first definition (Eq. 2.14), $\dot{m}_1$ is the mass flux originating from the fuel and $\dot{m}_2$ from the oxidizer stream. At last, a very common definition in experimental and numerical analysis is the definition from Bilger, 1988, which is the last one presented (Eq. 2.15). The terms Z_C, Z_H and Z_O denote the element mass fractions of C, H and O, and W_C, W_H and W_O their molecular weights, respectively. The terms m and n are the number of atoms of C and H in the fuel. All definitions have boundary conditions of $Z = 1$ in the fuel stream and $Z = 0$ in the oxidizer stream.

2.4 Detailed chemical kinetic modelling

The presented treatment of the chemical kinetic typically involves dozens of species, hundreds of reactions and different chemical time scales. The system of non-linear differential equations to be solved is strongly stiff and coupled, making the problem computationally demanding even for laminar flames.

This section describes the production or consumption of chemical species in the source term of the conservation equation of chemical species (Equation 2.5). Many elementary chemical reactions occurs simultaneously in the chemical reaction region of the flame. In general, those reactions are reversible and both directions have to be accounted for.

One generic chemical reaction j can be written as

$$\sum_{i=1}^{N_s} \nu'_{i,j}\mathcal{M}_i \rightleftharpoons \sum_{i=1}^{N_s} \nu''_{i,j}\mathcal{M}_i \tag{2.16}$$

where $\mathcal{M}_i$ represents the molecular formula of the species i, $\nu_{i,j}$ are the stoichiometric coefficients (that indicates how many moles of the species i are part of the reaction j), and the indexes $'$ and $''$ indicate reactants and products, respectively.

Following this notation, the net reaction rate for the j^{th} reaction is

$$\bar{\dot{\omega}}_j = k_{f,j} \prod_{i=1}^{N_s} [\mathcal{M}_i]^{\nu'_{i,j}} - k_{r,j} \prod_{i=1}^{N_s} [\mathcal{M}_i]^{\nu''_{i,j}}, \tag{2.17}$$

where the concentration of the species $\mathcal{M}_i$ is given by $[\mathcal{M}_i] = (Y_i MW/MW_i)(p_0/R_u T)$, and k represents the reaction rate coefficient. The subscripts f and r indicates the forward and the reverse directions of reactions, respectively.

The reaction rate coefficient k is given by the modified form of the Arrhenius expression:

$$k = AT^b \mathrm{e}^{-E_a/R_u T}. \tag{2.18}$$

where A is the pre-exponential factor, b is the temperature exponent and E_a is the activation energy. These parameters are determined empirically by adjusting procedures to recover experimental results, or theoretically from fundamental principles.

When the reverse reaction rate coefficient k_r is not specified, it can be calculated from the equilibrium constant K_c. In the equilibrium, the rate of change of any species concentration is zero ($\bar{\dot{\omega}}_j = 0$ from Eq. 2.17), leading to

$$\frac{k_{f,j}(T)}{k_{r,j}(T)} = \frac{\prod_i [\mathcal{M}_i]^{\nu''_{i,j}}}{\prod_i [\mathcal{M}_i]^{\nu'_{i,j}}}, \tag{2.19}$$

The LHS of Equation 2.19 is equal to the equilibrium constant $K_{c,j}$ of reaction j, which can be precisely calculated from the Gibbs free energy following the equilibrium formulation [Turns, 2000]. Lastly, the source term $\dot{\omega}_i$ of Equation 2.5 accounts all N_r reactions of the chemical kinetic mechanism containing the species i, and is given by

$$\dot{\omega}_i = MW_i \sum_{j=1}^{N_r} (\nu''_{i,j} - \nu'_{i,j}) \bar{\dot{\omega}}_j. \tag{2.20}$$

2.5 Simplified models

When dealing with complex combustion systems, there are two main streams of research which try to simplify the chemical kinetic modelling: laminar flamelet models and chemical reduction techniques. This section will talk about techniques which simplify the combustion modelling and those which were the start point for the developing of the Flamelet-Generated Manifold method, which is the technique used in the present work to simplify combustion chemistry. The infinitely fast reaction limit, flamelet-based models (SLDF, FPV, FPI, FGM) and the Intrinsic Low-Dimensional Manifold (ILDM) of Maas and Pope, 1992 are presented in the next sections.

2.5.1 Infinitely fast reaction limit

By assuming unity Lewis number for all species, the analysis of nonpremixed flames can be conducted through the mixture fraction Z space such that the results obtained are independent of the flame configuration. For the case of a one-step irreversible reaction with infinitely fast chemistry assumption, the earliest approximate solution of diffusion flames is the Burke-Schumann solution [Burke and Schumann, 1928], which relates linearly the species mass fractions and temperature to the mixture fraction (see Figure 2.1).

The usefulness of this approach is given by the fact that to solve the flame one needs to solve only a transport equation for Z, since the flame variables ψ are all dependent on Z only, yielding $\psi_i = f(Z)$. Another advantage is that the differential equation that describes the transport of Z does not have a source term. The general transport equation for Z can be given by

$$\frac{\partial \rho Z}{\partial t} + \rho \vec{u} \cdot \vec{\nabla} Z = \vec{\nabla} \cdot \left(\rho D \vec{\nabla} Z \right), \tag{2.21}$$

subjected to the boundary conditions already stated for Z. Since the unity Lewis number assumption is under consideration, the diffusion coefficient D is equivalent, in this case, to the thermal diffusivity.

Even though it is useful to have the flame structure solved in terms of a conserved scalar, $\psi_i = f(Z)$, most of the time it is interesting to have the flame variables related to the physical space, $\psi_i = f(x, y, z, t)$. Therefore, the solution of Z in the physical space, $Z = f(x, y, z, t)$, needs to be solved. Different solutions have been proposed for different

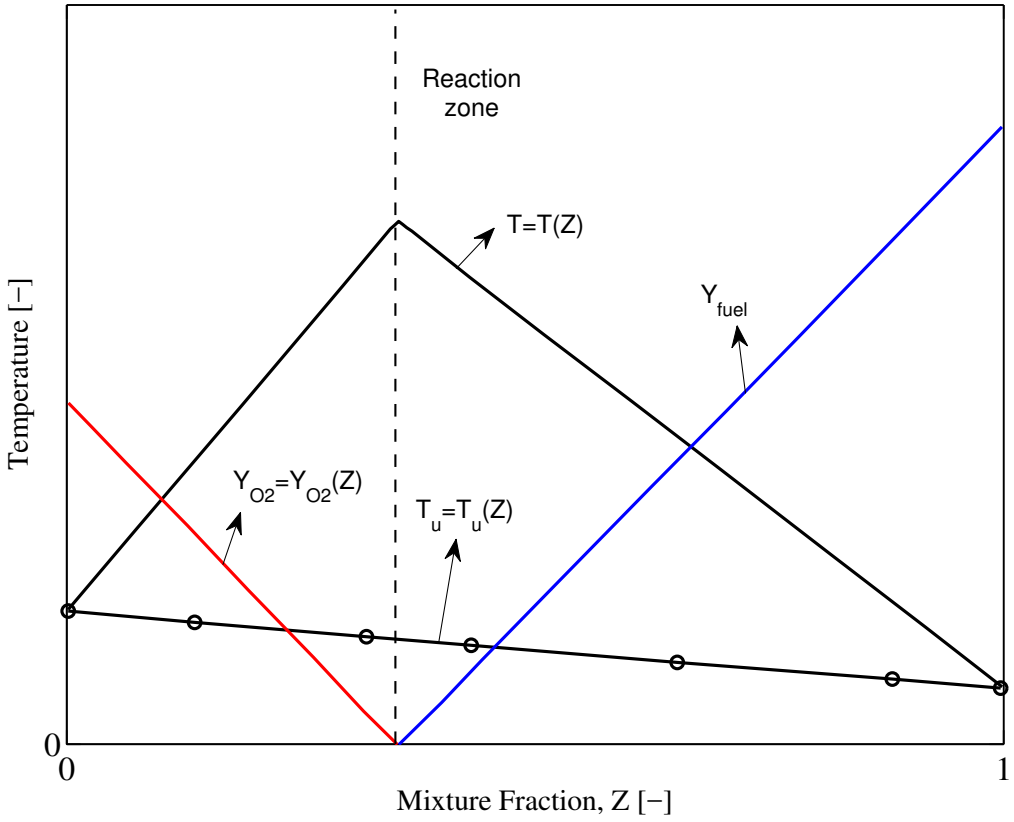

Figure 2.1 – Schematic Burke-Schumann solution of nonpremixed flames as function of mixture fraction (adapted from Peters, 2000).

flame configurations. As an example, for a one-dimensional counterflow flame its structure is time independent, and the three-dimensional Equation 2.21 can be reduced to its one dimensional form yielding

$$\rho v \frac{dZ}{dy} = \frac{d}{dy}\left(\rho D \frac{dZ}{dy}\right) \tag{2.22}$$

The solution of Equation 2.22 can be found in detail in Peters, 2000, in which one obtains the solution

$$Z = \frac{1}{2} erfc\left(\eta/\sqrt{2}\right), \tag{2.23}$$

through similarity analysis, where η is a nondimensional similarity coordinate which is, for the counterflow configuration, function of the strain rate a, ρ, D and the physical coordinate (y in this case). Therefore, one can find the mixture fraction field in the physical space, which is influenced by the strain rate a of the flow and by its properties.

2.5.2 Flamelet-based models

The essential feature of the calculation of non-premixed flames is the introduction of a conserved scalar, which is generally the mixture fraction, Z, as presented previously in section 2.3. Under the assumption of infinitely fast reaction limit, all the flame variables, such as temperature, mass fractions and properties can be uniquely described by Z. The solution of diffusion flames can then be obtained by only solving a transport equation for Z. The main advantage of such formulation is the absence of a chemical source term, which is extremely non-linear and leads to stiff solutions of the transport equations. However, such formulation fails when non-equilibrium effects are important. Therefore, the Steady Laminar Diffusion Flamelet model of Peters, 1984 extended the conserved scalar formulation to account for non-equilibrium effects, including the instantaneous scalar dissipation rate at stoichiometric conditions, χ_{st} , as a second variable. Later, derivations of this model arose with slightly different implementation processes which improve the SLDF model, such as the Flamelet-Generated Manifold (FGM), Flamelet Prolongation of the ILDM (FPI) and the Flamelet Progress Variable (FPV). Such models will be briefly described in the sequence and the FGM technique will be detailed in Chapter 3.

Flamelet equations in mixture fraction space

In non-premixed combustion, chemical reactions will occur if fuel and oxidizer are mixed at the molecular level [Pitsch et al., 2000]. The rate of the molecular scalar mixing is represented by the scalar dissipation rate χ. When dealing to finite rate chemistry models, χ appears as an important parameter in combustion models as the Flamelet model of Peters, 1984, which will be discussed in section 2.5.2. The χ parameter arises when the conservation equations given by Equations 2.5 and 2.8 suffer a coordinate transformation of Crocco-type (as performed at Peters, 1984), from the physical space to the mixture fraction Z space. The coordinate system (x, y, z, t) is transformed into the new one (Z, Z_2, Z_3, τ), in which the new coordinate mixture fraction Z is locally normal to the surface of stoichiometric mixture ($Z(x, y, z, t) = Z_{st}$), $Z_2 = y$, $Z_3 = z$ and $\tau = t$. The transformation rules applied are

$$\begin{aligned}
\frac{\partial}{\partial t} &= \frac{\partial}{\partial \tau} + \frac{\partial Z}{\partial t}\frac{\partial}{\partial Z}, \\
\frac{\partial}{\partial x} &= \frac{\partial Z}{\partial x}\frac{\partial}{\partial Z}, \\
\frac{\partial}{\partial y} &= \frac{\partial}{\partial Z_2} + \frac{\partial Z}{\partial y}\frac{\partial}{\partial Z}, \\
\frac{\partial}{\partial z} &= \frac{\partial}{\partial Z_3} + \frac{\partial Z}{\partial z}\frac{\partial}{\partial Z}.
\end{aligned} \tag{2.24}$$

For the inner reaction zone, a quasi-steady state regime can be considered for the flame structure and hence one can neglect the temporal terms. Also, in the inner reaction zone all terms involving derivatives with respect to Z_2 and Z_3 are of lower order compared to Z, which is the coordinate that comprises the highest gradients. The resultant equations in the mixture fraction space can hence be written by Eqs. 2.25 and 2.26. The energy equation is written in terms of temperature instead of sensible enthalpy, such it was in Equation 2.8, and only the species chemical source term is considered for convenience.

$$-\rho D\left(\vec{\nabla}Z\right)^2 \frac{\partial^2 Y_i}{\partial Z^2} = \dot{w}_i \tag{2.25}$$

$$\rho D\left(\vec{\nabla}Z\right)^2 \frac{\partial^2 T_i}{\partial Z^2} = S_h \tag{2.26}$$

The first term in the L.H.S of both equations above represents the influence of the flow field in the flame structure in the Z space. This term is the scalar dissipation rate and is given by

$$\chi = 2\rho D\left(\vec{\nabla}Z\right)^2. \tag{2.27}$$

In the flamelet concept, the scalar dissipation rate is used as a second variable to describe the flame and an analytical expression is used to calculate it. Depending on the flame configuration different expressions are obtained since it depends on the mixture fraction. For the counterflow configuration, whose solution is presented in Eq. 2.23, the scalar dissipation rate definition is given by

$$\chi = \frac{a}{\pi} exp\left(-2\left[erfc^{-1}(2Z)\right]^2\right). \tag{2.28}$$

The scalar dissipation rate, as already stated previously, quantifies the rate of the molecular scalar mixing. In the counterflow configuration, the expression of χ (Eq. 2.28) shows that χ is proportional to the strain rate a, which is a parameter that represents the intensity of the gradients in the flow field. It means that the higher the strain rate is, the higher the gradients will be and the higher will be the value of the scalar dissipation rate. That means the rate of the molecular scalar mixing will increase and the molecular diffusion time scale will decrease. Since the chemistry and diffusion time scales start to get closer with the increase of χ, its value can also be interpreted as a departure from the equilibrium regime. At a certain point, the scalar dissipation can be so high that leads the flame to locally quench. The perturbation from equilibrium regime being quantified by the scalar dissipation rate lead the flamelet approaches to use such parameter as the second variable to account for non-equilibrium effects.

Steady Laminar Diffusion Flamelet Model (SLDF)

The laminar flamelet concept was introduced by Peters, 1984 and views a turbulent diffusion flame as an ensemble of laminar diffusion flamelets. Such concept is derived from the basic idea of scales separation between chemistry and turbulence. Non-premixed flames have the diffusion time scale as dominant over convection and reaction ones. It is then intuitive to think that the assumption of infinitely fast chemistry is suitable for laminar flames. Such assumption is the basis for analytical models developed for non-premixed laminar flames, such as the Burk-Schumann [Burke and Schumann, 1928] solution, for instance. For turbulent flows, however, local diffusion time scales can vary considerably leading the infinitely fast chemistry assumption to be locally not valid, and hence non-equilibrium effects must be taken in account. Therefore, considering the flame reaction zone thin compared to the small turbulence scales yields to a local laminar structure of the flame even for turbulent flames.

The SLDF equations were previously presented in Eqs. 2.25 and 2.26 and can be written in a more general way as follows

$$-\frac{\chi}{2}\frac{\partial^2\psi_i}{\partial Z^2} = \dot{w} \tag{2.29}$$

where all the thermochemical quantities are a function of mixture fraction and scalar dissipation rate only. Therefore, all flame variables ψ in the steady laminar flamelet

model can be represented by

$$\psi = f_{\psi}\left(Z, \chi_{Z_{st}}\right), \tag{2.30}$$

where f_{ψ} represents the steady laminar flamelet library. The solution of these equations can be represented by the S-shaped curve, shown in Figure 2.2, where the stoichiometric temperature is graphed as function of the stoichiometric scalar dissipation rate. The upper and lower branches are the fully burning and fully frozen states, respectively. The turning point between the upper and the middle branch represents the quenching limit of the flame, while the turning point between the lower and the middle branch represents the igniting limit. It is important to note that the flamelet library from the steady laminar flamelet model in Equation 2.30 contains only the burning state solution of the S-shaped curve. One can note that there is no unique solution for each value of χ_{st} in the steady laminar flamelet model. The model proposed by Peters, 1984, does a vertical projection on the S-shaped curve when some point falls into the unstable branches. That means the steady laminar flamelet models which use the mixture fraction Z and the stoichiometric scalar dissipation rate χ_{st} for parametrization of all thermochemical quantities are unable to describe the transient states a flamelet experiences during the extinction and re-ignition processes [Ihme and Pitsch, 2008].

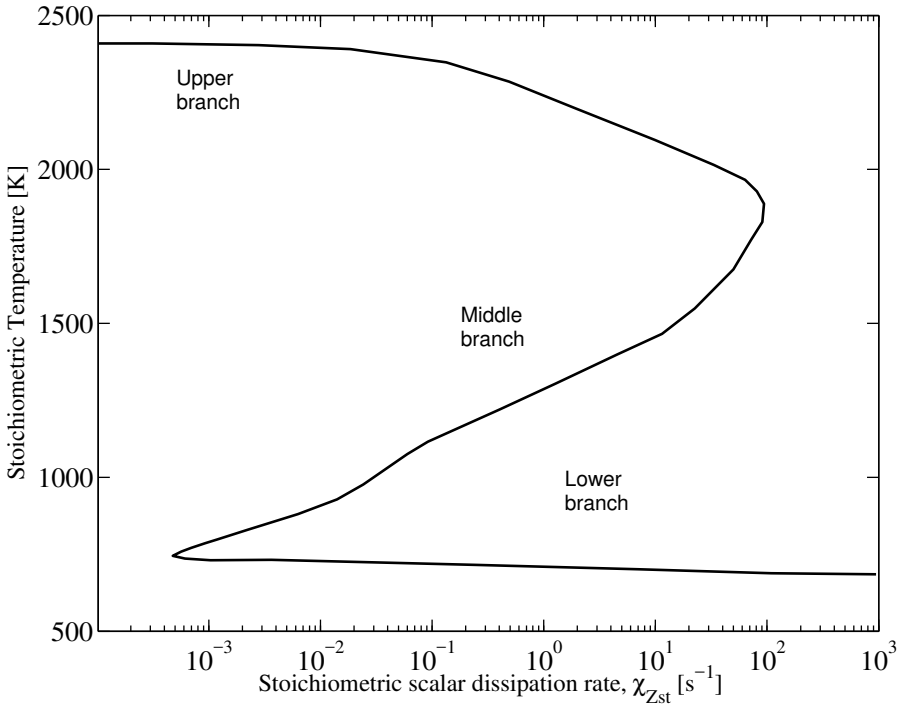

Figure 2.2 – Solution of the flamelet equations for methane/air combustion represented by the S-shaped curve, showing the stoichiometric temperature as function of the stoichiometric scalar dissipation rate (adapted from Ihme, 2007).

FGM, FPI and FPV models

After the introduction of the SLDF model, different methods arose in the literature which are very similar, differing slightly in their implementation process solely. In the years 2000, the Flamelet-Generated Manifold (FGM) technique was being developed by Van Oijen and de Goey, 2000 and, at the same time, the Flame Prolongation of the ILDM (FPI) was being independently developed by Gicquel et al., 2000. Later, Pierce and Moin, 2004 combined the SLDF model with the progress of reaction concept, proposing the Flamelet-Progress Variable (FPV) model. The FGM model will be explained in detail in Chapter 3. In the sequence, a brief explanation of the improvements of the mentioned techniques over the SLDF will be addressed.

The Flamelet Progress Variable (FPV) approach, proposed by Pierce and Moin, 2004, suggested the utilization of a reactive scalar as second control variable instead of the stoichiometric scalar dissipation rate in order to account flame dynamic effects into the steady laminar flamelet model. In practical terms, the introduction of this new reactive

scalar allowed an horizontal projection onto the S-shaped curve instead of a vertical one to the burning state only, as the steady laminar flamelet model of Peters, 1984 does (see Figure 2.3).

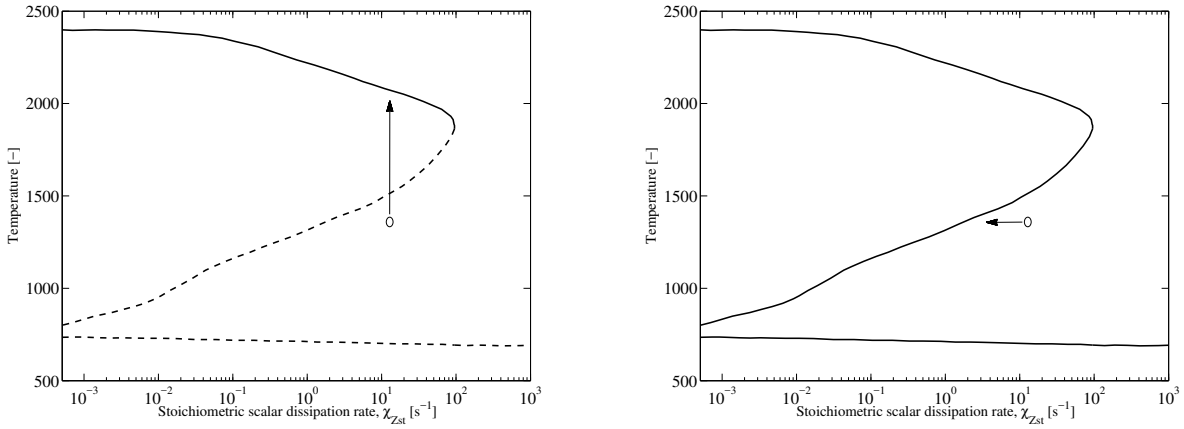

(a) SLDF flamelets solutions accessed.

(b) FPV flamelets solutions accessed.

Figure 2.3 – Schematic comparison of (a) SLDF model with (b) FPV model (adapted from Ihme, 2007). The solid lines represents the accessible solution in each mode, and the points and arrows represent the projections into the S-shaped curve of each model.

The new reactive scalar introduced is the progress parameter Λ, whose definition must be chosen such that it allows for a unique identification of all flamelets Ihme et al., 2005. Another constraint for the progress parameter Λ is that it must be statistically independent of the mixture fraction Z. If one chooses a generic reactive progress variable $\mathcal{Y}$ as being the temperature or a linear combination of the major chemical species, and wants to use it as second control variable along the mixture fraction, it would not be theoretically possible to ensure independence of those two variables ($\mathcal{Y}$ and Z). For this reason, the progress parameter Λ was defined as being a function of the progress variable $\mathcal{Y}$ at a certain condition of Z. A common definition used for Λ is

$$\Lambda = \mathcal{Y}|Z_{st}. \tag{2.31}$$

With the introduction of the progress parameter Λ in the FPV model, all flame variables can be described by

$$\psi = F_{\psi}\left(Z, \Lambda\right), \tag{2.32}$$

where F_ψ represents the FPV library. Note that it differs from Equation 2.30 since it includes all the solutions of the S-shaped curve, even the unstable branches.

The objective of the look-up techniques in combustion is to solve transport equations for a small number of control variables which can mimic the chemical kinetic of some detailed mechanism, instead of solving all the equations which describe it. Hence, from Equation 2.32, in the FPV model it would be necessary to solve transport equations for Z and Λ. A transport equation for Z is already solved in other techniques, but solving a transport equation for Λ would be too much complicated [Ihme, 2007]. It is common to solve a transport equation for a generic reactive progress variable, mainly in premixed flames, without extra complications. Therefore, it would be more convenient to use the progress variable $\mathcal{Y}$ as second control variable in order to solve a transport equation for it, instead of for Λ. To ensure it can be done, the definition of $\mathcal{Y}$ should be chosen such that the function that relates Λ and $\mathcal{Y}$ be bijective (invertible), yielding to a independent relation with the mixture fraction Z. This constraint is exactly the objective function used by Ihme et al., 2012, in his work dealing with an optimization algorithm to find a suitable definition for the progress variable.

2.5.3 Reduced chemical kinetic techniques

When dealing with the subject of simplifying the calculations necessary to describe the kinetic of combustion systems, several strategies arise. Classical methods like the Quasi-Steady State or Partial Equilibrium are used to find approximate algebraic relationships for the fast reactive species in terms of the slow reactive species. However, both need previous knowledge about the behavior of the reaction time scales in order to choose which species to be considered in quasi-steady state or elementary reactions to assume in partial equilibrium.

Another method for reducing chemical kinetic is the Intrinsic Low-Dimensional Manifold (ILDM) technique, firstly presented by Maas and Pope, 1992. The ILDM brings the advantage of automatically extract the required information from the detailed mechanism without relying on experience or intuition from the person applying it. Since the FGM method, which is the chosen method in the present work, was developed based on the flamelet-based models as well as on the ILDM technique, a brief explanation of the ILDM will be addressed in the sequence. The following text was written based on Maas

and Pope, 1992 and its reading is recommended for a complete explanation of the method.

Systems of Ordinary Differential Equations (ODE) which have time as an independent variable present local time scales which can be significant parameters depending on the application. For combustion systems, comprised of ODEs which describe the species mass fractions transport, the time scales in which each of them occur are very important parameters. The mathematical way to retrieve the different time scales due to the elementary reactions is to find the eigenvalues of the Jacobian matrix of the ODE system. A n_s-dimensional linear system of n_s first order ODEs can be represented by

$$\frac{d\mathbf{x}}{dt} = \mathbf{f}\left(x_1, x_2, ..., x_{n_s}\right), \tag{2.33}$$

where t is the independent variable, $\mathbf{x}$ is the vector of species mass fractions of length n_s, and x_i are the individual species mass fractions. The vector $\mathbf{f}$ comprises the functions describing the rates of change of the species mass fractions. In order to find the time scales associated with the solution at each point in the solution space, it is necessary to perform an eigenvalue analysis of the Jacobian matrix $\mathbf{J}$ at each point of the solution space, which is given by

$$\mathbf{J} = \begin{pmatrix} \frac{\partial f_1}{\partial x_1} & \frac{\partial f_1}{\partial x_2} & \cdots & \frac{\partial f_1}{\partial x_{n_s}} \\ \frac{\partial f_2}{\partial x_1} & \frac{\partial f_2}{\partial x_2} & \cdots & \frac{\partial f_2}{\partial x_{n_s}} \\ \vdots & \vdots & \ddots & \vdots \\ \frac{\partial f_{n_s}}{\partial x_1} & \frac{\partial f_{n_s}}{\partial x_2} & \cdots & \frac{\partial f_{n_s}}{\partial x_{n_s}} \end{pmatrix}. \tag{2.34}$$

The ILDM is based on the idea that the slow time scales dominate the behavior of the chemical kinetic over the fast time scales. Therefore, the slow elementary reactions should be identified through the eigenvalue analysis of the matrix of Equation 2.34 and be the basis for the creation of the solution trajectory. It is intuitive to think that the slowest reactions dominate the path of the chemistry over the fast time scales, which could be interpreted as being in steady state. There are many methods for finding the eigenvalues of the Jacobian matrix, however there are some that might be more useful than others in terms of implementation, such as the Schur decomposition, for instance. The next step is applying such technique at a certain known point of the manifold. A point which will always be in the manifold is the equilibrium point. Then, a numerical procedure to guess the next point in the manifold is performed extracting the eigenvalues

of the Jacobian matrix in such guessed point. The final result is a path which represents the lower dimensional manifold which should be representative of the detailed chemistry path (see Figure 2.4).

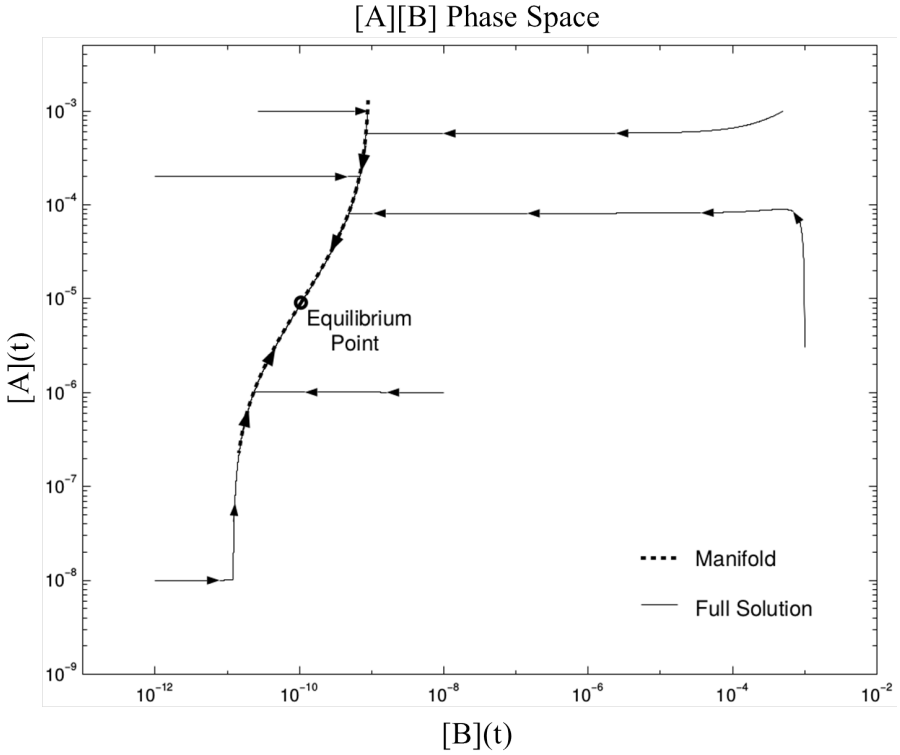

Figure 2.4 – Plot of a lower dimensional manifold along sample trajectories from different initial conditions (adapted from Maas and Pope, 1992).

3 FLAMELET-GENERATED MANIFOLD (FGM) TECHNIQUE

The FGM technique was independently developed at the same time by Van Oijen and de Goey, 2000 and Gicquel et al., 2000, in which the later calls it the Flame Prolongation of ILDM (FPI) method. The FGM is based on the observation that multidimensional turbulent flames can be represented by several unidimensional laminar flames, commonly called flamelets, which describe all the flame composition space. It combines the advantages of reducing the chemical space into a small number of representative control variables, like the Intrinsic Low-Dimensional Manifold (ILDM) method does [Maas and Pope, 1992], along the advantages of considering the flow characteristics by solving a set of flamelets, like the Steady Laminar Flamelet Model (SLDF) [Peters, 1984]. The later allows a better prediction of cold zones of the flame in comparison to the ILDM technique. Hence, the solutions of the flamelets (thermal, chemical and transport scalars that represent the combustion process) are stored in a manifold as function of the control variables. The choice of the control variables depends on the physics which will be simulated. They need to parametrize the entire thermochemical state of the flame. For premixed adiabatic flames, for instance, only a reactive progress variable is sufficient to properly map its physics, while for diffusion flames it is necessary the inclusion of the mixture fraction Z as additional control variable. Usually two or three dimensions are sufficient to properly solve most combustion systems, however, manifolds with higher dimensions may be necessary for more complex problems.

After constructing the manifold, it is further used in computational fluid dynamics codes to reconstruct the multidimensional flame. Note that in the FGM technique it is not necessary to solve all the chemical kinetic reaction equations neither the chemical species mass conservation or energy equations. Instead of it, transport equations for the control variables are solved along with the flow equations. This yields a reduction in the computational time up to 100 times in some cases [Van Oijen and de Goey, 2000]. In section 3.3 the equations solved in a multidimensional flame using FGM are presented. The Figure 3.1 shows a schematic representation of the FGM operation.

In the next sections, the flamelets equations used to construct the manifold will be presented in more detail. In the sequence, the process of manifold construction will be addressed and finally the equations which are solved in the multidimensional simulation

are presented. A discussion about the control variables is addressed in the next chapter, along the introduction of the optimization problem formulation.

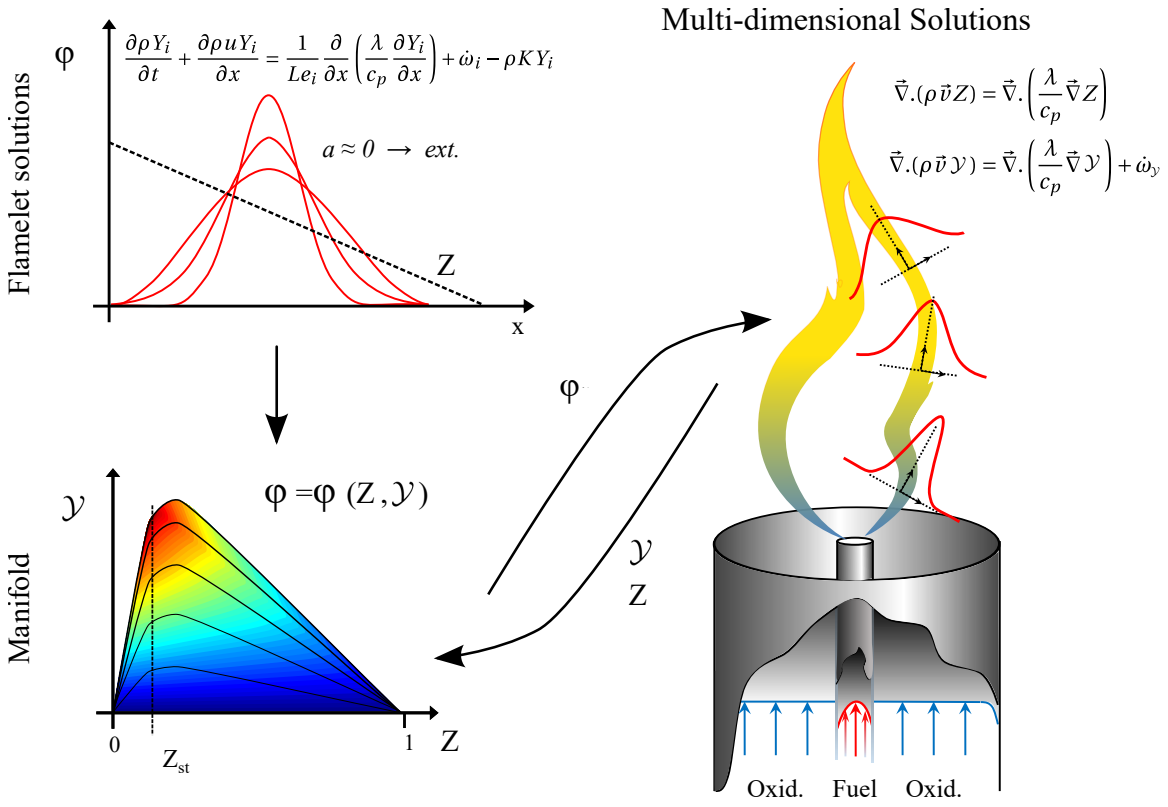

Figure 3.1 – Schematic representation of the operation of FGM technique [Hoerlle, 2017]. Hypothetical flamelet solutions are represented in physical space, for different strain rates a. Then, the flamelet solutions are stored in the manifold through the parametrization with the two controlling variables (Z and $\mathcal{Y}$). During the multidimensional simulation, the manifold is constantly accessed to retrieve the needed flame variables from the controlling variables.

3.1 Flamelet equations

Several unidimensional flames need to be solved for different conditions in order to build the manifold. In the case of diffusion flames being solved with the FGM technique, it is common to vary the strain rate a in counterflow flamelets from values close to equilibrium (small values of a) up to extinction (big values of a). The system of equations that is solved in the flamelets is derived from the three-dimensional conservation equations from section 2.1. They are simplified for one dimension and the stretch rate term is

introduced to account for multidimensional effects. The introduction of the stretch rate in the flamelet modelling is explained in detail in De Goey and Ten Thije Boonkkamp, 1999. It is also important to state that in the flamelet solutions the chemical kinetic is solved through a detailed mechanism. Therefore, there is information from the detailed mechanism in the FGM technique, which is stored in the manifold.

The system of flamelet equations for mass, species and enthalpy conservation is given by

$$\frac{\partial \rho}{\partial t} + \frac{\partial \rho u}{\partial x} = -\rho K, \tag{3.1}$$

$$\frac{\partial \rho Y_i}{\partial t} + \frac{\partial \rho u Y_i}{\partial x} = -\frac{\partial}{\partial x}\left(\rho Y_i \vec{V_i}\right) - \rho K Y_i + \dot{\omega}_i, \tag{3.2}$$

$$\frac{\partial \rho h}{\partial t} + \frac{\partial \rho u h}{\partial x} = -\frac{\partial}{\partial x}\left(-\frac{\lambda}{c_p}\frac{\partial h}{\partial x} + \sum_{i=1}^{N_s} h_i \rho Y_i \vec{V_i}\right) - \rho K h + \dot{q_R}, \tag{3.3}$$

in which x and u are, respectively, the spatial coordinate normal to the flame surface and the flow velocity. The x-momentum equation is superfluous since the continuity equation was used to find the velocity in the x direction. In addition, a transport equation was employed for the stretch rate (K), which was derived from the momentum equation in transverse direction. The conservation equation of K reads

$$\frac{\partial \rho K}{\partial t} + \frac{\partial \rho u K}{\partial x} = \frac{\partial}{\partial x}\left(\mu \frac{\partial K}{\partial x}\right) - \rho K^2 + \rho_2 a^2, \tag{3.4}$$

in which, a is the linear strain rate $a = -\partial u/\partial x$ [s^{-1}] and ρ_2 the density, both defined at a reference position, usually the oxidant side in non-premixed counterflow flames.

The stretch rate is defined as the relative rate of change of M as

$$K = \frac{1}{M}\frac{\mathrm{d}M}{\mathrm{d}t}. \tag{3.5}$$

where $M(t)$ is the mass contained in an infinitesimal flame volume $V(t)$

$$M(t) = \int_{V(t)} \rho \mathrm{d}x \tag{3.6}$$

that moves with the local velocity of the flame surface.

Finally, the set of differential equations is followed by the ideal gas law and the

caloric equation of state.

3.1.1 Counterflow flamelet modelling

The solution of the counterflow unidimensional flames was performed with the CHEM1D code (it is a CFD code to solve unidimensional flames developed in the Reactive Flow Group at the Eindhoven University of Technology). The code solves the system of conservation equations for reactive flows based on the finite volume method with a fully implicit modified Newton technique. Different domain lengths were used depending on the strain rate value, since the flame structure changes with it. The code employs a grid refinement algorithm to increase the number of control volumes in regions with steep gradients. The advective terms of the conservation equations were treated by the exponential discretization scheme, while the diffusive ones were treated by the central difference scheme. The conservation equations describe the conservation of mass, stretch rate, chemical species and enthalpy (set of equations 3.1-3.4).

The Figure 3.2 shows a schematic counterflow flame. In the present case, the fuel is injected in the left side ($-L$) while the oxidant is injected in the right side ($+L$). Both streams are injected along the x coordinate. A stagnation plane is formed between the injection tubes, and the flame commonly is formed closer to the oxidant side. For this flame, radial gradients can be neglected in transport equations because axial gradients are more significant.

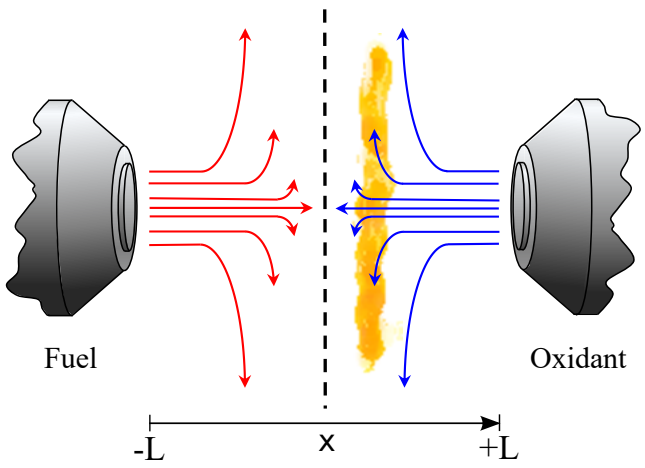

Figure 3.2 – Schematic counterflow flame configuration [Hoerlle, 2015].

The set of equations 3.1-3.4 are subjected to the following boundary conditions:

Fuel side	Oxidant side
$u(x=0)=0$	
$Y_i(x \to -L) = Y_{i,1}$	$Y_i(x \to +L) = Y_{i,2}$
$h(x \to -L) = h_1$	$h(x \to +L) = h_2$
$K(x \to -L) = a\sqrt{\rho_2/\rho_1}$	$K(x \to +L) = a$

The subscripts 1 and 2 represents the fuel and the oxidizer, respectively, while $-L$ (pure fuel) and $+L$ (pure oxidant) indicates the position of the boundary conditions. The stretch rate tends to the linear strain rate at the oxidant injection position $K(x \to +L) = a$.

In general, the multidimensional laminar flames retrieve information from the manifold related to the burning state of the S-shaped curve from Figure 2.2. In such cases, only the steady state solutions of the conservation equations above would be necessary, varying the strain rate from equilibrium conditions up to almost extinction of the flame. However, to guarantee that in the case the multidimensional flame wants to access regions closer to extinction and that it will be properly mapped by the control variables, it is a good practice to solve unsteady flamelets for a critical strain rate value which would lead to extinction. The Figure 3.3 below represents the regions of the S-shaped curve which are actually obtained with the flamelet solutions in the FGM technique. One may notice that this is different from the standard SLDF flamelet model, which only solves the fully burning branch, and from the FPV model, which solves all the branches, including the unstable ones. Instead of it, the FGM technique solves the fully burning state and solves a set of unsteady flamelets for only one critical strain rate until it reaches extinction. This is enough for adiabatic laminar flames which do not present local extinction phenomena or re-ignition effects.

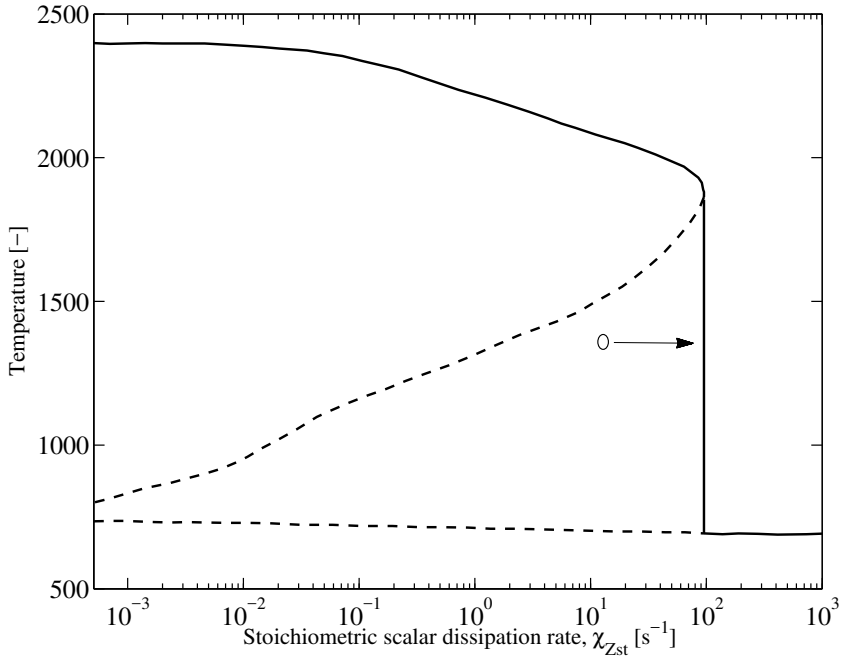

Figure 3.3 – Flamelets solutions accessed by the FGM technique. The fully burning branch is obtained by steady flamelets while unsteady flamelets are solved to obtain the solution up to fully extinction.

3.2 Manifold construction

The manifold is the look-up table which contains all the detailed thermochemical information obtained through the flamelets solutions. This manifold will be accessed during the multidimensional simulation for retrieving properties which are used in the transport equations, and later in a post-processing step to reconstruct the temperature and species mass fraction fields of the flame. For the case studied, a non-premixed laminar flame, a 2D manifold is sufficient to accurately capture the physics of the flame. The mixture fraction Z and a reactive progress variable $\mathcal{Y}$ are chosen as controlling variables for parametrization, the mixture fraction definition follows Bilger, 1988, defined by Equation 2.15. The reaction progress variable $\mathcal{Y}$ may acquire several different definitions. Such definition is crucial to the FGM accuracy and will be further discussed in next chapter.

The following steps comprise the 2D manifold construction from the flamelets solutions:

1. Reading of the chemical mechanism to retrieve the chemical species information;

2. Reading of flamelets solutions (comprised of steady-state and unsteady flamelets);
3. Definition of manifold discretization in Z and $\mathcal{Y}$ directions;
4. Calculation of mixture fraction through Bilger's definition (Equation 2.15);
5. Definition of $\mathcal{Y}$, generally defined as: $\mathcal{Y} = \sum_{k=1}^{N_s} \alpha_k Y_k$;
6. Interpolation of the flamelets solutions into Z space, followed by interpolation into $\mathcal{Y}$ space;
7. Calculation of all desirables variables to be in the manifold as function of Z and $\mathcal{Y}$;
8. Writing of manifold in specified format;

The result of the above process is a table with all thermochemical information of the flamelets stored in it. A graphical representation of the manifold for a generic variable ϕ in the $Z \times \mathcal{Y}$ space is shown in Figure 3.4.

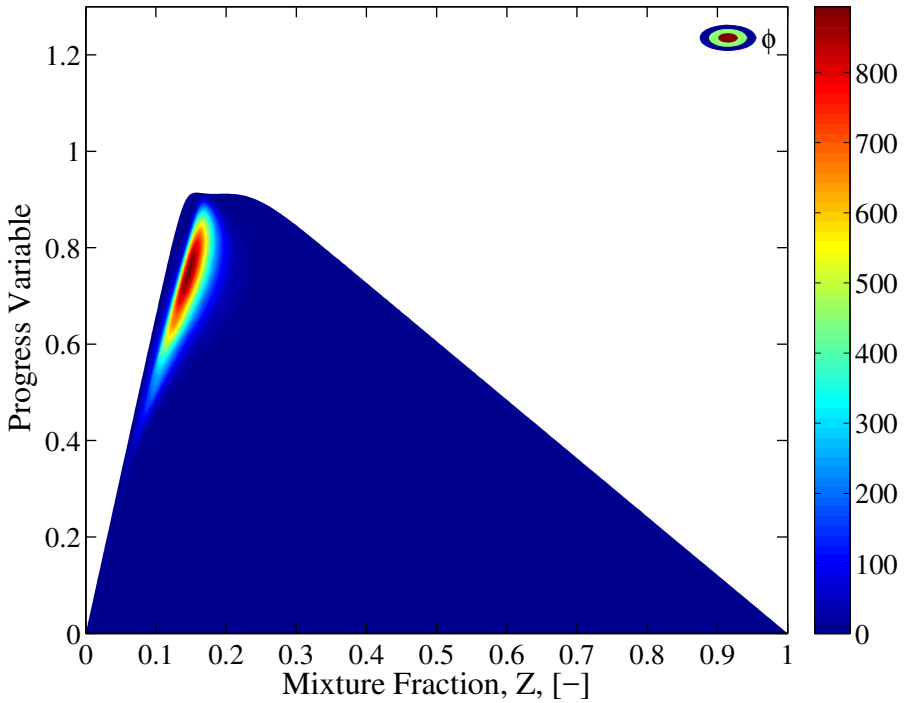

Figure 3.4 – Schematic representation of a generic flame variable ϕ as function of the controlling variables Z and $\mathcal{Y}$. The set of data for all flame variables is called a manifold.

From the point that the controlling variables are well defined, a manifold can be considered suitable if it allows a good search and interpolation procedure in the multidi-

mensional simulation of the flame. If a manifold has big gradients of the variables in the space of the controlling variables, it would need a more refined discretization of the manifold or a better interpolation algorithm in order to accurately retrieve its information. It is intuitive to think that most essential information of the flame is comprised around the stoichiometric mixture fraction value. Therefore, in the present work, all the manifolds have a bias in its discretization, in such way that the stoichiometric region has a more refined mesh.

3.3 Multidimensional simulations

After building the manifold from one-dimensional flamelets, a multidimensional flame can be simulated by retrieving information from such look-up table. This is performed by solving a transport equation for the controlling variables (Z and $\mathcal{Y}$ in this case) in addition to the total mass and momentum conservation equations. It is good to emphasize that the reduction in the computational time observed with the FGM technique is due to the replacement of the solution of all chemical reaction equations and the energy equation by the transport of the controlling variables. The studied cases in this work are adiabatic, however, in case of an non-adiabatic flame, the energy equation should be solved and the enthalpy is used as an additional controlling variable.

For simplicity it will be assumed the unity Lewis approximation $Le = 1$. Thus, the terms accounting for preferential diffusion in the controlling variable equations vanish. A detailed description of the flamelet equations including preferential diffusion is found elsewhere [Verhoeven et al., 2012, Donini et al., 2015 and Van Oijen et al., 2016].

Assuming the unity Lewis number, the transport equations for the controlling variables Z and $\mathcal{Y}$ are described as

$$\vec{\nabla} \cdot (\rho \vec{v} Z) = \vec{\nabla} \cdot \left(\frac{\lambda}{c_p} \vec{\nabla} Z \right), \tag{3.7}$$

$$\vec{\nabla} \cdot (\rho \vec{v} \mathcal{Y}) = \vec{\nabla} \cdot \left(\frac{\lambda}{c_p} \vec{\nabla} \mathcal{Y} \right) + \dot{\omega}_{\mathcal{Y}}, \tag{3.8}$$

where $\dot{\omega}_{\mathcal{Y}}$ is the source term for the progress variable $\mathcal{Y}$. It includes the source terms ($\dot{\omega}_{\mathcal{Y}} = \sum_i \alpha_i \dot{\omega}_i$) of the chemical species that constitute the progress variable. This term is tabulated in the manifold such that $\dot{\omega}_{\mathcal{Y}} = \dot{\omega}_{\mathcal{Y}}(\mathcal{Y}, Z)$ in adiabatic simulations.

The boundary conditions for the controlling variables transport equations in a co-flow flame are:

Fuel inlet	Oxidant inlet
$Z = 1$	$Z = 0$
$\mathcal{Y} = 0$	$\mathcal{Y} = 0$

and the remaining boundary conditions are defined as null derivatives.

Since the boundary conditions for the progress variable, which describes the combustion process, are null for all boundaries, it is necessary to perform an ignition process. This is done by imposing a value of progress variable correspondent to the maximum value of its source term, in the region of the multidimensional flame in which the mixture fraction assumes its stoichiometric value. During the multidimensional simulation, a field for Z and $\mathcal{Y}$ is obtained and for each cell of the domain the pair of values for the control variables are used by a search and interpolation algorithm. After solving Equations 3.7 and 3.8, the pair of values $(Z, \mathcal{Y})$ is used as input by the search and interpolation algorithm. The system comprises on finding the four closest combinations of Z and $\mathcal{Y}$ in the manifold and hence perform a bi-linear interpolation similar to the one used in Van Oijen, 2002.

The numerical methodology applied in the two-dimensional simulations will be presented in Chapter 6.

4 AUTOMATED CHOICE OF THE PROGRESS VARIABLE DEFINITION

Since the appearance of methods for reducing the chemical kinetic of complex mechanisms based on tabulation techniques, the definition of an accurate and feasible progress variable $\mathcal{Y}$ became one of the main concerns for achieving a good accuracy in such methods. Even though the literature contains several studies providing good results using tabulation techniques for combustion modelling, without a proper definition for $\mathcal{Y}$, such accuracy can not be reached. In general, $\mathcal{Y}$ is defined as a linear combination of major chemical species of the combustion products, and its coefficients are chosen arbitrarily or based on the user's experience. A linear combination of chemical species leads to simpler derivations of the transport equation of the progress variable, whose derivation start from the transport equation of the chemical species, mainly when preferential diffusion effects are included.

Studies have been performed in order to automate the $\mathcal{Y}$ definition by the use of Principal Component Analysis (PCA) [Najafi-Yazdi et al., 2012 and Chen et al., 2015], a method analogous to the eigenvalue analysis of ILDM, or by optimization methods [Ihme et al., 2012, Niu et al., 2013 and Prufert et al., 2015]. The result of both methods is a set of coefficients for each species which comprises the $\mathcal{Y}$ definition, which can now contain all the species of a detailed mechanism instead of only the major chemical species of combustion products, for instance.

This section presents the problem of finding a feasible progress variable as being equivalent to solving a constrained optimization problem, similar to Ihme et al., 2012, Niu et al., 2013 and Prufert et al., 2015. The characteristics of a feasible progress variable are addressed, the optimization problem formulation used in literature is presented and the difference of finding a suitable $\mathcal{Y}$ definition and a representative one is discussed.

4.1 Definition of a feasible progress variable

In tabulation techniques, the reaction progress variable $\mathcal{Y}$ describes the progress of combustion from the unburned to burned states of a flame. Ideally, it should mimic the chemical path of the detailed mechanism in which the tabulation is based on. However, it is only feasible if an adequate definition is applied to $\mathcal{Y}$, since the results obtained with

tabulation techniques are very sensitive to their definition. Different investigations were performed in the literature with different approaches, but they shared similar principles as the ones suggested by Ihme et al., 2012:

(a) The definition of $\mathcal{Y}$ should result in a transport equation that can be conveniently solved in a combustion simulation;

(b) The reactive scalars from which $\mathcal{Y}$ is constructed should all evolve on comparable time scales;

(c) All parameters that define the manifold should be independent of one another;

(d) The set of parameters from which the manifold is formed should uniquely characterize each point in the thermochemical state-space;

Most definitions of the progress variable reported in the literature fulfill principles (a) and (b). In such cases, the progress variable is formed by a linear combination of major species. Under the assumption of unity Lewis number, which yields equal species diffusivities, the transport equation for the progress variable can be conveniently solved in a combustion simulation, since the resultant transport equation is a simple summation of the transport equations of the chemical species which comprise its definition. Moreover, major product species are formed through reaction paths which generally evolve on similar time scales [Ihme et al., 2012]. This is the reason why only major species were taken into account on the optimization problem of Ihme et al., 2012, in which different linear combinations of CO_2, H_2O, CO and H_2 were tested.

4.2 Optimization problem formulation

In order to find a feasible progress variable through an optimization problem, different approaches can be used in terms of problem formulation. The objective function to be minimized is arbitrary and some studies in the literature have presented good results. One possible approach is based on the assumption of principle (d), considering the monotonicity of the progress variable as the objective function to be minimized [Ihme et al., 2012]. Another possible approach is to include the minimization of the chemical species gradients as well as the monotonicity requirement in the objective function definition [Niu et al., 2013 and Prufert et al., 2015].

4.2.1 Monotonicity of progress variable

Ihme et al., 2012 solved the problem of finding a feasible progress variable definition by imposing a cost function which minimizes the non-monotonicity of it. The requirement of the monotonicity of the progress variable can be expressed by the following expression for diffusion flames:

$$\left.\frac{d\mathcal{Y}}{da}\right|_{Z} > 0. \tag{4.1}$$

The expression above states that, for each value of mixture fraction Z, the difference between the values of the progress variable among different flamelets must continuously increase or decrease. The term a is the strain rate and is the parameter which identifies each flamelet. To illustrate such concept, the figure below shows different flamelets interpolated in the $Z \times \mathcal{Y}$ space, where an overlapping of the curves means non-monotonicity of the progress variable. The monotonicity of $\mathcal{Y}$ in respect of the strain rate guarantees the requirement (d), i.e., that the controlling variables (Z and $\mathcal{Y}$) uniquely map each point in the thermochemical state-space.

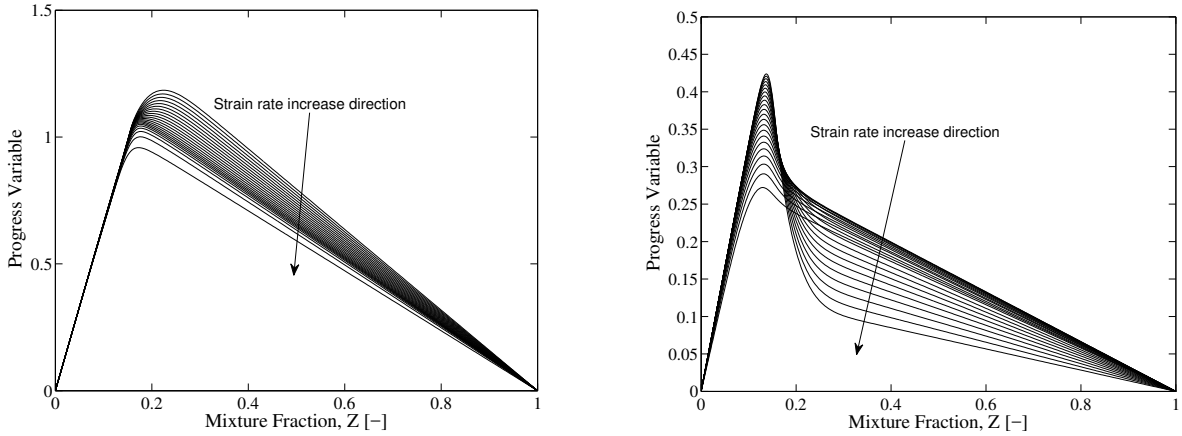

(a) Monotonic progress variable definition.

(b) Non-monotonic progress variable definition.

Figure 4.1 – Flamelet profiles in the $Z \times \mathcal{Y}$ space showing different monotonic behaviors using different progress variable definitions. Illustrative example for a generic counterflow diffusion flame.

In terms of an optimization problem, the objective function to be minimized can be expressed by

$$\begin{aligned} &\underset{\alpha_k \in \mathbb{R}^{\mathcal{S}}}{\text{minimize}} \quad \sum_{a=ext.}^{a=eq.} \sum_{Z=0}^{Z=1} \max\left[\mathcal{Y}\left(a;\alpha_k\right) - \mathcal{Y}\left(a+\delta;\alpha_k\right), 0\right] \\ &\text{subject to} \quad k \in \mathcal{S}. \end{aligned} \tag{4.2}$$

in which α is the set of coefficients which comprises the $\mathcal{Y}$ definition, k is the species index and $\mathcal{S}$ is the set of species which comprises the $\mathcal{Y}$ definition. When a non-monotonic set of α is found, the objective function will find a value greater than zero and will count it. The summation of the values greater than zero are the parts of the manifold which are non-monotonic. A perfectly monotonic manifold would imply in a null resultant objective function.

Figure 4.2 shows a schematic representation of Equation 4.2 usage. The figure on the left results in a negative value from the difference among consecutive progress variable values, resulting on the choice of the null value when choosing the maximum value. The opposite occurs in the figure on the right, in which the same difference calculated results in a positive value, which represents a non-monotonic behavior.

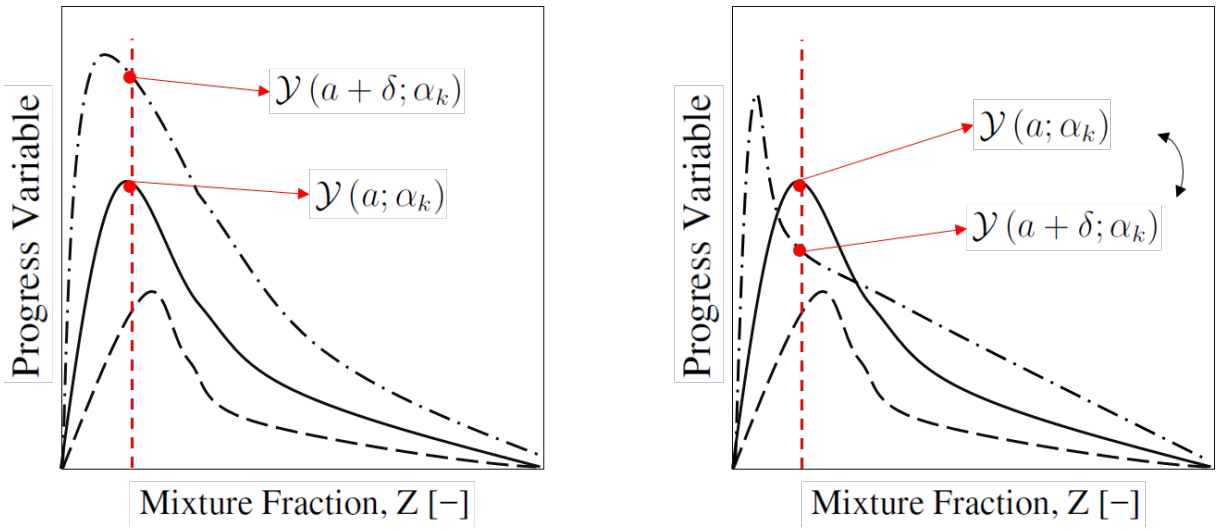

Figure 4.2 – Schematic representation of Equation 4.2 usage.

4.2.2 Minimization of chemical species gradient

As it will be presented in Tables 5.1 and 5.2 in next section, there are various possibilities of perfectly monotonic progress variable definitions. The optimization formulation of Equation 4.2 finds the most monotonic definition as possible, whose best possible value of the objective function is zero. This section treats about a different formulation from

the Equation 4.2, which considers the gradient of the chemical species as a parameter to be minimized as well. Such formulation is very similar to that used by Prufert et al., 2015. The idea is that a progress variable definition which is monotonic and also provides small gradients of the chemical species in the $Z \times \mathcal{Y}$ space is a good progress variable.

The new optimization problem formulation can now be expressed by

$$\begin{aligned} \underset{\alpha_k \in \mathbb{R}^{\mathcal{S}}}{\text{minimize}} \quad & \sum_{k=1}^{N_s} \sum_{Z=0}^{Z=1} \max_{j=1,\ldots,N_f} \left[\frac{dY_k}{d\mathcal{Y}} \right] + \sum_{a=ext.}^{a=eq.} \sum_{Z=0}^{Z=1} \mu \left(\max \left[\mathcal{Y}\left(a;\alpha_k\right) - \mathcal{Y}\left(a+\delta;\alpha_k\right), 0 \right] \right) \\ \text{subject to} \quad & k \in \mathcal{S}, \end{aligned} \tag{4.3}$$

where N_s is the number of species of the detailed mechanism, N_Z is the number of interpolated values of mixture fraction Z, N_f is the number of flamelets evaluated and Y_k is the mass fraction of species k. The gradients are evaluated by finite difference between consecutive flamelets in terms of strain rate a. The maximum gradient for each value of mixture fraction Z is evaluated and summed up for all values of mixture fraction evaluated. The objective function is hence the summation of this operation for all species of the detailed mechanism plus a penalty term accounting for non-monotonic definition. The μ is the penalty factor term and can be chosen as a very big value, enforcing only definitions which are perfectly monotonic. This value should be relaxed in cases where there is no monotonic definition possible in order to find the most monotonic definition as possible (this is the case for C_2H_4 flames, as will be shown).

4.3 Representativeness of the progress variable definition

The most recent methods which apply optimization algorithms to find a feasible progress variable definition relies on the assumptions that such feasible definition requires monotonicity and small gradients [Ihme et al., 2012, Niu et al., 2013 and Prufert et al., 2015]. Such assumptions are logic, since non-monotonicity yields bad results for one-dimensional and multidimensional flame solutions, and high gradients of flame variables relative to the progress variable in the look-up table yield errors in the search and interpolation algorithm. However, having a perfectly monotonic progress variable definition, and a look-up table with small gradients of the flame variables does not necessarily means that a representative solution of the flame exists. They only guarantee a good implementation

of the look-up table technique.

Both works of Ihme et al., 2012, Niu et al., 2013 and Prufert et al., 2015 present their results in terms of their objective functions, instead of solutions of the flame. They proved that their implementation reduced the respective objective function proposed, however, there is no guarantee that the definitions found with their algorithms yield representative solutions of the flame in one-dimensional or multidimensional space. In the present work, several perfectly monotonic definitions were found with similar optimization formulations used in the literature, however, not all of them provided good results.

A different approach that apparently results in a representative progress variable definition is the approach of Najafi-Yazdi et al., 2012, whose method is based on a Principal Component Analysis (PCA) of species mass fractions in the composition space. It is analogous to an eigenvalue analysis of the ILDM method and provides a rigorous mathematical formulation for flamelet-based tabulation methods. This is not the case of methods such as FPI and FGM, since the definition of the progress variable has been chosen arbitrarily resulting in a weak mathematical foundation. The PCA applied for chemistry tabulation results in the minimum number of linearly independent progress variables for a user-prescribed desirable accuracy, with their respective coefficients for each specie. However, Najafi-Yazdi et al., 2012 did not solved a CFD simulation with the optimized progress variable, such as Ihme et al., 2012, Niu et al., 2013 and Prufert et al., 2015. The only work which carried about using the optimized progress variable in a CFD solver was Chen et al., 2015, which similarly to Najafi-Yazdi et al., 2012 used PCA to find a progress variable for flamelet-based methods.

In the next chapters, 1D and 2D CFD simulations of different flames will be presented in order to evaluate the representativeness of the progress variables found with the optimization algorithm implemented. It will be shown that some definitions, even though perfectly monotonic, presented bad results. However, most of definitions that the algorithm suggested agree well with detailed mechanism results. This shows the potential of such methods since it can improve the efficiency of the progress variable definition choice for users of chemistry tabulation techniques.

4.4 Coupling of optimization algorithm in the FGM technique

This section aims to briefly explain the coupling between the optimization algorithm and the FGM technique. When using any of the objective functions presented in the previous sections, defined by Equations 4.2 and 4.3, not all the steps in the creation of the manifold (presented in section 3.2) is necessary. There is no need to calculate and interpolate variables from the flamelet solutions in terms of Z and $\mathcal{Y}$ if such variables are not used in the objective functions calculation (temperature and properties, for instance). This implies in a big reduction of the computational time of the optimization algorithm, since the calculation of specific heats is very costly during the look-up table construction. In the case of the monotonicity requirement being the objective function (Eq. 4.2), only the interpolation of the controlling variables need to be performed. In the case of the minimization of the gradients of the chemical species in relation to the progress variable being the objective function (Eq. 4.3), the interpolation of the chemical species is necessary. Figure 4.3 shows a schematic diagram of the manifold construction in the FGM technique, coupled to the optimization algorithm.

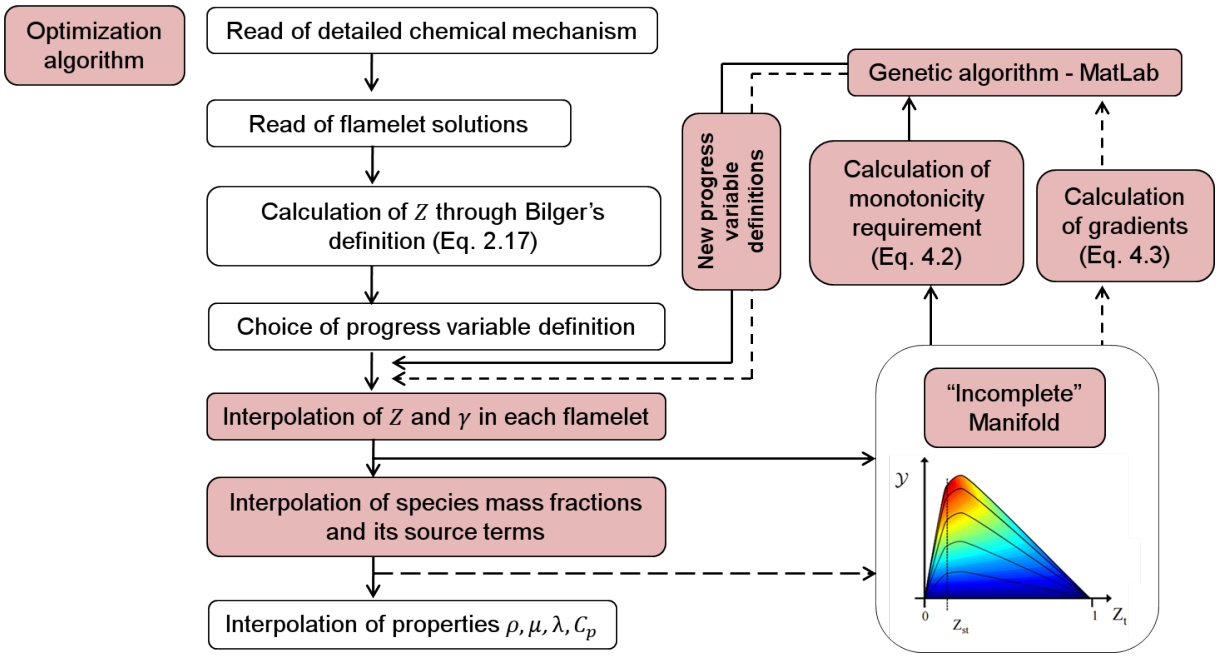

Figure 4.3 – Schematic representation of the steps for constructing the manifold in the FGM technique, coupled to the optimization algorithm (steps in red).

4.5 Genetic algorithm parameters

This section aims to provide the parameters used in the genetic algorithm toolbox of MatLab. The literature does not provide any general correlation for defining the input parameters when solving an optimization problem via genetic algorithm. It is understood that such parameters are very dependent on the particular problem of interest and might be defined based on experience. Parameters like number of generations, population size, upper and lower boundaries and stopping threshold considerably influence the computational time of the optimization algorithm. The population size determines how many different combinations will be generated by the algorithm at each generation. The number of generations determines how many adaptations will be made based on the crossover and mutation functions. The upper and lower boundaries determine the range of possible solutions for the variable parameters of the optimization problem. In the present work, such range was also restricted to integer values, and later scaled to be between -1 and 1. Finally, the stopping threshold defines when the algorithm should stop, which is when the population does not produce offspring which are significantly different from the previous generation.

In the present work, different parameters were used for the methane and ethylene flames. For the methane flames, the parameters which provided the results presented in the next sections within a reasonable computational time are the following:

- population size: 30
- number of generations: 100
- upper and lower boundaries: [-20,20]
- stopping threshold: 0.0001

For the ethylene flames, the use of the same range of the methane ones caused recurrent convergence of the optimization algorithm to a null set of coefficients, since null coefficients leads to a null objective function, which mathematically means monotonicity but in practical terms means in a non-sense progress variable definition. Therefore, the set of parameters which lead to reasonable computational times are the following:

- population size: 35

- number of generations: 150
- upper and lower boundaries: [0,20]
- stopping threshold: 0.001

5 ONE-DIMENSIONAL EVALUATION OF OPTIMIZED PROGRESS VARIABLES

As mentioned in the previous chapter, the monotonicity requirement and smaller gradients in the look-up table are necessary, however, do not guarantee a representativeness of the flame solution in the physical space. Therefore, it is still important to analyze the flame solution instead of only looking at such requirements. In this section, one-dimensional flames are evaluated with the FGM technique and compared to the detailed mechanism whose look-up tables were built from. Major and minor species mass fraction profiles are analyzed and compared among different definitions. In the first analysis, pure methane was used as fuel and several definitions were found. Since Hoerlle et al., 2017 and Zimmer, 2016 presented a worsen in the results when using the standard definition of $\mathcal{Y}$ to simulate methane flames diluted with CO_2 and ethylene flames, respectively, such cases were chosen as additional tests. The evaluation of the monotonicity by Equation 4.2 was applied to the definitions used in Hoerlle et al., 2017 and Zimmer, 2016 to analyze their monotonicity.

The next sections present the results for each case tested, whose configuration is briefed below:

- 100% CH_4, flamelets simulated with DRM19 (Kazakov and Frenklach, 2005) mechanism;
- 60% CH_4 / 40% CO_2, flamelets simulated with DRM19 (Kazakov and Frenklach, 2005) mechanism;
- 100% C_2H_4, flamelets simulated with GRI-MEC 3.0 (Smith et al., 2000) mechanism;

All of them were simulated with the FGM technique, building the manifold with the respective detailed mechanisms. Steady-state one-dimensional flamelets were solved with strain rate values varying from a condition close to equilibrium up to close to extinction, and transient one-dimensional flamelets with the critical strain rate value describing the extinction of the flame. Those solutions follow the solid curve presented in Figure 3.3. The counterflow flamelets modelling is described in previous section 3.1.1.

5.1 100% CH_4 results

In most applications of the FGM technique for methane flames, the progress variable definition used is correspondent to definition A_1 in Table 5.1, which has been providing accurate results. Equation 4.2 was used to evaluate its monotonicity and it was found that it is perfectly monotonic, justifying such tendency of finding good results so far. The optimization algorithm found other definitions which presented perfectly monotonic behavior as well. None of them provided significant improvements compared to definition A_1, even because definition A_1 already presents excellent agreement to detailed mechanisms for methane. Most of them also presented good accuracy, except definitions A_7, A_{10} and A_{12}, which provided poor results for some species profiles. Table 5.1 below shows some definitions found by the optimization algorithm (except definition A_1) as being perfectly monotonic, fulfilling the objective function given by Equation 4.2.

Table 5.1 – Different progress variable definitions found by the optimization algorithm for 100% CH_4.

100%CH_4			
Definition label	$\mathcal{S}$	α	Monotonicity evaluation
A_1 (standard pure methane)	$[H_2O, CO_2, CO, H_2]$	$[1, 1, 0, 1]$	0
A_2	$[H_2O, CO_2, CO, H_2]$	$[0.95, 0.4, 0.4, 0.422]$	0
A_3	$[H_2O, CO_2, CO, H_2]$	$[0.2, 0.85, 0.5, 0.065]$	0
A_4	$[H_2O, CO_2, CO, H_2]$	$[0.3, 0.5, 0.45, 0.135]$	0
A_5	$[H_2O, CO_2, CO, H_2]$	$[1, 0.7, 0, 0.931]$	0
A_6	$[H_2O, CO_2, CO, H_2]$	$[1, 0.6, 0.5, 0.9]$	0
A_7	$[H_2O, CO_2, CO, H_2]$	$[0.2, 0.5, 0.4, 0.42]$	0
A_8	$[H_2O, CO_2, CO, H_2]$	$[0.35, 0.7, 0.45, 0.482]$	0
A_9	$[H_2O, CO_2, CO, H_2]$	$[0.2, 0.45, 0.4, 0.167]$	0
A_{10}	$[H_2O, CO_2, CO, H_2]$	$[0.2, 0.25, 0, 0.506]$	0
A_{11}	$[H_2O, CO_2, CO, H_2]$	$[0.95, 0.6, 0.45, 0.729]$	0
A_{12}	$[H_2O, CO_2, CO, H_2]$	$[0.7, -0.1, -0.1, 0.349]$	0
A_{13}	$[H_2O, CO_2, CO, H_2]$	$[0, 0.75, 0.55, 0.049]$	0

In the FGM technique, the first analysis that can be performed regarding the quality of the progress variable definition is the observation of the manifold data as function of the controlling variables. In the case of the present work, which used the mixture fraction Z and the progress variable $\mathcal{Y}$ as controlling variables, Figure 5.1 shows some data of the manifold plotted in the $Z \times \mathcal{Y}$ space. Such manifold corresponds to definition A_{11}, which was one of the resultant definitions of the optimization algorithm which provided accurate results, as will be shown later. Figure 5.1a shows some steady-state flamelets of various

strain rates graphed as function of the controlling variables. The fact that there is no overlapping between the flamelets means this definition provided a unique parametrization of the composition space of the flame (as also schematically shown in Figure 4.1a). In the other figures it is possible to understand how the progress variable mapped each of the variables in the $Z \times \mathcal{Y}$ space.

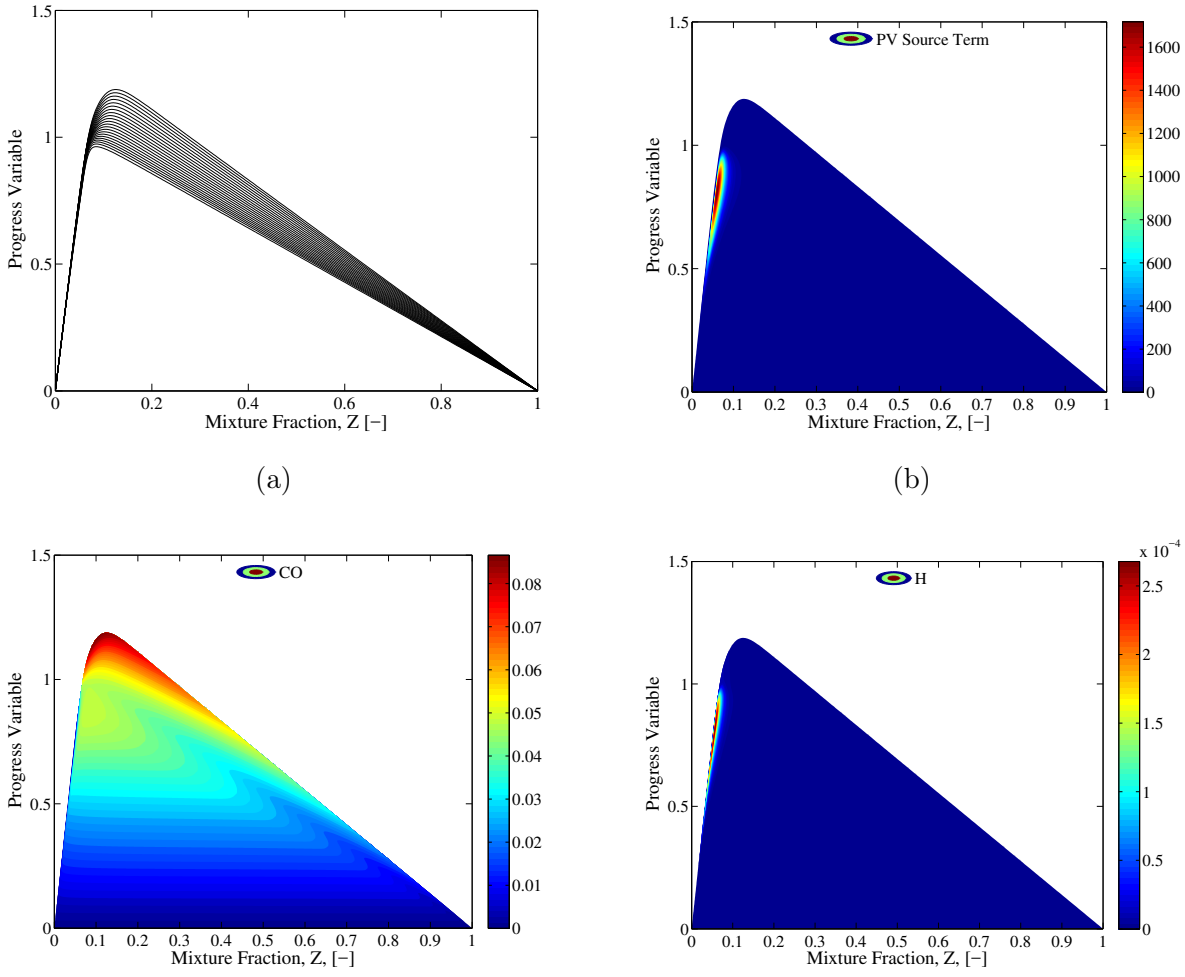

Figure 5.1 – Manifold data visualization for definition A_{11} of 100% CH_4 case, in the $Z \times \mathcal{Y}$ space: (a) flamelets for different strain rates (only steady-state flamelets are shown), (b) contour plot of source term of progress variable [kg/m^3.s], (c) contour plot of CO mass fraction, (d) contour plot of H mass fraction.

In Figure 5.1b, which shows the contour of the source term of the progress variable, one may notice its higher values are concentrated in the region close to the stoichiometric mixture fraction value (in this case, around $Z_{st} = 0.055$). The Figures 5.1c and 5.1d

presents the data for the CO and H mass fraction, showing very different behavior in the $Z \times \mathcal{Y}$ space. While the CO species presents significant values of mass fraction in all the mixture fraction range, from lean to rich mixtures, the H species is only significantly present in the stoichiometric region, which agrees to a radical species behavior.

In Figure 5.2, one-dimensional flamelet calculations were performed for 5 different strain rate values: 0.09 (close to equilibrium condition), 1.15, 11.5, 115 and 615 (close to extinction) $[s^{-1}]$. Three major species (CO_2, CO and H_2O) and three minor species (H, OH and O) are shown in the mixture fraction space. A comparison between the detailed solution and the FGM technique with progress variable defined by definition A_{11} of Table 5.1 is presented. It can be noticed that the FGM results agree very well with the detailed solution for conditions from equilibrium up to close to extinction. Even for minor species concentration, which have very small mass fraction values, the FGM technique was able to produce accurate results. Such good accuracy is also encountered with definition A_1 from Table 5.1, which is the standard definition used in the literature for pure methane flames.

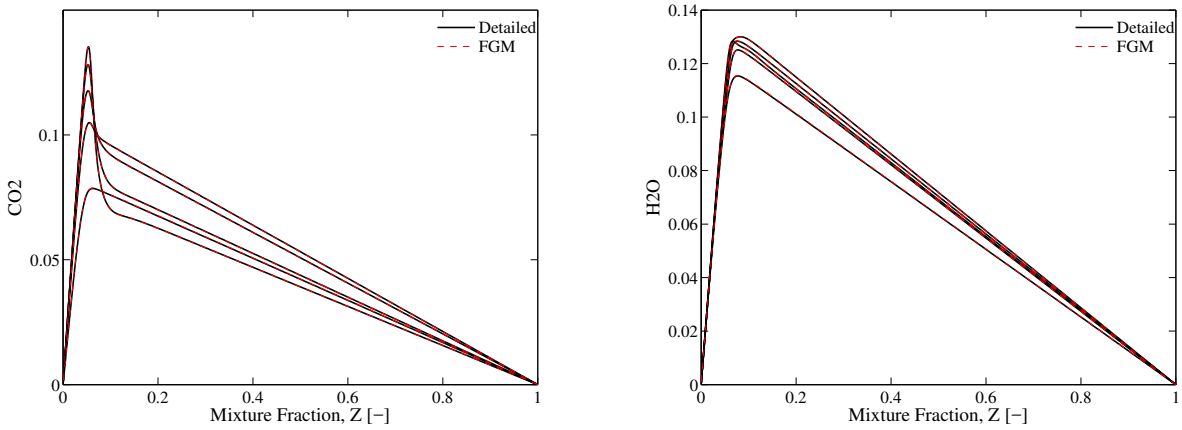

(a) CO_2 mass fraction profile.

(b) H_2O mass fraction profile

Figure 5.2 – Specie mass fraction profiles for the definition A_{11} of Table 5.1, computed for several strain rate values.

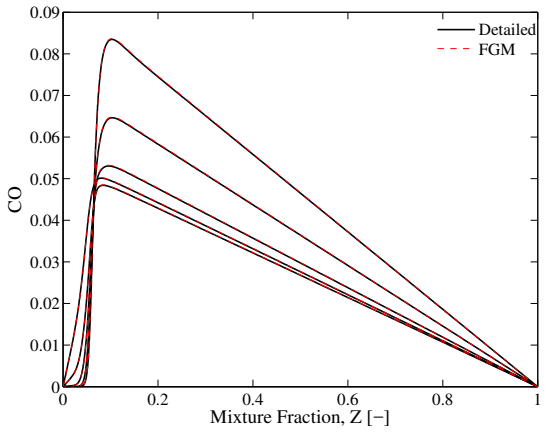

(c) CO mass fraction profile.

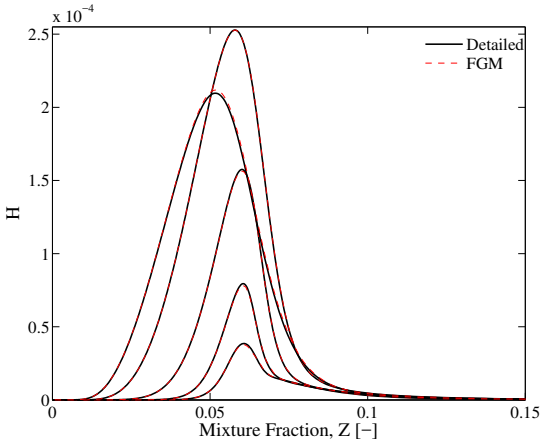

(d) H mass fraction profile

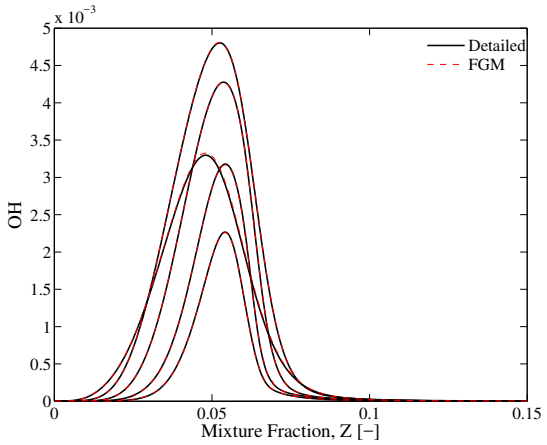

(e) OH mass fraction profile

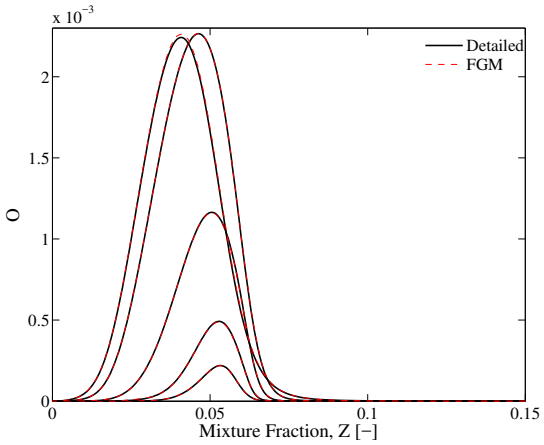

(f) O mass fraction profile

Figure 5.2 – Specie mass fraction profiles for the definition A_{11} of Table 5.1 (cont.), computed for several strain rate values.

However, even when a certain definition is fully monotonic according to Equation 4.2, that does not guarantee that the monotonicity requirement is enough for a good representativeness of the flame with such definition. This is shown through results with definition A_{12} from Table 5.1, which is a resultant definition from the optimization algorithm that is fully monotonic as well. However, the one-dimensional comparison with the detailed solution fails in the prediction of some species mass fractions for some strain rate conditions. The Figures 5.3 show some examples of curves which do not agree well with the detailed mechanism and even present non-physical behavior (with sparked curves instead of continuous ones).

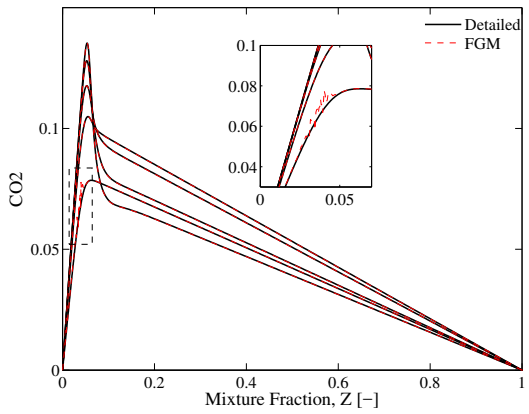

(a) CO_2 mass fraction profile.

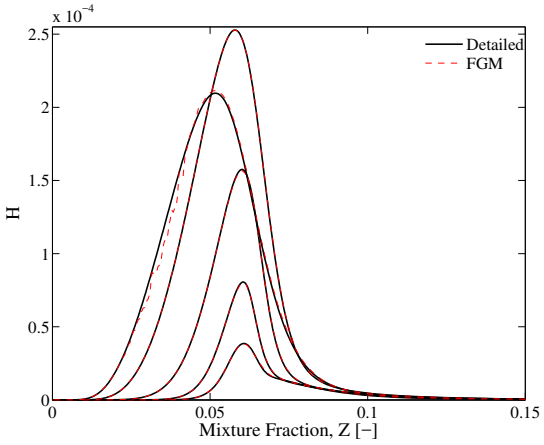

(b) H mass fraction profile

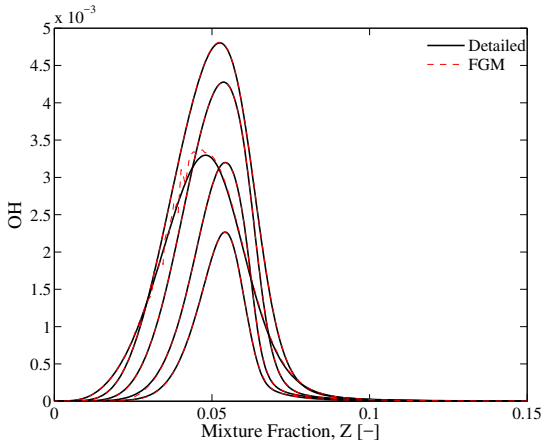

(c) OH mass fraction profile

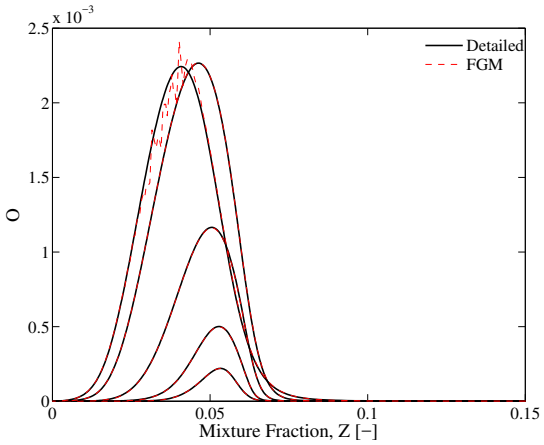

(d) O mass fraction profile

Figure 5.3 – Specie mass fraction profiles for definition A_{12}, computed for several strain rate values.

The above results reinforce the discussion of section 4.3. The optimization algorithm formulated according to Equation 4.2 found that definition A_{12} was perfectly monotonic. However, this requirement did not guarantee a good representation of the flame in the one-dimensional CFD simulation for all conditions. There are some conditions for which this definition is not representative. In a multidimensional simulation, there might be regions in which the solution falls into such condition, and hence the accuracy of the FGM technique will fail. This was not the case for the co-flow burner simulated in the present work, in which definition A_{12} was as accurate as the definition A_{11} (which is the one presented in next section). There might be other flame configurations in which the state-space accessed in the manifold falls into this problematic region, leading to poor

results. This happened for the next case shown (methane with 40% CO_2 dilution) in next section. Such results show the importance of analyzing the optimized progress variable definition in a CFD solver instead of only looking at the composition space data, as done in Ihme et al., 2012, Niu et al., 2013, Prufert et al., 2015 and Najafi-Yazdi et al., 2012.

5.2 60% CH_4 40% CO_2 results

In order to use the optimization technique for a more difficult situation, it was tested in cases of methane with 40% of CO_2 dilution. In Hoerlle et al., 2017, the definitions B_1, B_2 and B_3 for 40% CO_2 dilution in CH_4 were tested for a 2D diffusion laminar flame. In such work, the definition B_1, which works well for pure methane, provided slightly deviations for the CO species profile, as well as presented non-physical behavior near the flame front for this species. Such non-physical behavior was not captured in the simulations of the present work with definition B_1. Some differences between present results and from Hoerlle et al., 2017 might be explained by different ways of building the look-up table (different strain rates simulated in the flamelets, different discretization of the manifold, etc.). On the other hand, changing the species H_2 by the species CO in the $\mathcal{Y}$ definition lead to better predictions of some species mass fraction profiles. Such definition is the definition B_3 in Table 5.2, whose objective function value shows it is perfectly monotonic, while definitions B_1 and B_2 are not.

Table 5.2 – Different progress variable definitions found by the optimization algorithm for 60% CH_4 and 40% CO_2.

60%CH_4, 40%CO_2			
Definition label	$\mathcal{S}$	α	Monotonicity evaluation
B_1 (standard pure methane)	$[H_2O, CO_2, CO, H_2]$	$[1, 1, 0, 1]$	0.002591
B_2 (Hoerlle et al., 2017)	$[H_2O, CO_2, CO, H_2]$	$[1, 1, 1, 1]$	0.000224
B_3 (Hoerlle et al., 2017)	$[H_2O, CO_2, CO, H_2]$	$[1, 1, 1, 0]$	0
B_4	$[H_2O, CO_2, CO, H_2]$	$[0.3, 0, 0, 0.111]$	0
B_5	$[H_2O, CO_2, CO, H_2]$	$[0.5, 0.1, 0, 0.214]$	0
B_6	$[H_2O, CO_2, CO, H_2]$	$[0.4, 0, -0.15, 0.414]$	0
B_7	$[H_2O, CO_2, CO, H_2]$	$[0.25, 0.05, 0, 0.127]$	0
B_8	$[H_2O, CO_2, CO, H_2]$	$[0.35, 0.05, -0.15, 0.387]$	0
B_9	$[H_2O, CO_2, CO, H_2]$	$[0.3, 0.2, 0, 0.348]$	0
B_{10}	$[H_2O, CO_2, CO, H_2]$	$[0.9, 0, 0, 0.258]$	0
B_{11}	$[H_2O, CO_2, CO, H_2]$	$[0.4, 0, -0.1, 0.394]$	0
B_{12}	$[H_2O, CO_2, CO, H_2]$	$[0.8, 0, -0.05, 0.833]$	0
B_{13}	$[H_2O, CO_2, CO, H_2]$	$[0.6, 0, 0, 0.068]$	0

The next results show one-dimensional flamelet calculations performed for 5 differ-

ent strain rate values: 0.09 (close to equilibrium condition), 0.95, 11.5, 115 and 395 (close to extinction) $[s^{-1}]$. Figures 5.4 show the improvement in the mass fraction profiles prediction by using CO instead of H_2 in the progress variable definition. Such improvement can be seen mainly for CO mass fraction profile. One may observe that for definition B_1, which is not perfectly monotonic, most of the curves agree well with the detailed mechanism, apart from species CO and H_2 in flamelets with strain rate correspondent to a condition close to equilibrium (small values of strain rate). Even though it was only inaccurate in a very specific condition, that was enough to lead to a bad representation of the flame in a two-dimensional simulation, as reported by Hoerlle et al., 2017. Since the two-dimensional flames simulated in such work as well as in the present work are adiabatic laminar flames, in which there is no local extinction phenomena or any physical behavior which departures the flame from the equilibrium condition, it is important that the progress variable definition is accurate in regions with small strain rates. A turbulent non-adiabatic flame, for instance, might need a good accuracy in a wider range of strain rates.

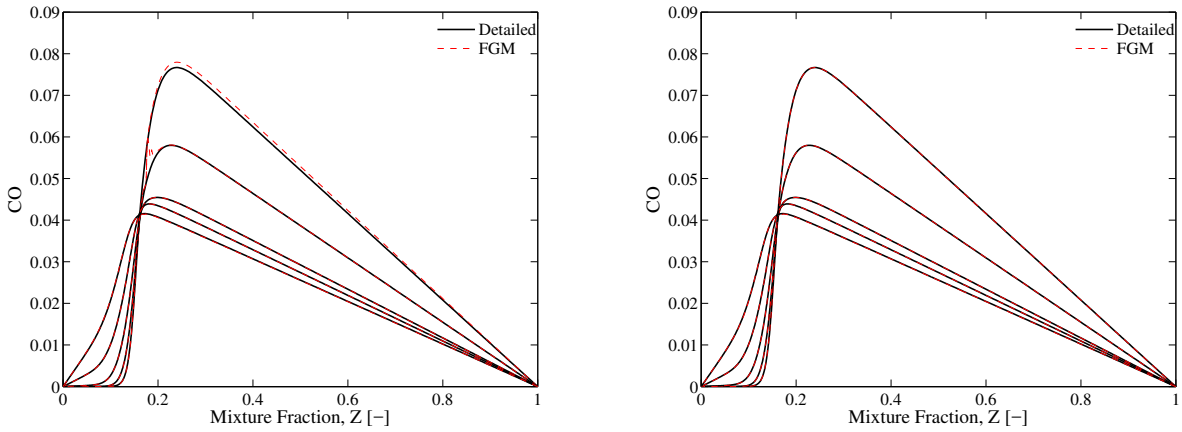

(a) CO mass fraction profile for definition B_1.

(b) CO mass fraction profile for definition B_3.

Figure 5.4 – Comparison of species mass fraction profiles between non-monotonic (B_1) and a monotonic (B_3) definition (Hoerlle et al., 2017), computed for several strain rate values.

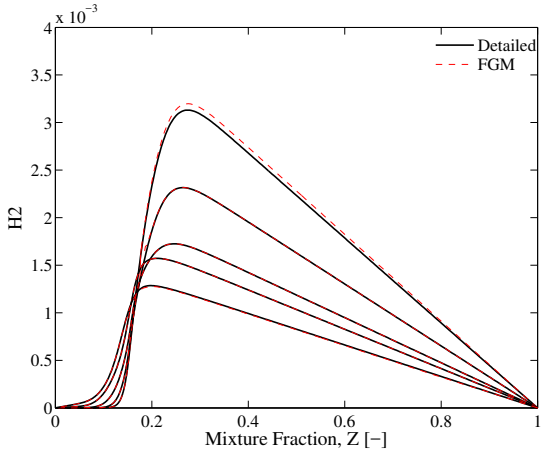

(c) H_2 mass fraction profile for definition B_1.

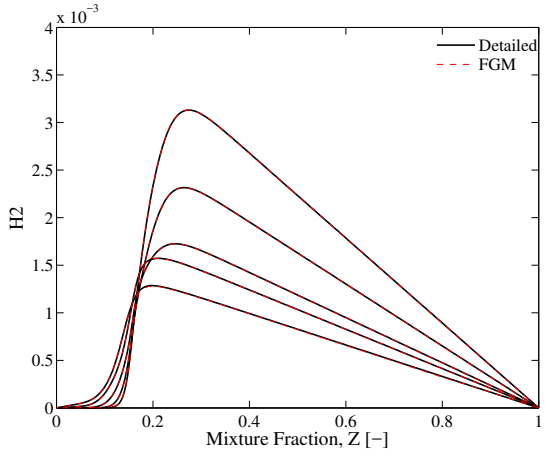

(d) H_2 mass fraction profile for definition B_3.

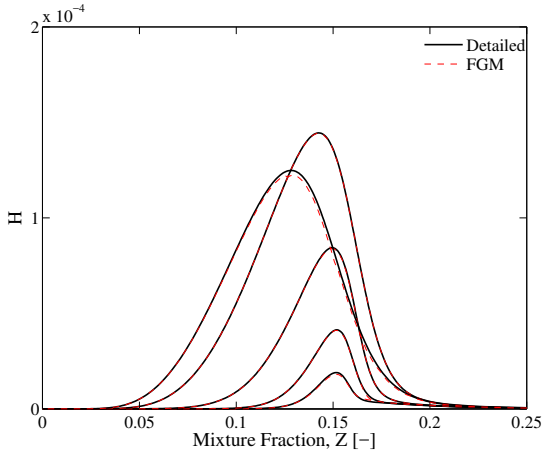

(e) H mass fraction profile for definition B_1.

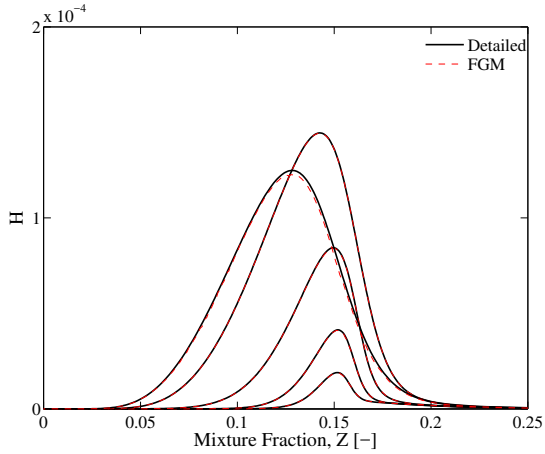

(f) H mass fraction profile for definition B_3.

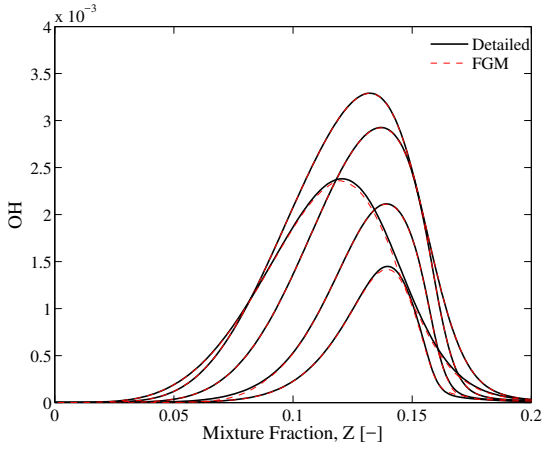

(g) OH mass fraction profile for definition B_1.

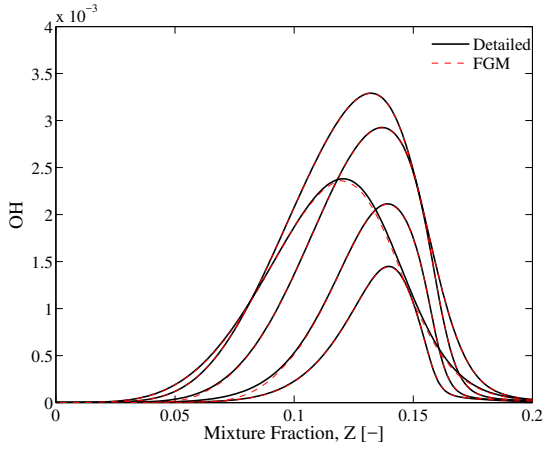

(h) OH mass fraction profile for definition B_3.

Figure 5.4 – Comparison of species mass fraction profiles between non-monotonic (B_1) and a monotonic (B_3) definition (Hoerlle et al., 2017), computed for several strain rate values (cont.).

Hoerlle et al., 2017 stated that using definition B_2 lead to difficulties in the convergence for the 2D case. Such behavior can be explained by its non-monotonicity, as it can be seen in Table 5.2. Most species profiles presented bad agreement with the detailed case when comparing to the other definitions. Figures 5.5 show some results for definition B_2.

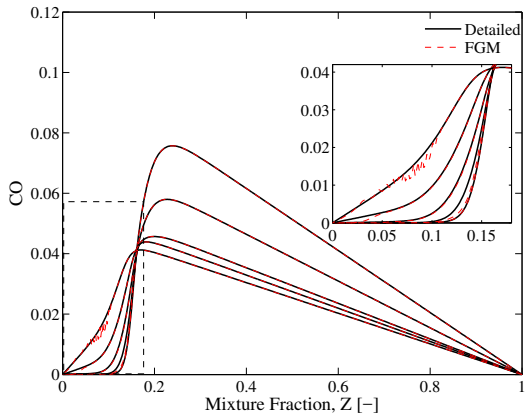

(a) CO mass fraction profile.

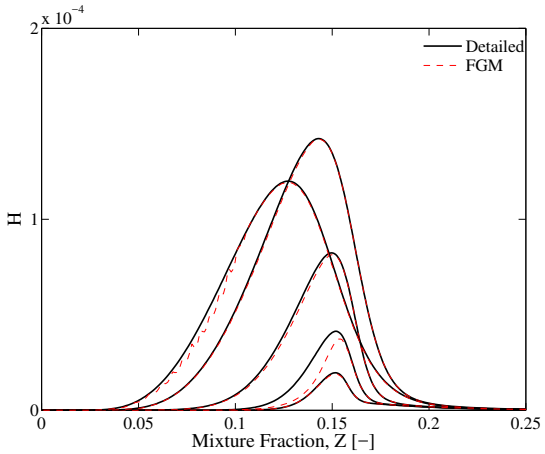

(b) H mass fraction profile

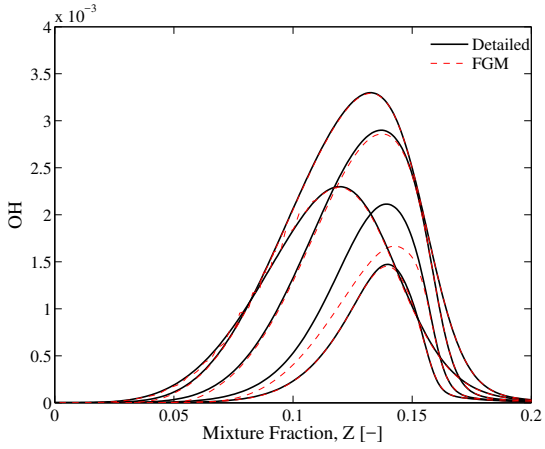

(c) OH mass fraction profile

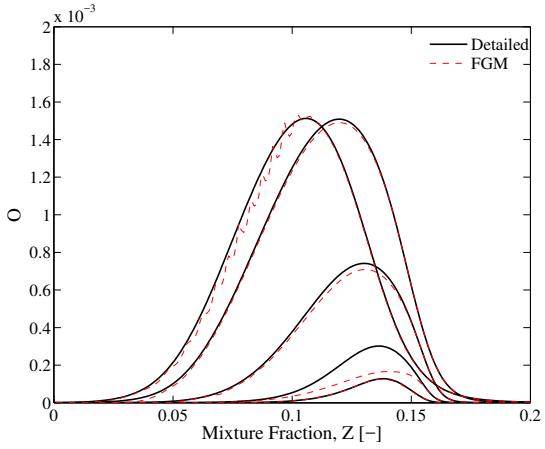

(d) O mass fraction profile

Figure 5.5 – Specie mass fraction profiles for definition B_2, computed for several strain rate values.

Among the definitions presented in Table 5.2 which were found by the optimization algorithm, only definition B_{12} provided bad results for species H, OH and O even though it resulted in a perfectly monotonic progress variable definition, while all the others presented good results for all species evaluated. Figures 5.6 show results for definition B_8, found by the optimization algorithm to be perfectly monotonic and also presented good results for

all the profiles evaluated.

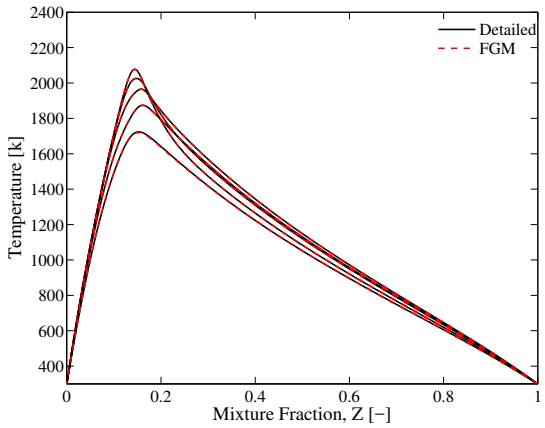

(a) Temperature profile.

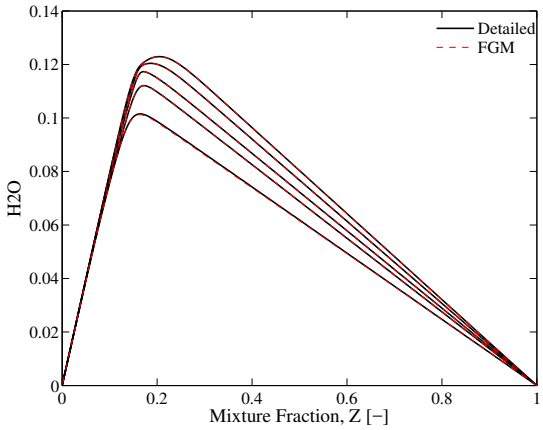

(b) H_2O mass fraction profile

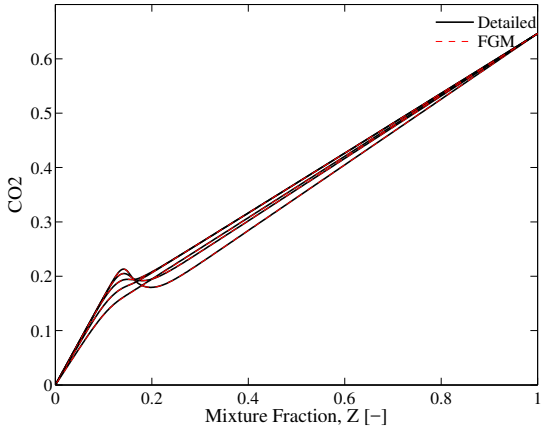

(c) CO_2 mass fraction profile

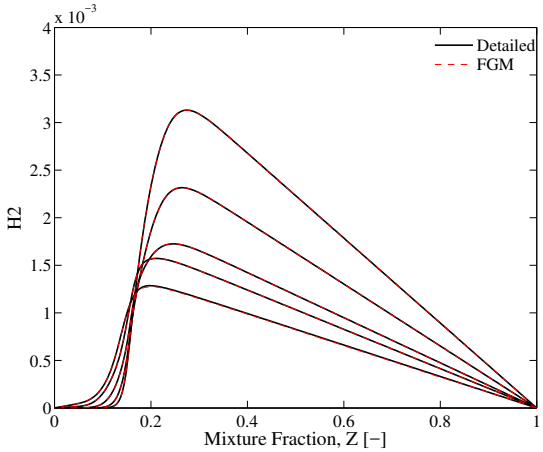

(d) H_2 mass fraction profile

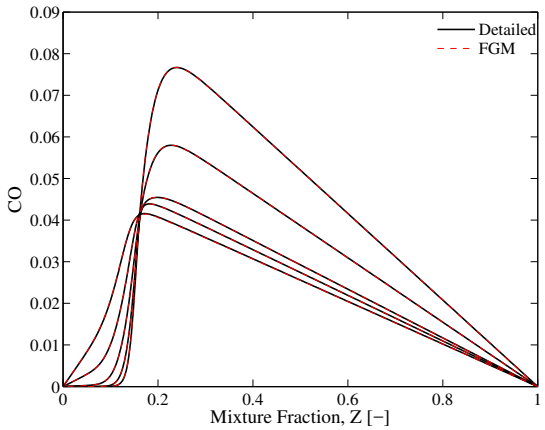

(e) CO mass fraction profile.

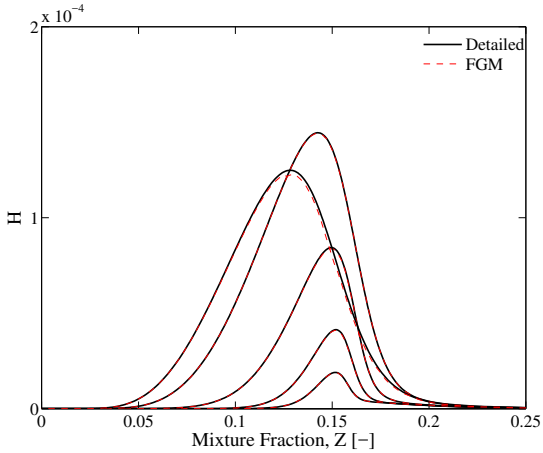

(f) H mass fraction profile

Figure 5.6 – One dimensional profiles for definition B_8, computed for several strain rate values.

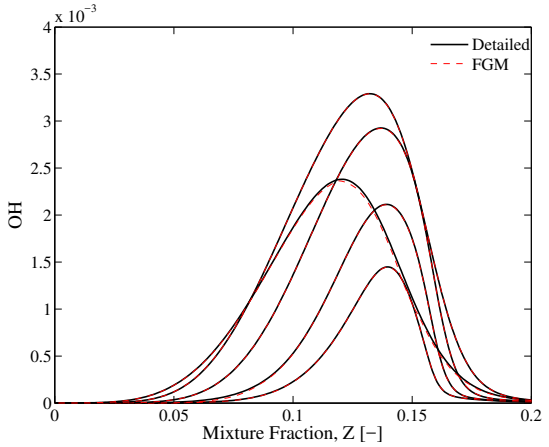

(g) OH mass fraction profile

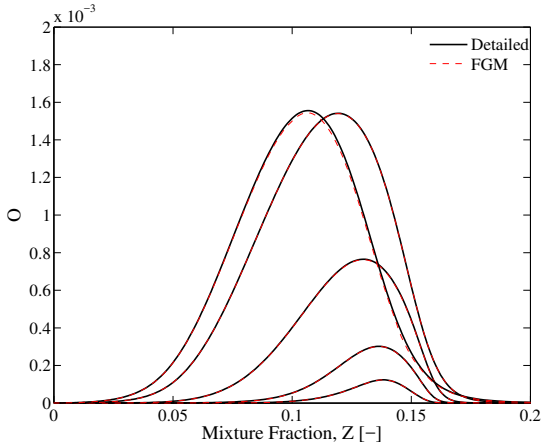

(h) O mass fraction profile

Figure 5.6 – One dimensional profiles for definition B_8, computed for several strain rate values (cont.).

Similarly to the previous section results, among the perfectly monotonic progress variables found by the optimization algorithm, not all of them presented good accuracy in the one-dimensional simulations for all variables. With definition B_{12} from Table 5.2, it was not possible to achieve convergence in the flamelets simulations with the FGM technique for the strain rate value of 0.95 $[s^{-1}]$ (one may notice that only 4 curves were presented in Figures 5.7 instead of 5, as it was being done for all cases). Also, not good accuracy was found for all species, as it can be observed in Figures 5.7. In previous section, definition A_{12} (from Table 5.1) presented bad results for the 1D problem for some specific conditions but good agreement in the two-dimensional case. This is probably because the region of inaccuracy was not accessed in the manifold by the multidimensional simulation. In the present case, the inaccuracy of definition B_{12} (from Table 5.2) lead to a non-convergence of the two-dimensional simulation. That means the conditions (strain rates values) for which definition B_{12} failed in its accuracy were accessed during the multidimensional simulation, leading to its non-convergence.

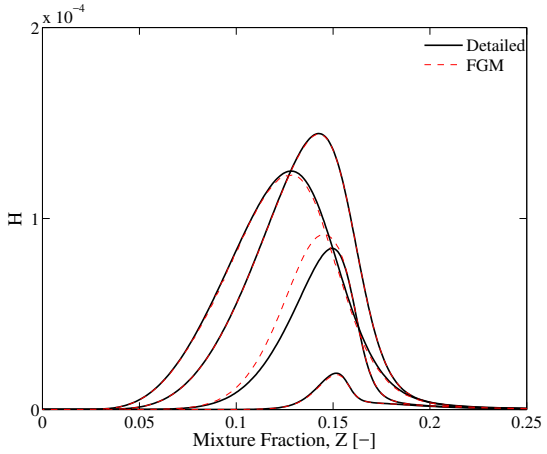

(a) H mass fraction profile

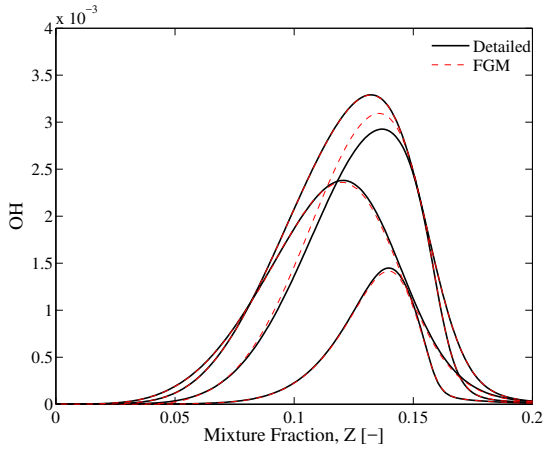

(b) OH mass fraction profile

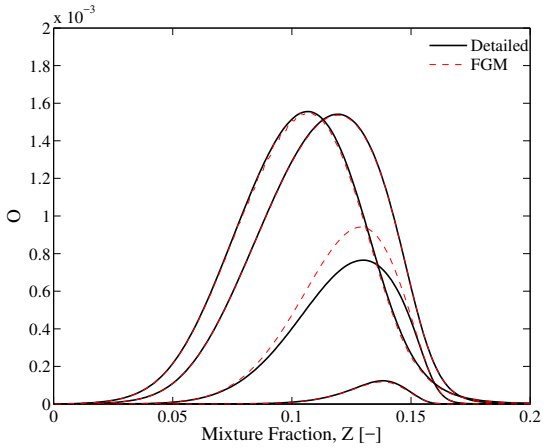

(c) O mass fraction profile

Figure 5.7 – One dimensional profiles for definition B_{12}, computed for several strain rate values.

5.3 100% C_2H_4 results

For ethylene flames under the assumption of unity Lewis number and only gas-phase, Zimmer, 2016 suggested that the definition C_1 from Table 5.3 was a good definition since it provided a monotonic result. Such definition lead to reasonable results in a 2D simulation, but presenting relevant differences for C_2H_2 species prediction. Different authors may use different discretization and number of flamelets to evaluate the monotonicity and that can lead to different values of Equation 4.2. In the present work, 800 values of mixture fraction were interpolated and flamelets with strain rate values from equilibrium condition up to extinction, varying its value 5% from one flamelet to another,

were used in the calculation of Equation 4.2. Such discretization lead to a non-monotonic value for definition C_1 as well.

The optimization algorithm found the definition C_2 as the most monotonic under the imposed constraints. When comparing the one-dimensional results to the definition C_1 (Zimmer, 2016), there is an improvement of the agreement of some species mass fraction profiles, mainly for specific flamelets. Such improvement might be explained by the higher value of non-monotonicity of definition C_1 (see Table 5.3). Figures 5.8 show different profiles comparing definitions C_1 and C_2. The strain rate values analyzed in the next figures were 0.11 (close to equilibrium), 1.2, 11.0, 111.0, 1080.0 and 2800 (close to extinction) $[s^{-1}]$.

Table 5.3 – Progress variable definitions for 100% C_2H_4.

100%C_2H_4			
Definition label	$\mathcal{S}$	α	Monotonicity evaluation
C_1 (Zimmer, 2016)	$[H_2O, CO_2, CO, H_2]$	$[1, 1, 0.9, 0]$	0.618097
C_2	$[H_2O, CO_2, CO, H_2]$	$[0.333, 1, 0.833, 0.167]$	0.000285

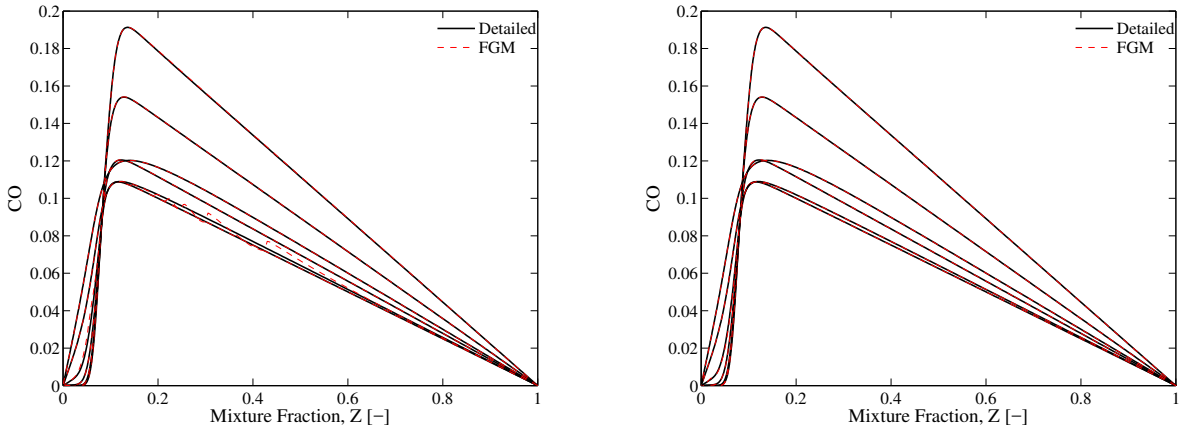

(a) CO mass fraction profile for definition C_1.

(b) CO mass fraction profile for definition C_2.

Figure 5.8 – Comparison of species mass fraction profiles between Zimmer, 2016 definition (C_1) and definition C_2, computed for several strain rate values.

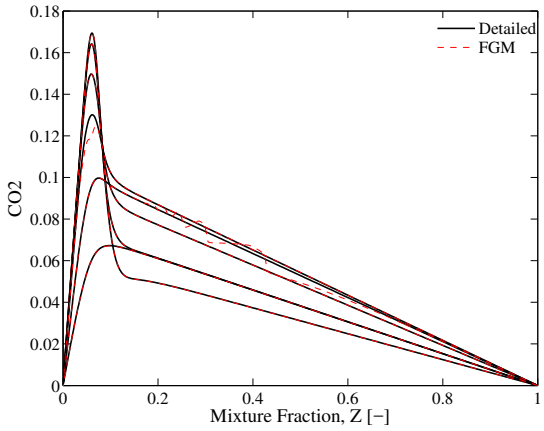

(c) CO_2 mass fraction profile for definition C_1.

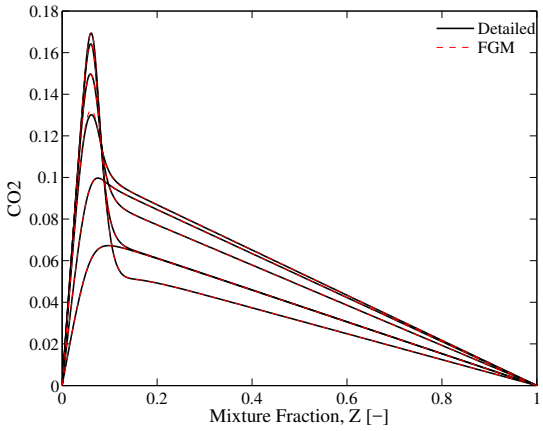

(d) CO_2 mass fraction profile for definition C_2.

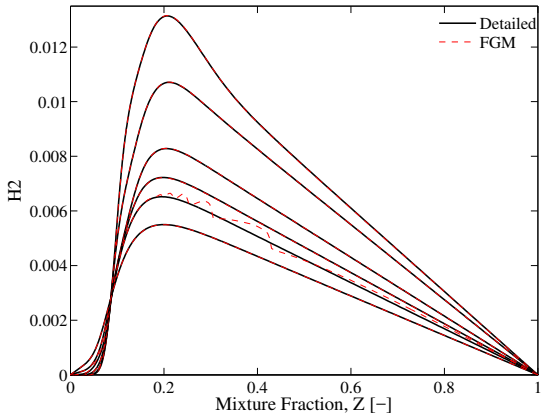

(e) H_2 mass fraction profile for definition C_1.

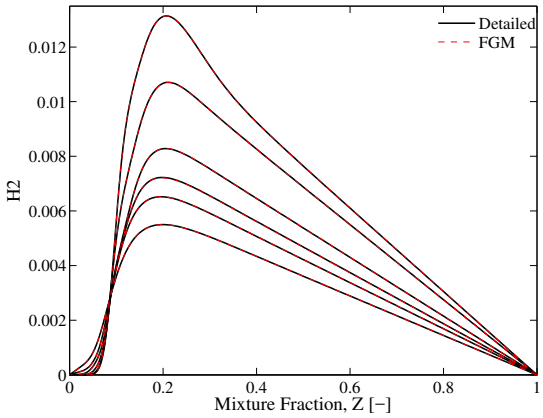

(f) H_2 mass fraction profile for definition C_2.

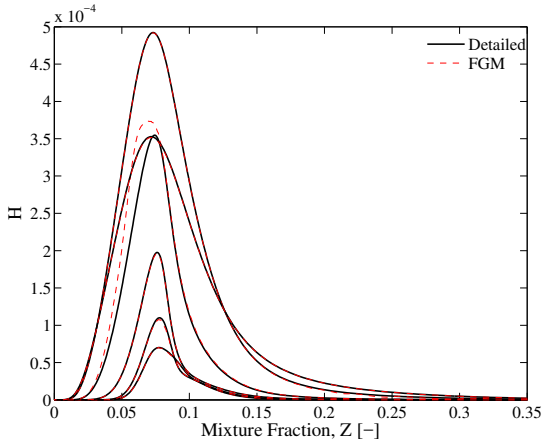

(g) H mass fraction profile for definition C_1.

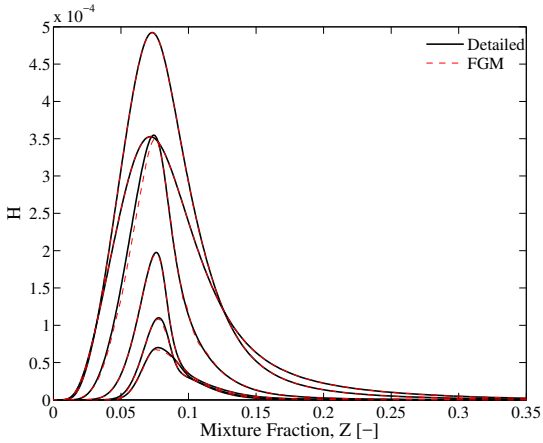

(h) H mass fraction profile for definition C_2.

Figure 5.8 – Comparison of species mass fraction profiles between Zimmer, 2016 definition (C_1) and definition C_2, computed for several strain rate values (cont.).

5.4 One-dimensional results remarks

In this chapter, one-dimensional flamelets were simulated for three different fuels in order to evaluate the functionality of the optimization algorithm implemented for different conditions. Pure methane, CO_2 dilution and ethylene flames were simulated with the FGM technique using definitions found by the optimization algorithm. It was found that the monotonicity requirement yield a tendency of finding good agreement when comparing it to detailed flamelets. A significant improvement in the agreement of some species mass fraction profiles were found mainly for the ethylene case, which was shown to be a difficult case for finding a monotonic progress variable (Zimmer, 2016). However, even though perfectly monotonic definitions could be found for the methane cases, some of the resultant definitions did not result in good agreement of the flame profiles for some specific conditions. Such bad results indicate that there is no guarantee of a good representativeness of the flame only by satisfying the monotonicity requirement. Also, finding a representative solution in one-dimensional flames using a certain definition does not mean that it will still be representative in a multidimensional flame.

In the next section, two-dimensional co-flow burners will be simulated with the FGM technique using some of the definitions presented in this section, and its evaluation will be addressed comparing it to detailed mechanisms.

6 TWO-DIMENSIONAL EVALUATION OF OPTIMIZED PROGRESS VARIABLES

In this section, an assessment of the two-dimensional representativeness of the FGM technique will be addressed by simulating a co-flow laminar adiabatic flame and comparing the FGM results to standard solution with direct integration of the detailed chemical kinetic mechanism. The same cases evaluated in the one-dimensional simulations are evaluated in this section. Some relevant contours and species mass fractions profiles in axial direction will be presented. Major species like CO_2 and H_2O, and minor species like CO, H_2, O, H and OH are analyzed. Radial profiles for different heights are presented in the Appendix A. The same progress variable definitions which presented good results in the one-dimensional simulations are now applied to the 2D problem.

6.1 Description of the problem

The computational domain is a coflow burner formed by two concentric tubes. Figure 6.1 shows the boundary conditions applied for each chemical kinetic approach. Different burners and values of boundary conditions were applied depending on the case studied. For all cases studied, the fuel is injected in the inner tube, assuming a parabolic fully developed profile, while external tube represents an annular section of uniform air injection. For the pure methane and CO_2 dilution cases, the inner tube has a 1.2 cm diameter and the external tube has a 8.0 cm diameter. Such burner is similar to the one simulated at Verhoeven et al., 2012, with the difference of including the fuel wall tube as a no-thickness wall. This is done in order to capture temperature gradients towards the inlet boundary, since it improves the FGM accuracy according to Zimmer, 2016. The velocity of the constant air stream is 23 cm/s and the maximum velocity of the parabolic profile for the fuel stream is also 23 cm/s.

For the pure ethylene case, the burner simulated is formed by a 1.11 cm diameter for the fuel tube and 10.16 cm diameter for the air tube. It was chosen the same burner used by Zimmer, 2016 in order to compare the FGM results with the ones from the present work. This is the Santoro et al., 1983 flame, recommended for soot studies due to the good amount of experimental data. The mean velocity of the fuel stream is 3.98 cm/s and 8.9 cm/s for the air stream. The fuel tube also extends beyond the exit plane of the

air tube in 4 mm for the same reasons of the methane cases.

For both cases, the axial origin ($z = 0$ cm) is at the exit plane of the fuel tube.

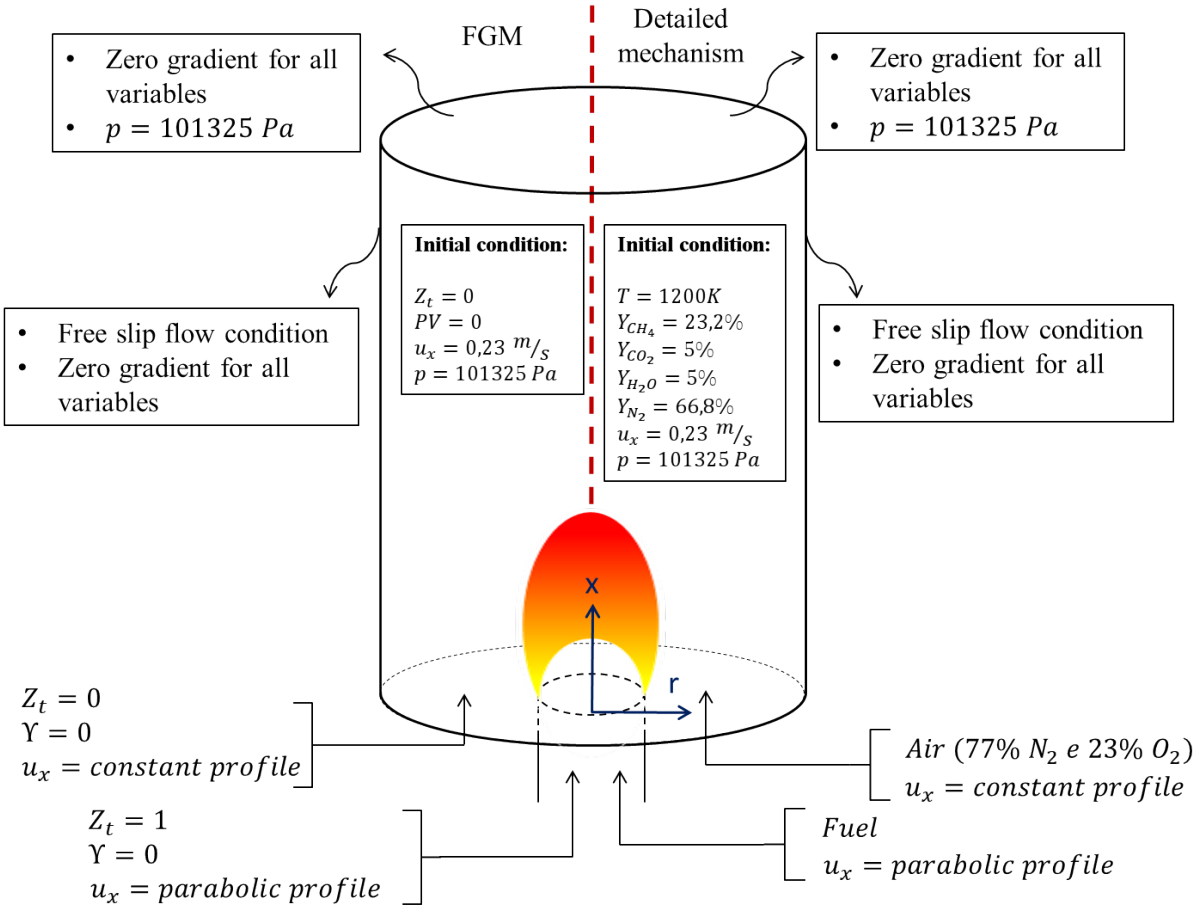

Figure 6.1 – Generic coflow burner scheme. Boundary conditions applied for both chemistry approaches: FGM and detailed kinetic mechanism.

6.2 Numerical method

The modelling of the 2D laminar coflow flame follows section 2.4 for detailed chemical kinetics and section 3 for the FGM technique. No heat losses by radiation are accounted for. Non-uniform mesh is used to save computational time and finer mesh is applied in the region of flame front, which comprises the higher gradients. An adaptive mesh refinement based on gradients of the flame was applied to choose the regions of refinement, and the resultant mesh is presented in Figure 6.2. The total number of volumes was 50.575 for the methane flames and 37.085 for the ethylene flames. All the simulations converged under a convergence criteria of 10^{-6}.

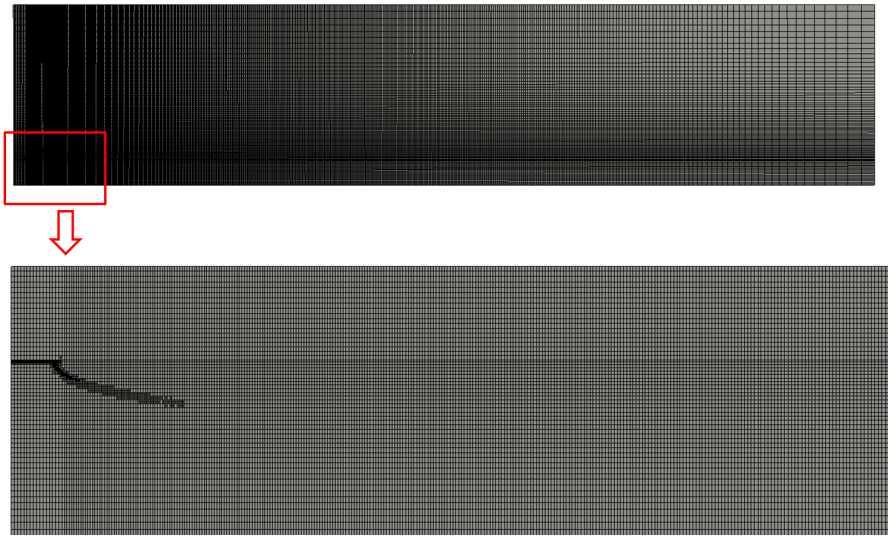

Figure 6.2 – Adaptive refinement in the flame front region.

The system of equations described by Equations 2.1 - 2.8 for axisymmetrical coordinate system was solved with the commercial software ANSYS Fluent®v16.1 for steady state conditions. It was used a segregated pressure-based solver with the SIMPLE algorithm to treat the pressure-velocity coupling. The advective terms were discretized by second order upwind while the diffusion terms were discretized by second order central difference scheme.

It was necessary to include User Defined Functions in ANSYS Fluent®code to perform the following tasks:

- inlet fuel velocity profile when applicable (for both FGM and direct integration solution);
- calculation of dynamic viscosity and thermal conductivity through Equations 2.12 and 2.13 for the direct integration solutions;
- retrieval from look-up table of properties (density and dynamic viscosity) for the FGM solutions;
- inclusion of transport equations for the controlling variables in the FGM solutions;
- retrieval of all flame variables from the look-up table for post-processing of the FGM solutions;

6.3 100% CH_4 bi-dimensional results

In order to verify the FGM results, the *skeleton*-mechanism DRM19 (Kazakov and Frenklach, 2005) was used for comparison. Two different definitions were used in the FGM technique, the standard definition used in the literature for pure methane flames (definition A_1 of Table 5.1), and definition A_{11} of Table 5.1, respectively given by

$$\begin{aligned} \mathcal{Y}_{A_1} &= Y_{H_2O} + Y_{CO_2} + Y_{H_2}, \\ \mathcal{Y}_{A_{11}} &= 0.95Y_{H_2O} + 0.60Y_{CO_2} + 0.45Y_{CO} + 0.729Y_{H_2}. \end{aligned} \tag{6.1}$$

It is important to state that both definitions presented fully monotonic behavior when calculated with Equation 4.2. Also, a CFD simulation was performed for the optimized definition A_{12} (from Table 5.1), since it failed to predict some species mass fractions in certain conditions, but a general good agreement was found for this definition and the results are omitted. Only results for definition A_{11}, which presented the best accuracy in the one-dimensional simulation, are shown.

Figures 6.3 show contour fields for some flame variables, like temperature, velocity magnitude and CO and OH species mass fractions comparing the FGM technique to direct chemistry integration (referred to as DCI) simulations. The temperature field visually present a very accurate agreement with the optimized definition A_{11} in the FGM technique. This is confirmed by Figures 6.4 and by Appendix A. The velocity magnitude field also shows a visual good agreement (Figure 6.3b). The CO mass fraction field (Figure 6.3d) is over-predicted by the FGM technique, and the OH field presents some little discrepancies in the region just above the flame front. Other species mass fraction behaviors are shown in the axial profiles of Figures 6.4.

In the axial profiles plotted in Figure 6.4, it is possible to compare two different definitions of progress variable used in the FGM technique along with the results of direct chemistry integration. It is possible to observe the over-prediction of CO and H_2 mass fractions in the axial profiles in Figures 6.4d and 6.4e. However, in a general way, good agreement was found with the optimized progress variable.

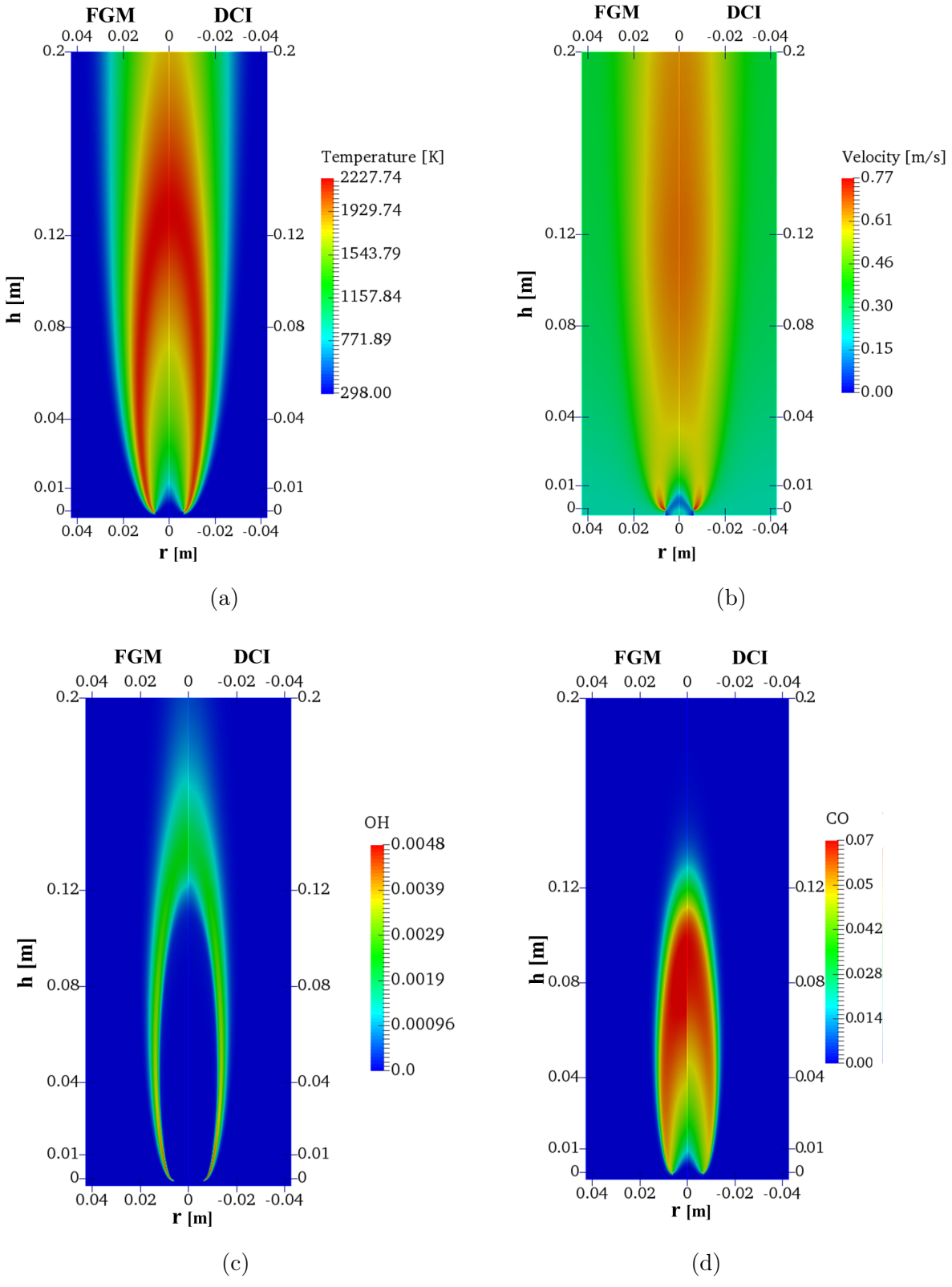

Figure 6.3 – Contour fields for 100% CH_4 with FGM (left), using definition A_{11}, and DCI (right): (a) temperature, (b) velocity magnitude, (c) OH mass fraction and (d) CO mass fraction.

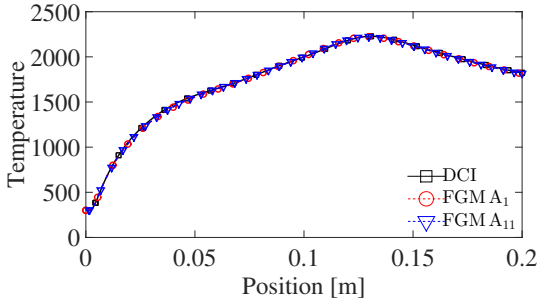

(a) Axial temperature profile.

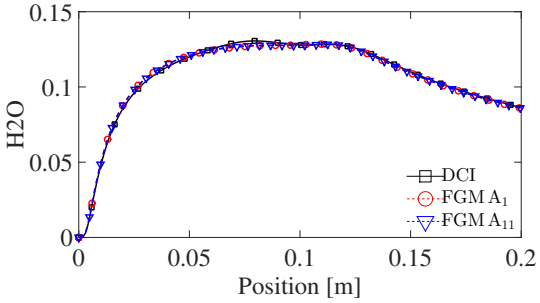

(b) Axial H_2O mass fraction profile.

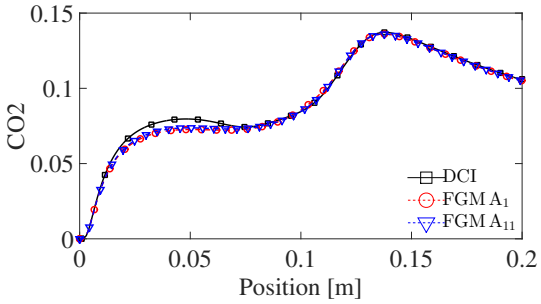

(c) Axial CO_2 mass fraction profile.

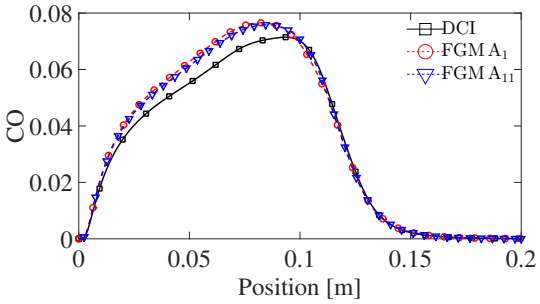

(d) Axial CO mass fraction profile.

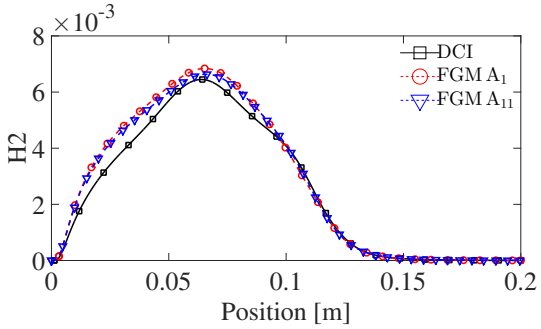

(e) Axial H_2 mass fraction profile.

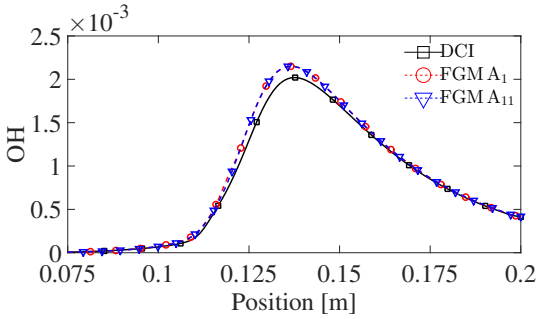

(f) Axial OH mass fraction profile.

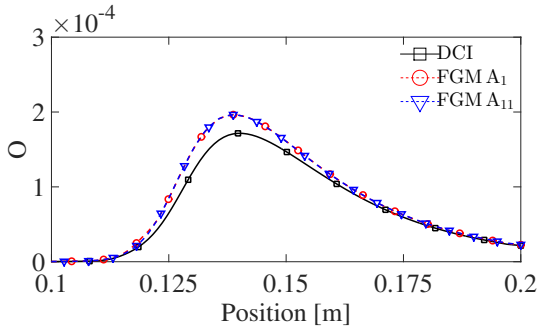

(g) Axial O mass fraction profile.

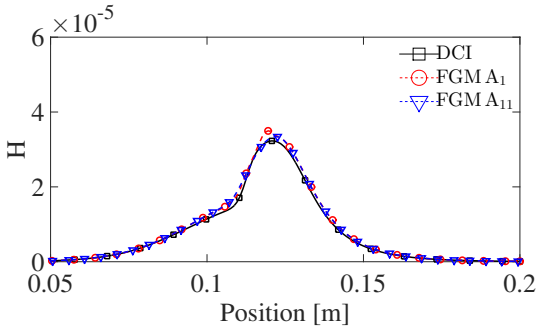

(h) Axial H mass fraction profile.

Figure 6.4 – Axial profiles in the center of the fuel jet for 100% CH_4, comparing direct chemistry integration (DCI) to the FGM technique.

6.4 60% CH_4 40% CO_2 bi-dimensional results

For the following results, the reader may use as reference the Table 5.2 for the labels referred to. The definition B_1 is the standard definition used for pure methane. The definition B_3 corresponds to the definition found by Hoerlle et al., 2017 which provided better results when adding CO_2 into the methane stream. The definition B_8 correspond to a definition found by the optimization algorithm implemented in the present work. They are respectively given by

$$\begin{aligned} \mathcal{Y}_{B_1} &= Y_{H_2O} + Y_{CO_2} + Y_{H_2}, \\ \mathcal{Y}_{B_3} &= Y_{H_2O} + Y_{CO_2} + Y_{CO}, \\ \mathcal{Y}_{B_8} &= 0.35Y_{H_2O} + 0.05Y_{CO_2} - 0.15Y_{CO} + 0.387Y_{H_2}. \end{aligned} \tag{6.2}$$

Definitions B_3 and B_8 presented fully monotonic behavior when calculated with Equation 4.2. The definition B_{12} (from Table 5.2), which presented non-convergence in the one-dimensional flamelets for one strain rate value, as well as provided poor agreement for some other conditions, also lead to problems in the multidimensional simulation. It was not possible to achieve convergence in the two-dimensional co-flow burner simulation using the FGM technique with definition B_{12} as progress variable.

The Figure 6.5 shows some contour fields comparing the FGM technique using definition B_8 to the direct chemistry integration (DCI) simulation. It was possible to find an optimized progress variable which resulted in accurate prediction of most flame variables, as it can be observed.

In Figures 6.6 below, definitions B_1, B_3 and B_8 are plotted along the direct chemistry integration (DCI) results. It is possible to see that all of them have a general good accuracy in the prediction of temperature and species mass fraction profiles, even for minor species. As mentioned in Hoerlle et al., 2017, definition B_1 slightly over-predicted the axial profile for CO species mass fraction. However, the non-physical behavior encountered in such work was not found in the present work. A small over-prediction for the H_2 species mass fraction also can be noticed. In general, the optimization algorithm was able to find a feasible progress variable for the case of methane with CO_2 dilution as it had done with the pure methane case, leading to accurate predictions of the flame variables in the two-dimensional simulation.

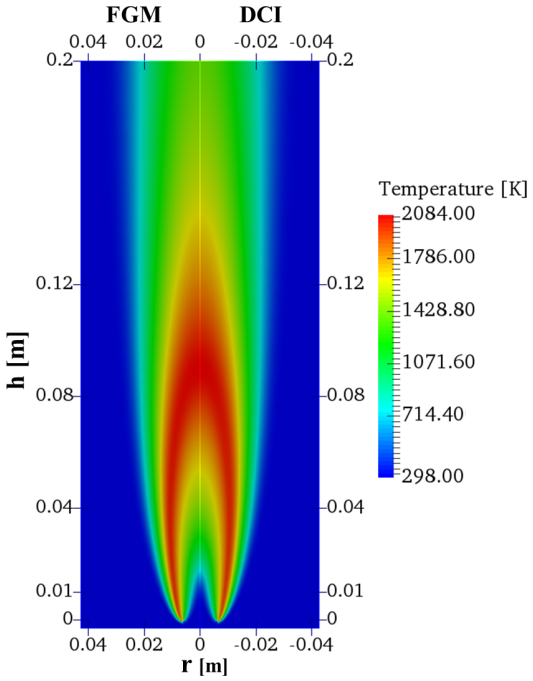

(a) Temperature field

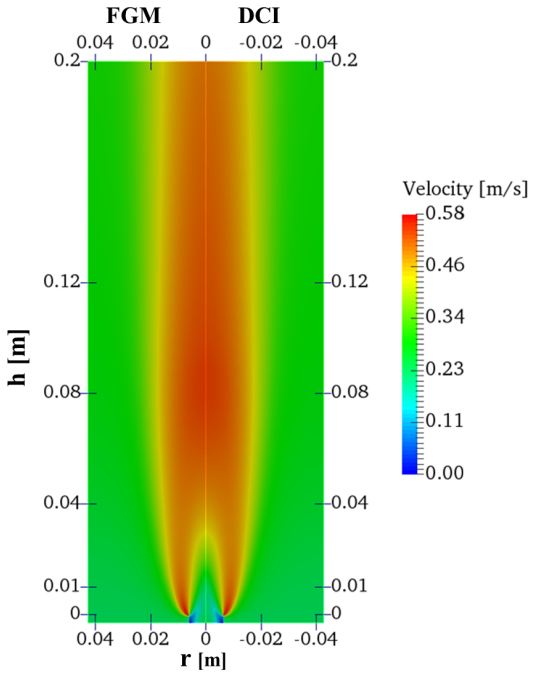

(b) Velocity magnitude field

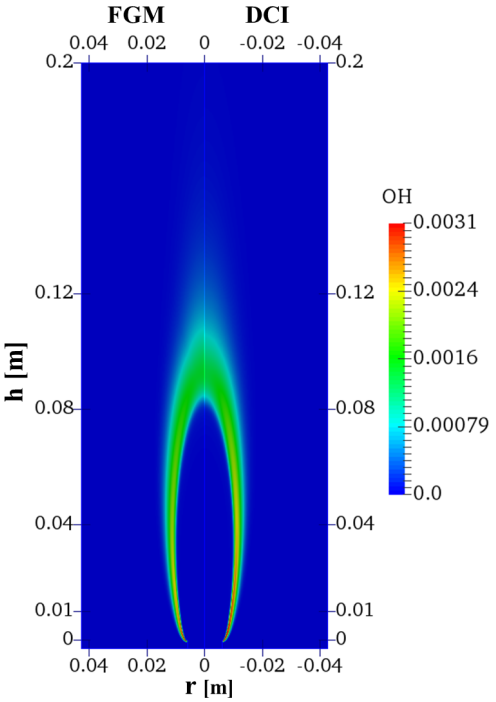

(c) OH mass fraction field

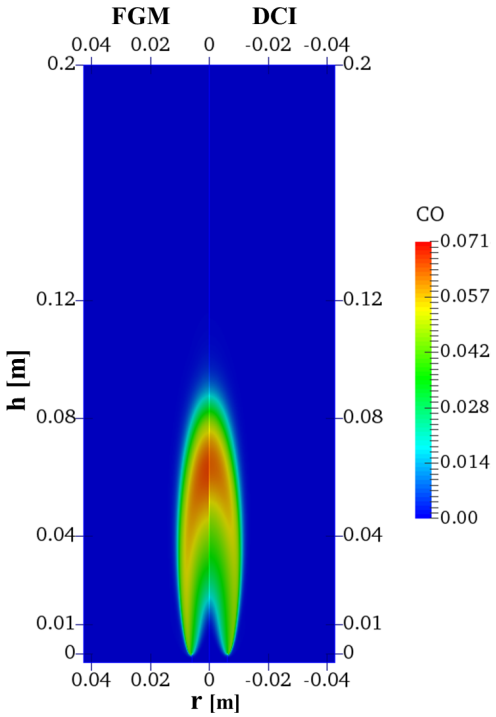

(d) CO mass fraction field

Figure 6.5 – Contour fields for methane with 40% CO_2 dilution with FGM (left), using definition B_8, and DCI (right): (a) temperature, (b) velocity magnitude, (c) OH mass fraction and (d) CO mass fraction.

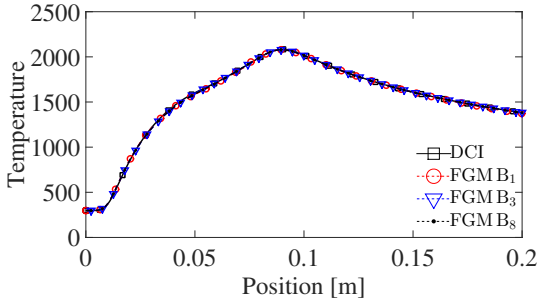

(a) Axial temperature profile.

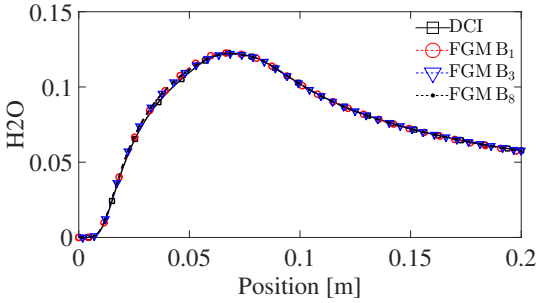

(b) Axial H_2O mass fraction profile.

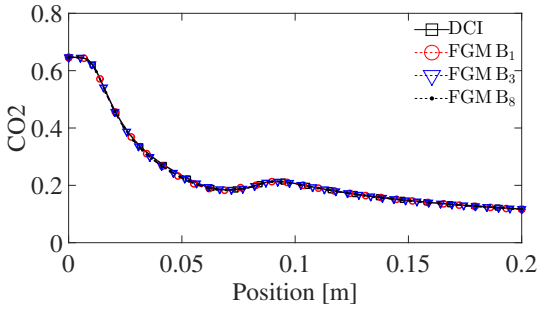

(c) Axial CO_2 mass fraction profile.

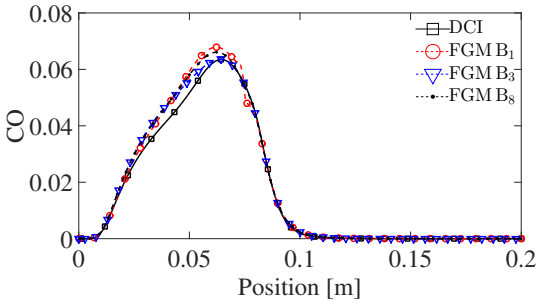

(d) Axial CO mass fraction profile.

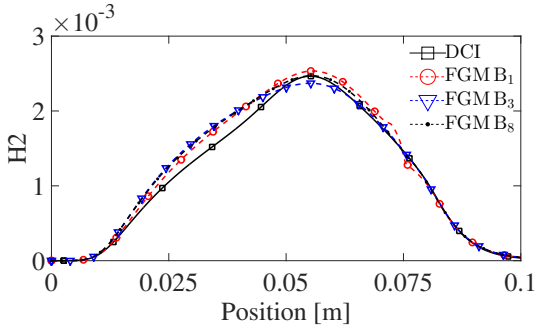

(e) Axial H_2 mass fraction profile.

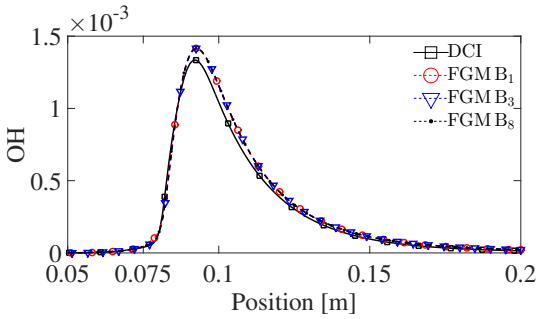

(f) Axial OH mass fraction profile.

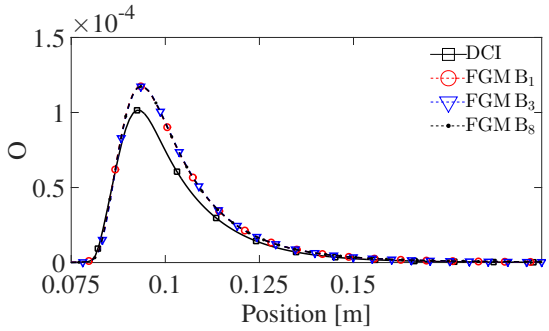

(g) Axial O mass fraction profile.

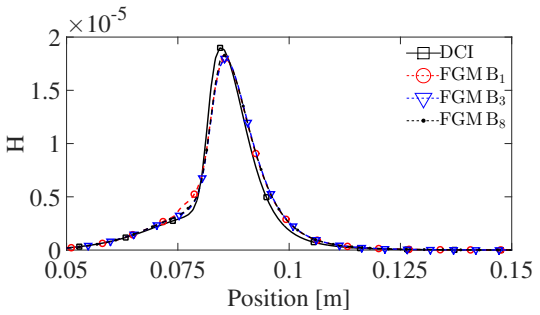

(h) Axial H mass fraction profile.

Figure 6.6 – Axial profiles in the center of the fuel jet for methane with 40% CO_2 dilution, comparing direct chemistry integration (DCI) to the FGM technique.

6.5 100% C_2H_4 bi-dimensional results

For the ethylene flames, the FGM results are compared to the adapted GRI-MEC 3.0 (Smith et al., 2000) detailed mechanism using direct chemistry integration. Since Zimmer, 2016 found a good definition for the progress variable when dealing with gas-phase only and under unity Lewis number assumption, his definition will be used as reference of an accurate FGM result (definition C_1 of Table 5.3). Along those two results, the optimized definition will be compared (definition C_2 of Table 5.3). Using Equation 4.2 to evaluate the monotonicity of the definitions, it was found that both definitions were not perfectly monotonic, being definition C_2 more monotonic than definition C_1 (see Table 5.3 for specific values of non-monotonicity). The definitions C_1 and C_2 are respectively given by

$$\begin{aligned} \mathcal{Y}_{C_1} &= Y_{H_2O} + Y_{CO_2} + 0.9Y_{CO}, \\ \mathcal{Y}_{C_2} &= 0.333Y_{H_2O} + 1Y_{CO_2} + 0.833Y_{CO} + 0.167Y_{H_2}. \end{aligned} \tag{6.3}$$

Good accuracy was presented in Zimmer, 2016 with definition C_1 for major species and temperature contours, apart from acetylene specie, which shown some deviations. The Figure 6.7b below shows the acetylene contours for the optimized progress variable of the present work in comparison to the direct chemistry integration (DCI) simulation. Very similar fields were found with both definitions C_1 and C_2 and no significant improvement could be observed with definition C_2. Figures 6.7 show other fields presenting an overall good accuracy of the FGM technique with definition C_2. However, even though significant improvements on the accuracy were not found, it is important to state that the benefits of using an automated procedure to establish the progress variable definition is notorious. Several attempts of finding a feasible progress variable might be done through trial and error approach by Zimmer, 2016, while the automated procedure provides a definition in a couple of hours.

Axial profiles in the center of the fuel jet for temperature, major and minor species are presented in Figures 6.8. It can be shown that the overall behavior of both definitions in the FGM technique are similar, even though definition C_2 is more monotonic than definition C_1. This induces the conclusion that the non-monotonicity of definition C_1 occurs in regions that are not that important for the results observed. In Appendix A radial profiles for different heights show a more complete set of data.

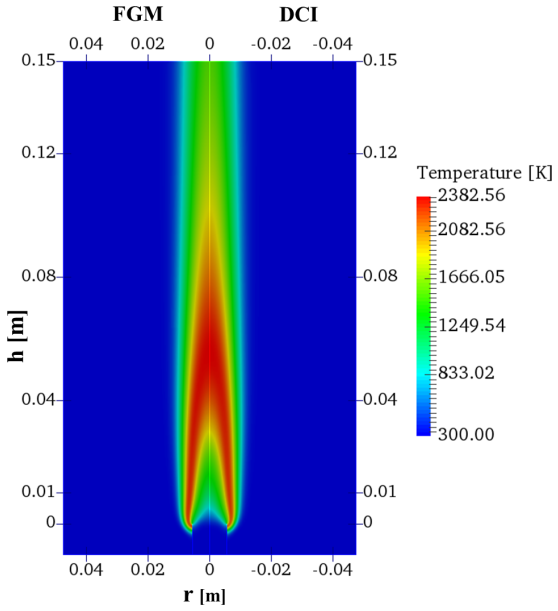

(a) Temperature field

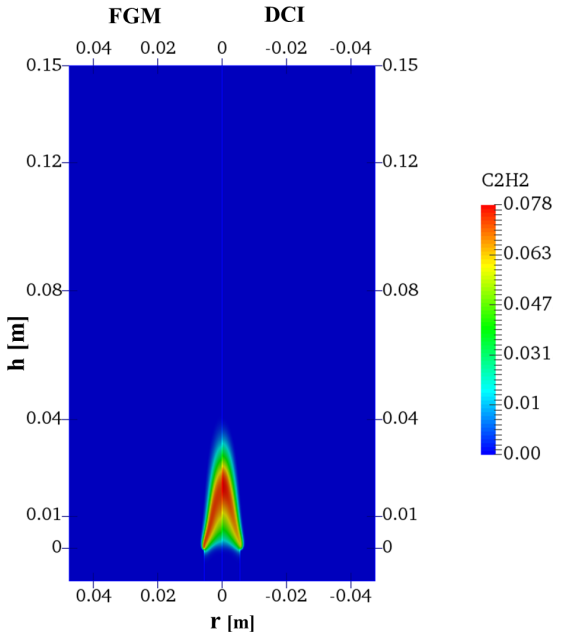

(b) C_2H_2 mass fraction field

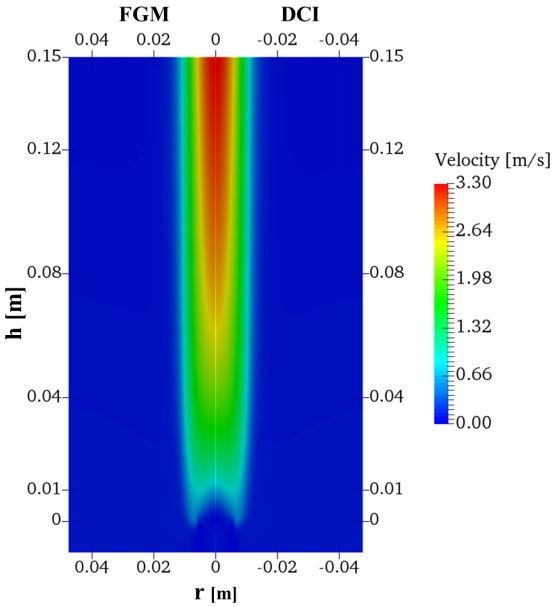

(c) Velocity magnitude field

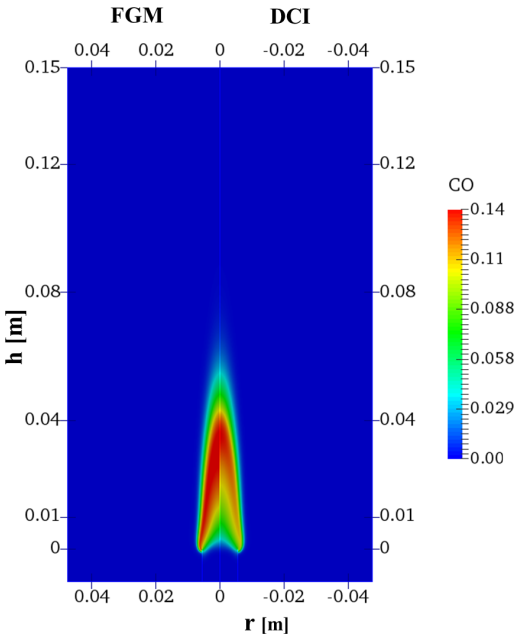

(d) CO mass fraction field

Figure 6.7 – Contour fields for 100% C_2H_4 with FGM (left), using definition C_2, and DCI (right): (a) temperature, (b) C_2H_2 mass fraction, (c) velocity magnitude and (d) CO mass fraction.

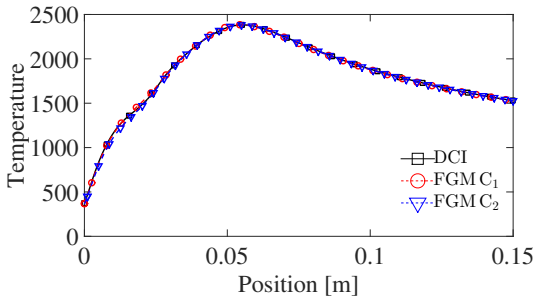

(a) Axial temperature profile.

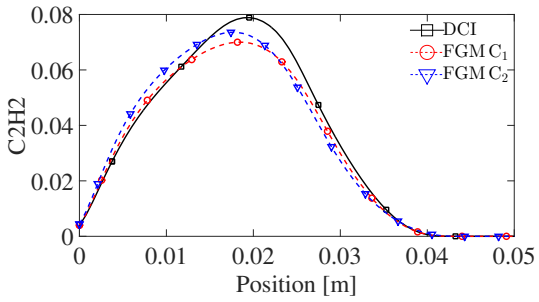

(b) Axial C_2H_2 mass fraction profile.

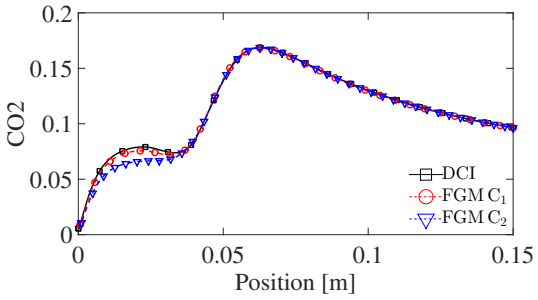

(c) Axial CO_2 mass fraction profile.

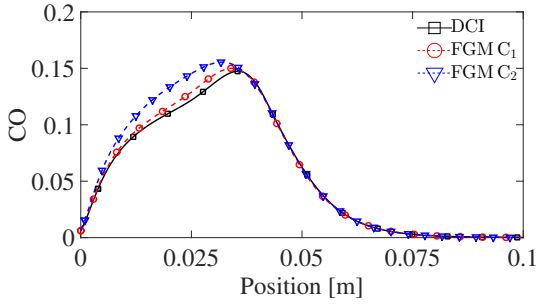

(d) Axial CO mass fraction profile.

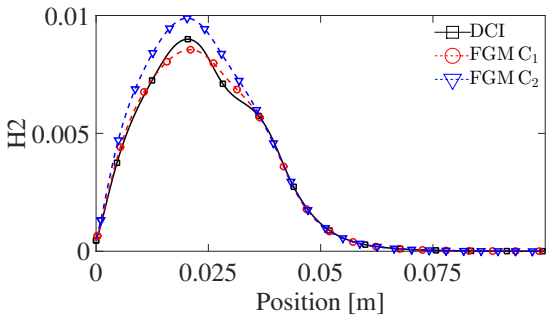

(e) Axial H_2 mass fraction profile.

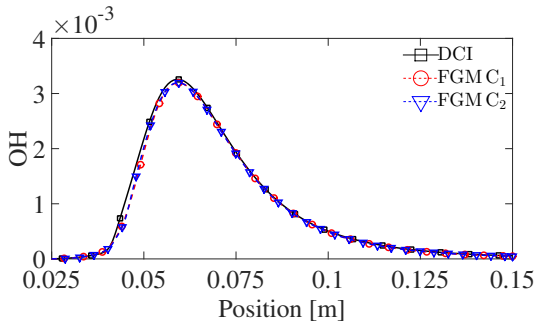

(f) Axial OH mass fraction profile.

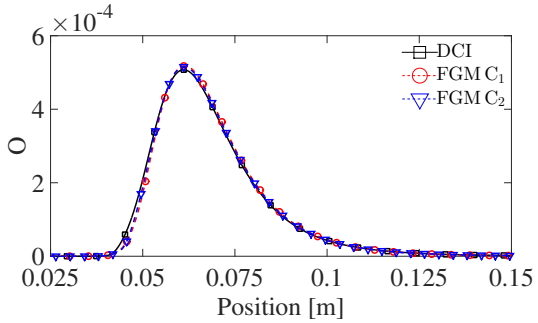

(g) Axial O mass fraction profile.

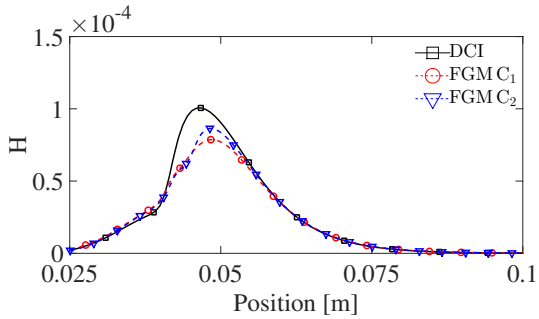

(h) Axial H mass fraction profile.

Figure 6.8 – Axial profiles in the center of the fuel jet for 100% C_2H_4, comparing direct chemistry integration (DCI) to the FGM technique.

Since improving the acetylene field prediction would be an important result, mainly

for future soot modelling studies, the objective function of Prufert et al., 2015 was used in the optimization algorithm. This objective function was calculated through Equation 4.3 and includes the gradients of the species mass fractions as parameter to be optimized as well. Along this, a penalty factor takes into account the monotonicity requirement. The resultant progress variable from such optimization (called definition C_3 in this section) was given by

$$\mathcal{Y}_{C_3} = 0.4Y_{H_2O} + 1Y_{CO_2} + 0.8Y_{CO} + 0.2Y_{H_2}. \tag{6.4}$$

The Table 6.1 presents the evaluation of Equations 4.2 and 4.3 for definitions C_1, C_2 and C_3 for ethylene flames.

Table 6.1 – Evaluation of two different objective functions applied for definitions C_2 and C_3 in the 100% C_2H_4 flames (and comparison to definition C_1).

	100%C_2H_4	
Definition label	Monotonicity evaluation (Eq. 4.2)	Gradients minimization (Eq. 4.3).
C_1 (Zimmer, 2016)	0.618097	2.130,66
C_2 (objective function of Eq. 4.2)	0.000285	2.972,80
C_3 (objective function of Eq. 4.3)	0.000290	2.665,06

The optimized progress variable C_3 presented very similar values for the monotonicity requirement compared to definition C_2, and a reduction in the maximum gradients values. However, definition C_3 did not shown any improvement and presented very similar results to the ones obtained with the other definitions. The results were omitted since it would be a repetition of the curves from Figures 6.8.

6.6 Two-dimensional results remarks

In this chapter, two-dimensional simulations were performed for three different fuels using some definitions found by the optimization algorithm and previously evaluated through one-dimensional simulations (Chapter 5). In the pure methane case, the definition A_{12} (Table 5.1) presented bad accuracy for some specific strain rate values in the one-dimensional simulations. However, it was not problematic in the two-dimensional co-flow burner when simulated with the FGM technique. That leads to the conclusion that the problematic region of the manifold was not accessed during the multidimensional simulation. However, it is expected that a turbulent non-adiabatic flame presents worsen

results with such problematic flamelets, since there will be regions which departure from the equilibrium condition. In the methane with 40% CO_2 dilution case, the definition B_{12} (Table 5.2), which presented bad results for other strain rates, resulted in a non-convergence of the two-dimensional simulation. That leads to the conclusion that, in this particular case, the two-dimensional simulation tried to access such problematic regions in the manifold, leading to a non-convergence of the problem (but could be inaccurate predictions as well). Those results show the importance of evaluating the flamelet-based models results in both one-dimensional and multidimensional simulations, instead of only looking at the former one. The one-dimensional solutions are indicatives of good accuracy and representativeness of the progress variable, but depending on the flame configuration being simulated in the multidimensional solution they can be enough or not.

Among the results presented with the FGM technique using optimized progress variables, there were no significant improvement compared to well known accurate definitions from other studies. However, the benefits of using an automated procedure to define the progress variable are notorious for users of flamelet-based models. When non-standard fuels or dilution is the problem of interest, finding a feasible progress variable is not trivial, and a trial and error approach is often applied. The optimization algorithm used in the present work under the already stated conditions, took around 2 hours to provide a definition. An estimation of the computational time for the co-flow burner simulations in the present work are presented in Table 6.2 below. Different burners and progress variable definitions might take different computational times in the FGM and direct integration solutions. Also, the computational time of the optimization algorithm depends on a lot of factors, like population number, stopping threshold, number of variable parameters, etc.

Table 6.2 – Estimated computational time of optimization algorithm, FGM and direct integration solution.

—	Computational time
Optimization algorithm	1-2 hours
FGM solution	30-45 minutes
Direct chemistry integration	72-100 hours

7 CONCLUSIONS AND FUTURE WORKS

The present work aimed to implement and couple an optimization algorithm to find a feasible progress variable to the Flamelet-Generated Manifold technique. To fulfill the lack of studies in the literature which solve a CFD simulation using the optimized progress variable, one-dimensional and two-dimensional simulations were performed for different flame configurations. Non-premixed flames of pure methane, methane diluted with CO_2 and pure ethylene flames were analyzed. The optimization algorithm was applied for all cases and the representativeness of the progress variable was discussed.

For the methane cases, several perfectly monotonic definitions were found by the algorithm. It was shown that, even though most of the monotonic definitions for the methane cases presented good agreement to the direct chemistry integration results, there were definitions which failed to predict some species mass fractions for certain strain rate values in the one-dimensional solutions. For the pure methane case, definition A_{12} ended up providing accurate results when using it in a two-dimensional CFD simulation, even though there were some inaccuracies in the one-dimensional profiles. The conclusion is that such problematic regions of the manifold were not accessed during the 2D CFD solution. On the other hand, for the methane diluted to CO_2 case, the definition which presented bad behavior in the one-dimensional case lead to a non-convergence on the 2D CFD simulation (definition B_{12} from Table 5.2). Besides that, in the one-dimensional flamelets, this definition did not converge for a strain rate value of $0.95[s^{-1}]$, which is close to equilibrium condition. Also, bad results were found for smaller values of strain rate.

It is possible to take the following main conclusions about the presented study:

- the monotonicity requirement really tends to yield accurate results in one-dimensional and multidimensional solutions. Most of definitions found by the optimization algorithm provided accurate results in the present work. However, there might be situations in which a monotonic definition is not representative, which was the case of definition B_{12}, for instance. In order to find a representative definition, other techniques might be necessary in which the chemical kinetic mechanism is analyzed instead of only selecting major species from the gas water shift reaction.

- in a multidimensional simulation, it is necessary that the accessed regions in the

manifold be representative. A first approach of verifying the quality of the manifold on such regions is taking a look into one-dimensional FGM solutions and comparing it to direct chemistry integrated solutions. If the one-dimensional simulations fail to predict such regions is expected that the multidimensional solution yields bad results or even non-convergence of the simulation. For instance, definition A_{12} failed in the prediction of some flamelets solutions but provided accurate results in the multidimensional solution, while definition B_{12} also failed in the prediction of some flamelets solutions but, in this case, it lead to non-convergence of the multidimensional simulation. The difference between both cases is the strain rate values whose flamelets solutions were not accurate. While definition A_{12} failed in higher strain rate values, close to extinction region, definition B_{12} failed in smaller strain rate values, corresponding to regions closer to equilibrium condition. It is expected that an adiabatic laminar flame presents a thermochemical state which falls into the equilibrium regime, since it will not show too much local extinction phenomena, for instance, such as a non-adiabatic turbulent flame would do.

The main contributions of the present work can be divided in the following:

- an optimization algorithm coupled to the FGM technique, which allows finding a probable feasible progress variable without the use of a trial and error approach;
- discussion about the representativeness of the progress variable, showing that the monotonicity requirement, commonly employed in optimization works in the literature, does not guarantee a representative solution;
- discussion about the relations between representative one-dimensional solutions and representative multidimensional ones, showing that depending on the case of interest, different regions of the manifold must be, in fact, representative;

7.1 Future works

An extensive study about the factors which affect the representativeness of the progress variable definition is still missing in the literature. It might be possible to predict in advance if a definition will suit in a multidimensional simulation by only looking at one-dimensional CFD solutions, if prior knowledge of the physics to be simulated in the 2D/3D

case is known. Simpler problems, like laminar non-premixed flames, might not necessarily need an entire accurate mapping of the flamelets. The accuracy might be relaxed for regions which will probably not be accessed in the manifold, for instance. It is necessary to perform a higher number of tests comparing one-dimensional and multidimensional simulations and their regions which are accessed in the manifold to achieve a more precise conclusion.

There are other methodologies, like the multistage FGM proposed by Göktolga et al., 2017, which could be coupled to an optimization algorithm for each stage of combustion. Other methodologies which are based on more rigorous mathematical foundations might be more assertive in relation to the representativeness of the progress variable, like the Principal Component Analysis (PCA) used by Najafi-Yazdi et al., 2012 and Chen et al., 2015. When optimization tools are coupled to flamelet-based techniques such as performed in the present work, CFD simulations are still necessary to guarantee that the optimized progress variable yields to representative solutions of the flame. It is, however, notorious that methodologies based on optimization of the progress variable, even though based only on the monotonicity requirement, decreases significantly the complexity of finding a probable good definition.

BIBLIOGRAPHY

Bekdemir, C., Somers, L. M. T., and De Goey, L. P. H. Modeling diesel engine combustion using pressure dependent Flamelet Generated Manifolds, **Proceedings of the Combustion Institute**, vol. 33(2), p. 2887–2894, 2011.

Bilger, R. W. **Turbulent flows with nonpremixed reactants**. In *Topics in Applied Physics*, volume 6, pages 239–239, 1980.

Bilger, R. W. The structure of turbulent nonpremixed flames, **Symposium (International) on Combustion**, vol. 22(1), p. 475–488, 1988.

Burke, S. P. and Schumann, T. E. W. Diffusion Flames, **Industrial**, vol. 20(10), p. 998–998, 1928.

Cao, S., Ma, B., Bennett, B. A., Giassi, D., Stocker, D. P., Takahashi, F., Long, M. B., and Smooke, M. D. A computational and experimental study of coflow laminar methane/air diffusion flames: Effects of fuel dilution, inlet velocity, and gravity, **Proceedings of the Combustion Institute**, vol. 35(1), p. 897–903, 2015.

Chen, J., Liu, M., and Chen, Y. Optimizing progress variable definition in flamelet-based dimension reduction in combustion, **Applied Mathematics and Mechanics (English Edition)**, vol. 36(11), p. 1481–1498, 2015.

De Goey, L. P. H. and Ten Thije Boonkkamp, J. H. A flamelet description of premixed laminar flames and the relation with flame stretch, **Combustion and Flame**, vol. 119(3), p. 253–271, 1999.

de Lange, H. C. Modelling of premixed laminar flames using, **Combustion Science and Technology**, vol. 161(1), 1992.

Donini, A., Bastiaans, R. J. M., Van Oijen, J. A., and De Goey, L. P. H. A five dimensional implementation of the flamelet generated manifolds technique for gas turbine application, **AIP Conference Proceedings**, vol. 1648, 2015.

Egüz, U., Ayyapureddi, S., Bekdemir, C., Somers, B., and De Goey, L. P. H. Manifold resolution study of the FGM method for an igniting diesel spray, **Fuel**, vol. 113, p. 228–238, 2013.

Fiorina, B., Baron, R., Gicquel, O., Thevenin, D., Carpentier, S., and Darabiha, N. Modelling non-adiabatic partially premixed flames using flame-prolongation of ILDM, **Combustion Theory and Modelling**, vol. 7(3), p. 449–470, 2003.

Gicquel, O., Darabiha, N., Thévenin, D., Emc, L., and Cha, F. Liminar premixed hydrogen/air counterflow flame simulations using flame prolongation of ILDM with differential diffusion, **Proceedings of the Combustion Institute**, vol. 28(2), p. 1901–1908, 2000.

Göktolga, M. U., Van Oijen, J. A., and De Goey, L. P. H. Modeling MILD combustion using a novel multistage FGM method, **Proceedings of the Combustion Institute**, vol. 36(3), p. 4269–4277, 2017.

Hoerlle, C. A. Estudo numérico de chamas laminares difusivas de CH4 diluído com CO2 empregando mecanismos cinéticos globais e a técnica Flamelet-Generated Manifold, 2015.

Hoerlle, C. A. **Numerical modeling of soot forma- tion based on the Discrete Sectional Method coupled to the Flamelet- Generated Manifold technique**. Qualification, UFRGS, 2017.

Hoerlle, C. A., Zimmer, L., and Pereira, F. M. Numerical study of CO2effects on laminar non-premixed biogas flames employing a global kinetic mechanism and the Flamelet-Generated Manifold technique, **Fuel**, vol. 203, p. 671–685, 2017.

Ihme, M. **Pollutant Formation and Noise Emission in Turbulent Non-Premixed Flames**. Phd, Stanford University, 2007.

Ihme, M., Cha, C. M., and Pitsch, H. Prediction of local extinction and re-ignition effects in non-premixed turbulent combustion using a flamelet/progress variable approach, **Proceedings of the Combustion Institute**, vol. 30(1), p. 793–800, 2005.

Ihme, M. and Pitsch, H. Prediction of extinction and reignition in nonpremixed turbulent flames using a flamelet/progress variable model. 2. Application in LES of Sandia flames D and E, **Combustion and Flame**, vol. 155(1-2), p. 90–107, 2008.

Ihme, M., Shunn, L., and Zhang, J. Regularization of reaction progress variable for application to flamelet-based combustion models, **Journal of Computational Physics**, vol. 231(23), p. 7715–7721, 2012.

Kazakov, A. and Frenklach, M. **Reduced Reaction Sets based on GRI-Mech 1.2**, 2005.

Lam, S. H. Using CSP to Understand Complex Chemical Kinetics, **Combustion Science and Technology**, vol. 89(5-6), p. 375–404, 1993.

Lam, S. H. and Goussis, D. A. The CSP method for simplifying kinetics, **International Journal of Chemical Kinetics**, vol. 26(4), p. 461–486, 1994.

Law, C. K. **Combustion physics**. volume 9780521870, 2006.

Maas, U. and Pope, S. B. Simplifying chemical kinetics: Intrinsic low-dimensional manifolds in composition space, **Combustion and Flame**, vol. 88(3-4), p. 239–264, 1992.

MathWorks. **MatLab**, 2012.

MME. **Balanço Energético Nacional**. Technical report, 2017.

Najafi-Yazdi, A., Cuenot, B., and Mongeau, L. Systematic definition of progress variables and Intrinsically Low-Dimensional, Flamelet Generated Manifolds for chemistry tabulation, **Combustion and Flame**, vol. 159(3), p. 1197–1204, 2012.

Niu, Y. S., Vervisch, L., and Tao, P. D. An optimization-based approach to detailed chemistry tabulation: Automated progress variable definition, **Combustion and Flame**, vol. 160(4), p. 776–785, 2013.

Peters, N. Laminar diffusion flamelet models in non-premixed turbulent combustion, **Progress in Energy and Combustion Science**, vol. 10(3), p. 319–339, 1984.

Peters, N. **Turbulent Combustion**, 2000.

Pierce, C. D. and Moin, P. Progress-variable approach for large-eddy simulation of non-premixed turbulent combustion, **International Review of Mechanical Engineering**, vol. 4(3), p. 358–363, 2004.

Pitsch, H., Riesmeier, E., and Peters, N. Unsteady Flamelet Modeling of Soot Formation in Turbulent Diffusion Flames, **Combustion Science and Technology**, vol. 158(1), p. 389–406, 2000.

Prufert, U., Hartl, S., Hunger, F., Messig, D., Eiermann, M., and Hasse, C. A constrained control approach for the automated choice of an optimal progress variable for chemistry tabulation, **Flow, Turbulence and Combustion**, vol. 94(3), p. 593–617, 2015.

Santoro, R. J., Semerjian, H. G., and Dobbins, R. A. Soot Particle Formation in Diffusion Flames, **Combustion and Flame**, vol. 51, p. 203–218, 1983.

Santoro, R. J., Yeh, T. T., Horvath, J. J., and Semerjian, H. G. The Transport and Growth of Soot Particles in Laminar Diffusion Flames, **Combustion Science and Technology**, vol. 53(2-3), p. 89–115, 1987.

Smith, G. P., Golden, D. M., Frenklach, M., Moriarty, N. W., Eiteneer, B., Goldenberg, M., Bowman, C. T., Hanson, R. K., Song, S., Jr., W. C. G., Lissianski, V. V., and Qin, Z. **GRI-MECH 3.0**, 2000.

Smooke, M. D. and Giovangigli, V. **Lecture Notes in Physics and Asymptotic Approximations**, 1991.

Smooke, M. D., Long, M. B., CONNELLY, B. C., Colket, M. B., and HALL, R. J. Soot formation in laminar diffusion flames, **Combustion and Flame**, vol. 143(4), p. 613–628, 2005.

Turns. **An Introduction to Combustion**, 2000.

Van Oijen, J. A. 2ss Flamelet-Generated Manifolds : Development and Application to Premixed Laminar Flames, (september), p. 125, 2002.

Van Oijen, J. A. and de Goey, L. P. H. Modelling of Premixed Laminar Flames using Flamelet-Generated Manifolds, **Combustion Science and Technology**, vol. 161(1), p. 113–137, 2000.

Van Oijen, J. A. and De Goey, L. P. H. Modelling of premixed counterflow flames using the flamelet-generated manifold method, **Combustion Theory and Modelling**, vol. 6(3), p. 463–478, 2002.

Van Oijen, J. A., Donini, A., Bastiaans, R. J., ten Thije Boonkkamp, J. H., and De Goey, L. P. H. State-of-the-art in premixed combustion modeling using flamelet generated manifolds, **Progress in Energy and Combustion Science**, vol. 57, p. 30–74, 2016.

Verhoeven, L. **Radical Tar Removal; Numerical modeling of tar conversion in a partial combustion reactor**. Number november, 2011.

Verhoeven, L. M., Ramaekers, W. J., van Oijen, J. A., and De Goey, L. P. H. Modeling non-premixed laminar co-flow flames using flamelet-generated manifolds, **Combustion and Flame**, vol. 159(1), p. 230–241, 2012.

Xuan, Y. and Blanquart, G. Numerical modeling of sooting tendencies in a laminar co-flow diffusion flame, **Combustion and Flame**, vol. 160(9), p. 1657–1666, 2013.

Zimmer, L. **Numerical Study of Soot Formation in Laminar Ethylene Diffusion Flames**. Phd, UFRGS, 2016.

APPENDIX A – Radial Profiles of 2D Simulations

In this Appendix, radial profiles at $10mm$, $40mm$, $80mm$ and $120mm$ height for temperature, major and minor species are presented. The three cases simulated are divided into three different sections.

100% CH_4 two-dimensional results

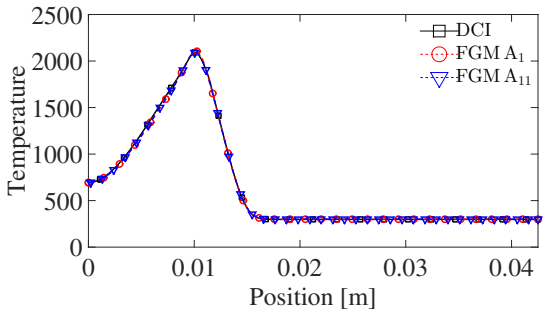

(a) Temperature profile at $10mm$ height.

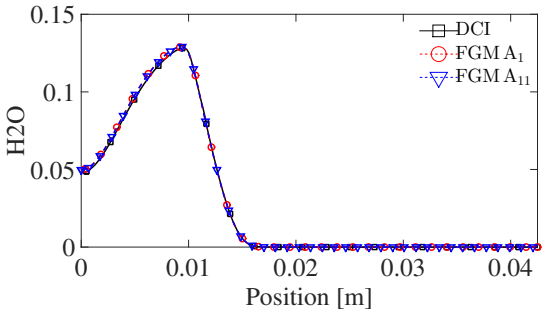

(b) H_2O profile at $10mm$ height.

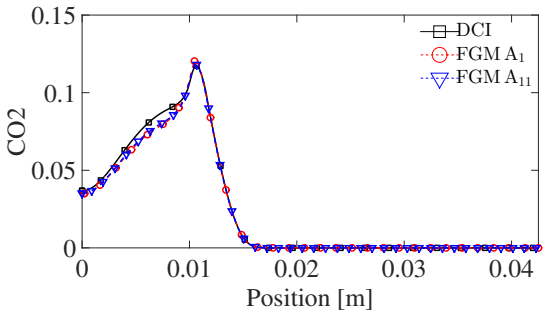

(c) CO_2 profile at $10mm$ height.

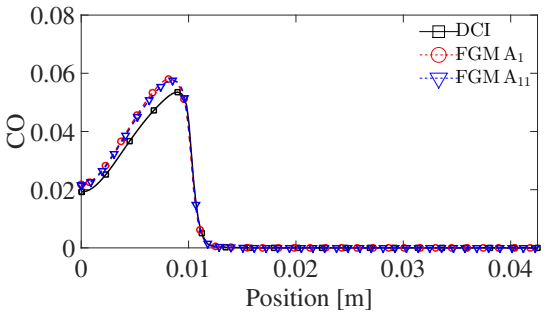

(d) CO profile at $10mm$ height.

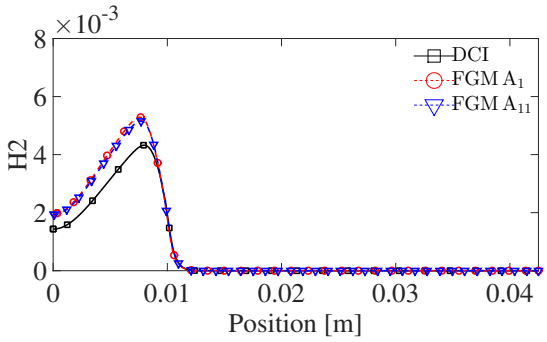

(e) H_2 profile at $10mm$ height.

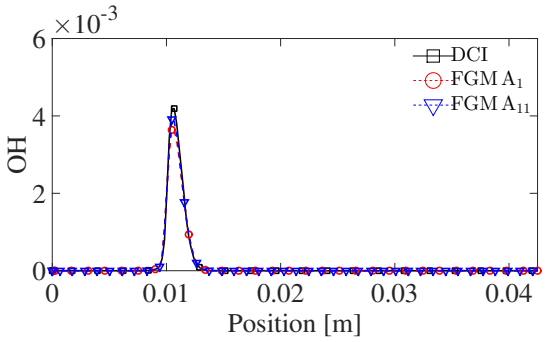

(f) OH profile at $10mm$ height.

Figure A.1 – Radial species mass fraction profiles at $10mm$ height for 100% CH_4.

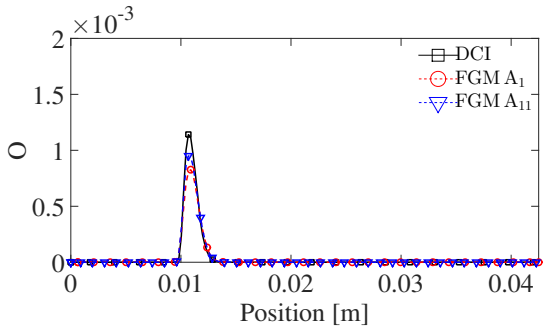

(g) O profile at $10mm$ height.

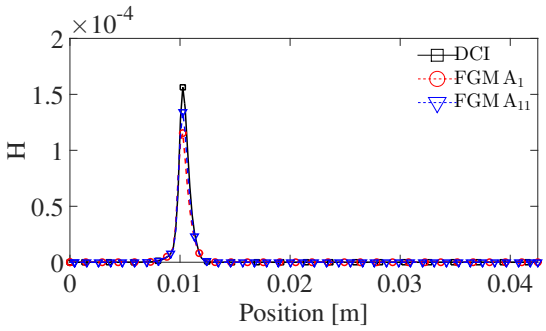

(h) H profile at $10mm$ height.

Figure A.1 – Radial species mass fraction profiles at $10mm$ height for 100% CH_4 (cont.).

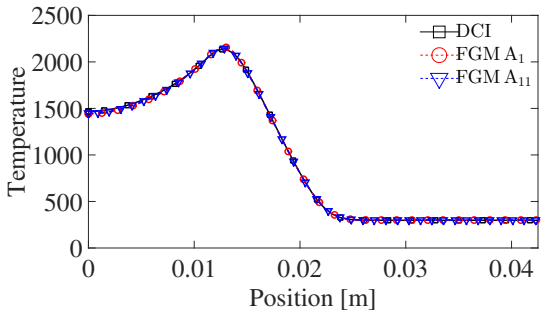

(a) Temperature profile at 40mm height.

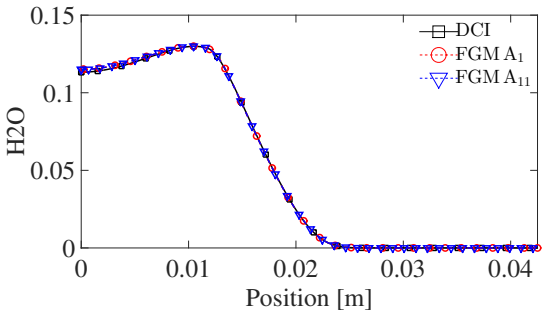

(b) H_2O profile at 40mm height.

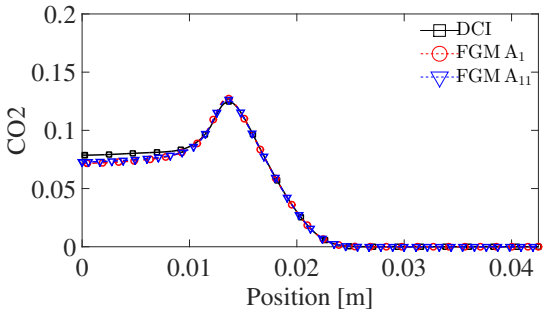

(c) CO_2 profile at 40mm height.

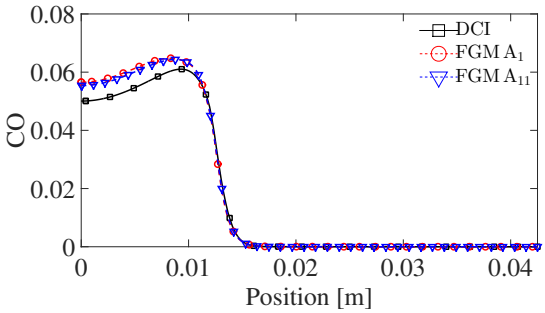

(d) CO profile at 40mm height.

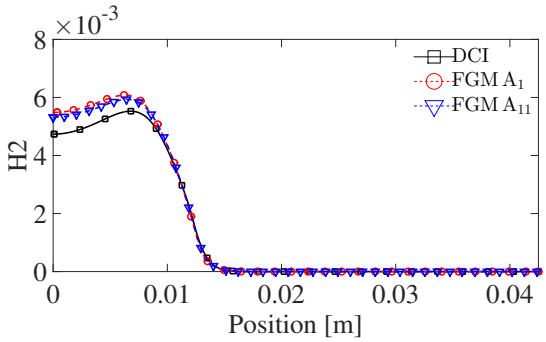

(e) H_2 profile at 40mm height.

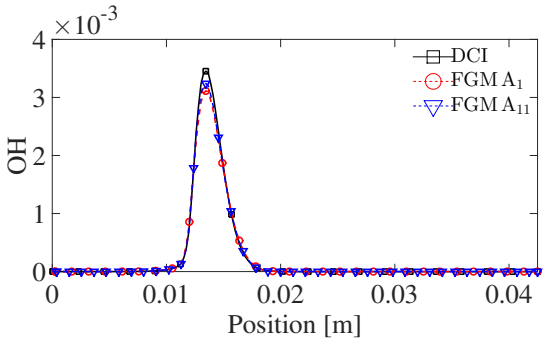

(f) OH profile at 40mm height.

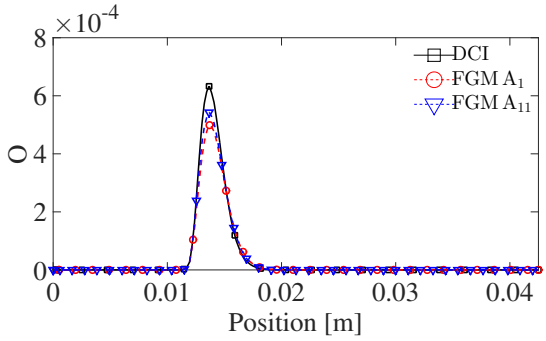

(g) O profile at 40mm height.

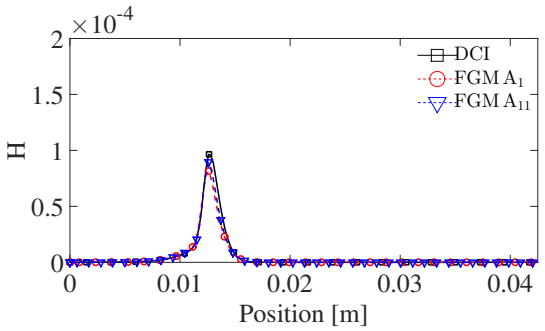

(h) H profile at 40mm height.

Figure A.2 – Radial species mass fraction profiles at 40mm height for 100% CH_4

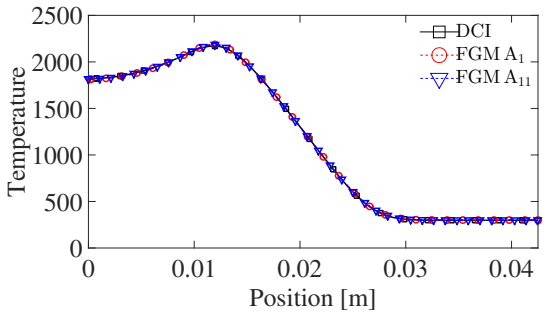

(a) Temperature profile at 80mm height.

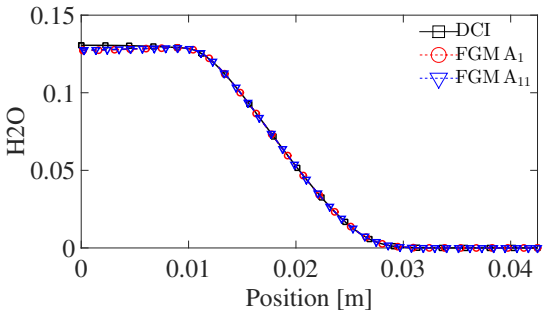

(b) H_2O profile at 80mm height.

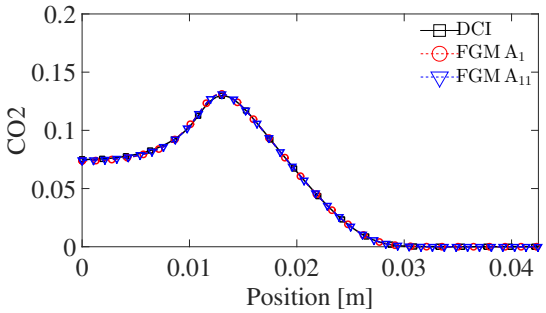

(c) CO_2 profile at 80mm height.

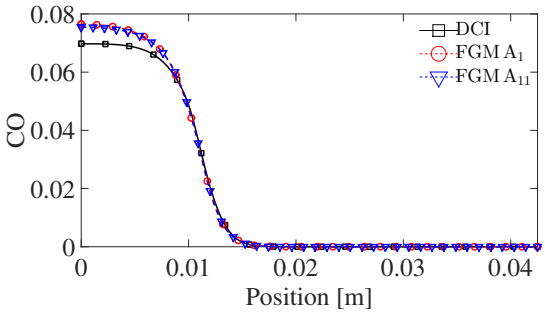

(d) CO profile at 80mm height.

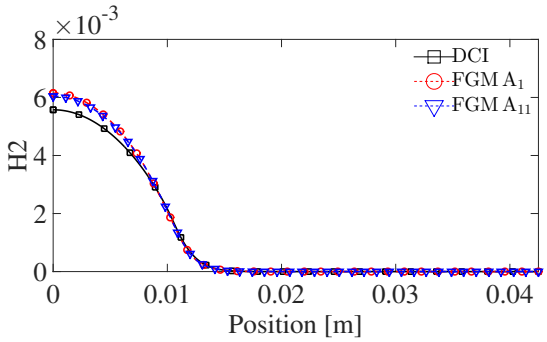

(e) H_2 profile at 80mm height.

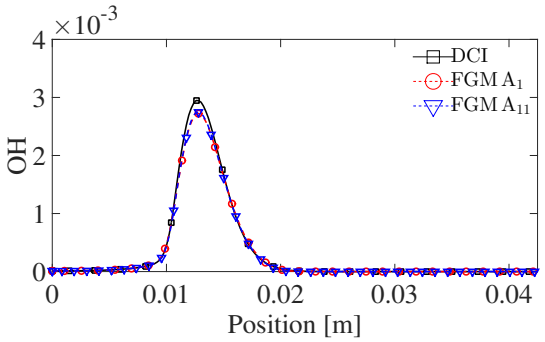

(f) OH profile at 80mm height.

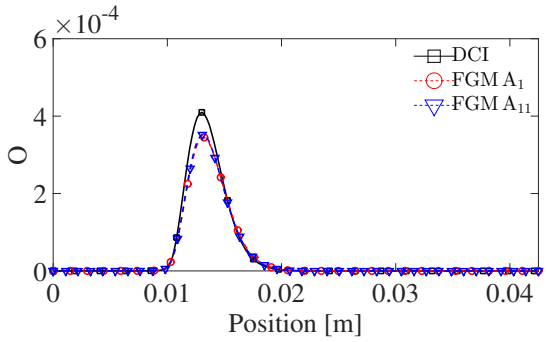

(g) O profile at 80mm height.

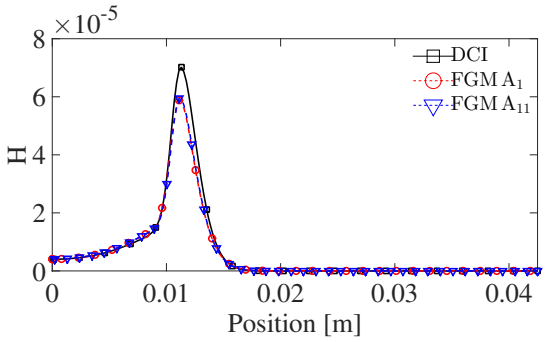

(h) H profile at 80mm height.

Figure A.3 – Radial species mass fraction profiles at 80mm height for 100% CH_4

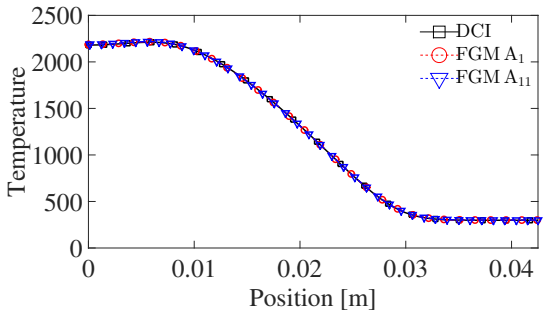

(a) Temperature profile at 120mm height.

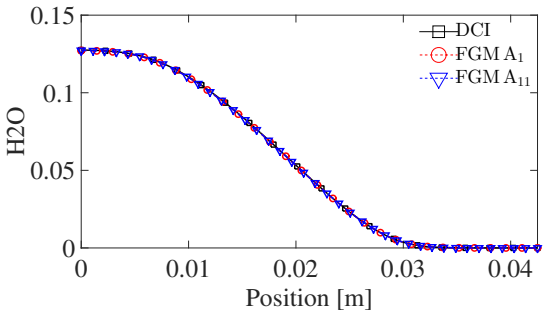

(b) H_2O profile at 120mm height.

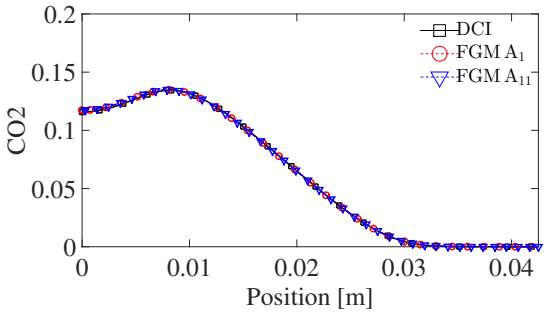

(c) CO_2 profile at 120mm height.

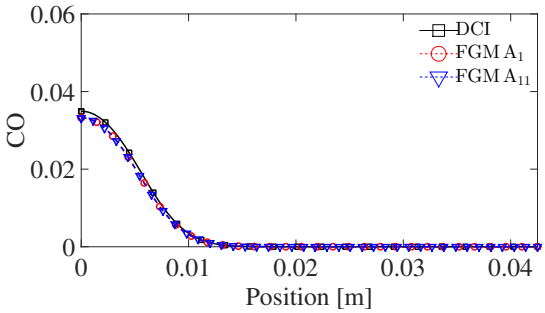

(d) CO profile at 120mm height.

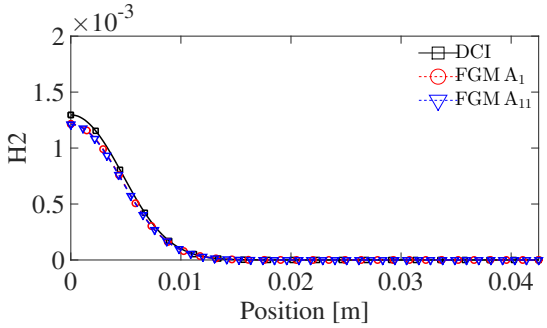

(e) H_2 profile at 120mm height.

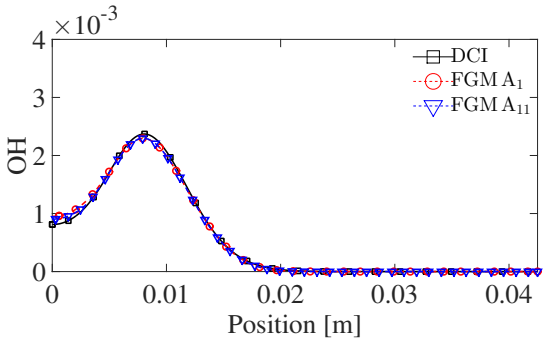

(f) OH profile at 120mm height.

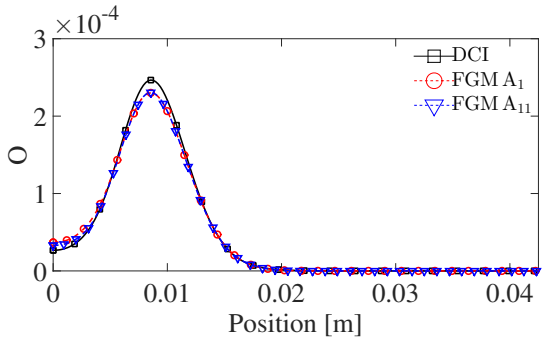

(g) O profile at 120mm height.

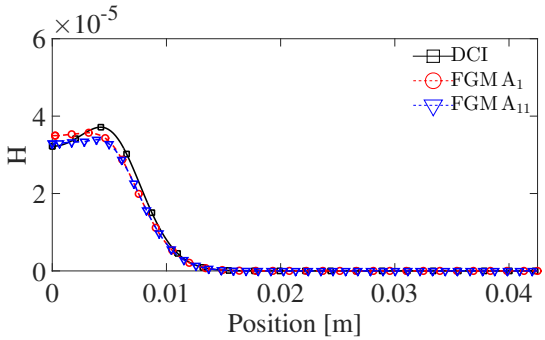

(h) H profile at 120mm height.

Figure A.4 – Radial species mass fraction profiles at 120mm height for 100% CH_4

60% CH_4 40% CO_2 two-dimensional results

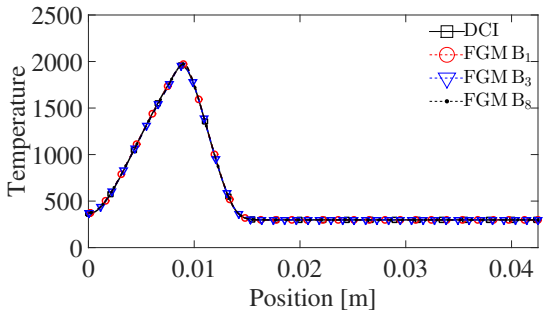

(a) Temperature profile at 10mm height.

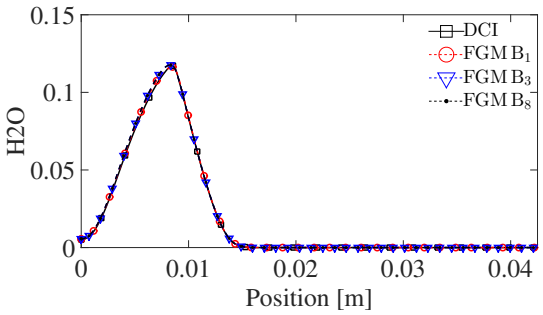

(b) H_2O profile at 10mm height.

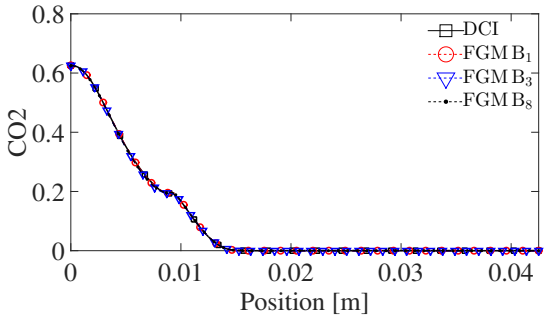

(c) CO_2 profile at 10mm height.

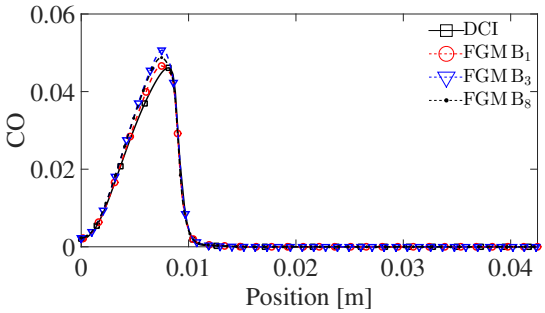

(d) CO profile at 10mm height.

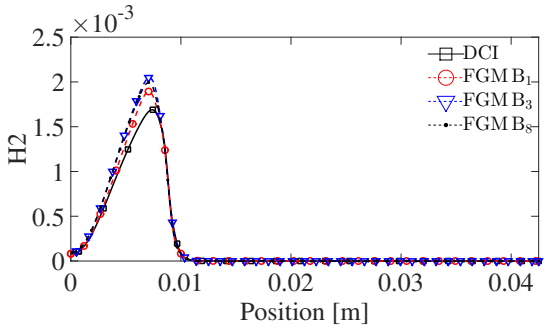

(e) H_2 profile at 10mm height.

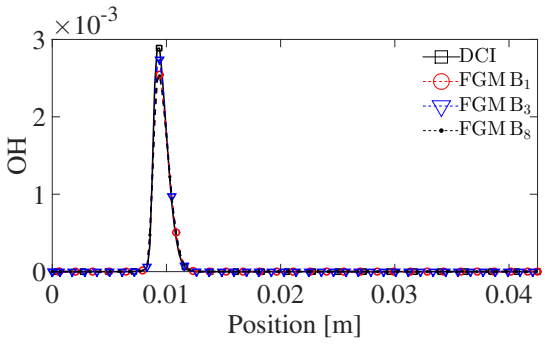

(f) OH profile at 10mm height.

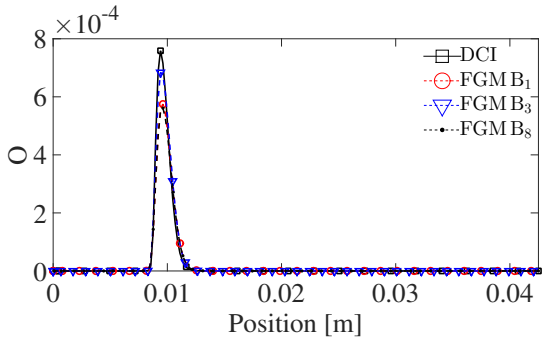

(g) O profile at 10mm height.

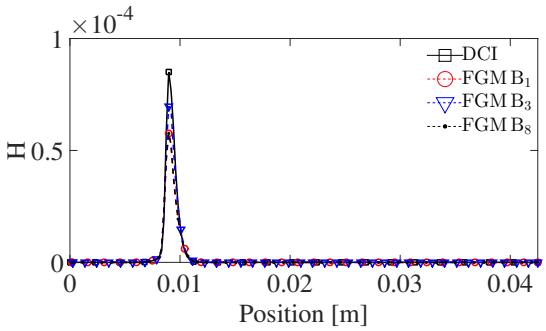

(h) H profile at 10mm height.

Figure A.5 – Radial species mass fraction profiles at 10mm height for methane with 40% CO_2 dilution

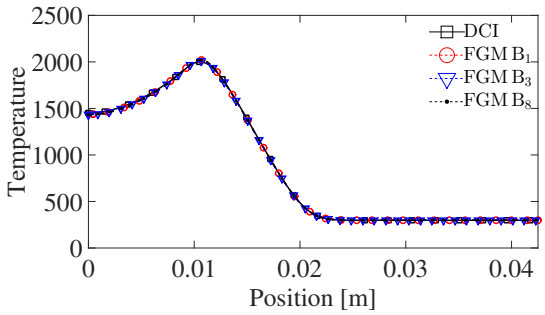

(a) Temperature profile at 40mm height.

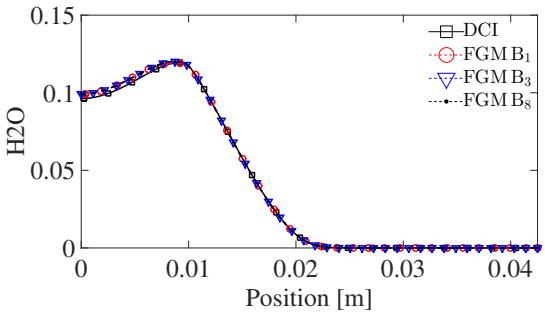

(b) H_2O profile at 40mm height.

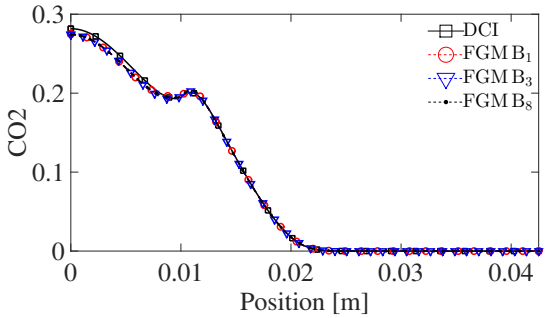

(c) CO_2 profile at 40mm height.

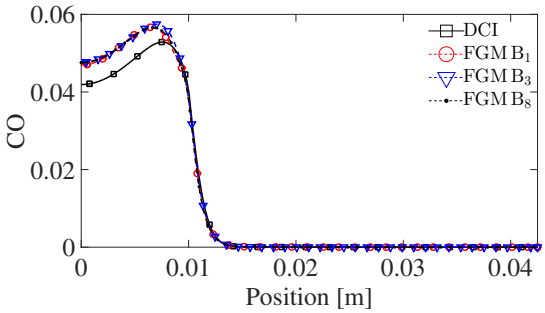

(d) CO profile at 40mm height.

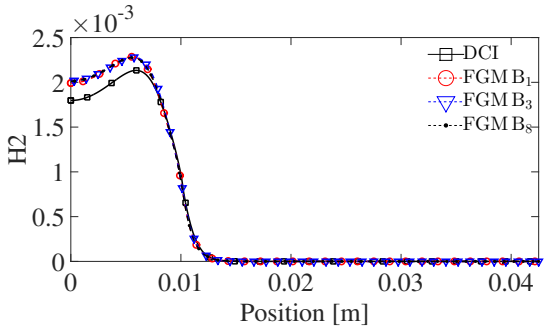

(e) H_2 profile at 40mm height.

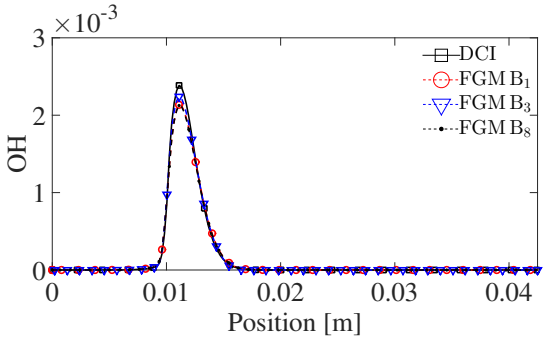

(f) OH profile at 40mm height.

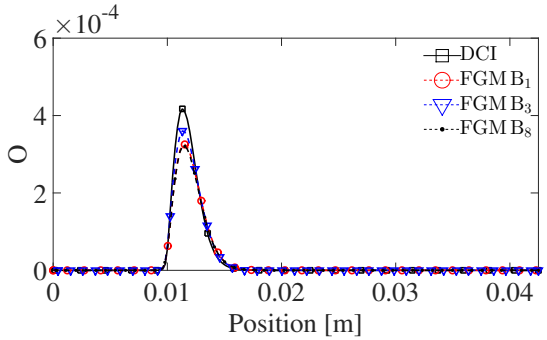

(g) O profile at 40mm height.

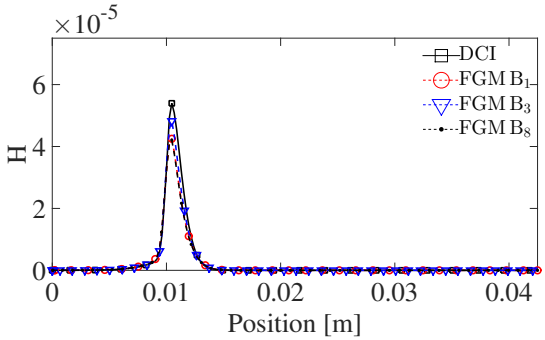

(h) H profile at 40mm height.

Figure A.6 – Radial species mass fraction profiles at 40mm height for methane with 40% CO_2 dilution

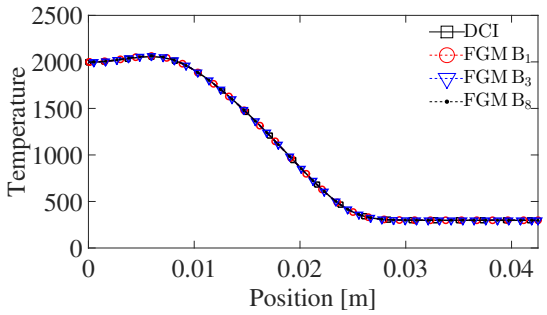

(a) Temperature profile at 80mm height.

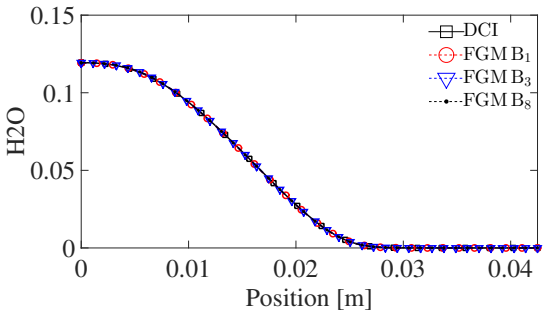

(b) H_2O profile at 80mm height.

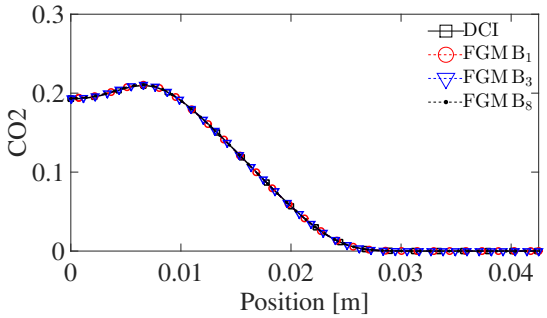

(c) CO_2 profile at 80mm height.

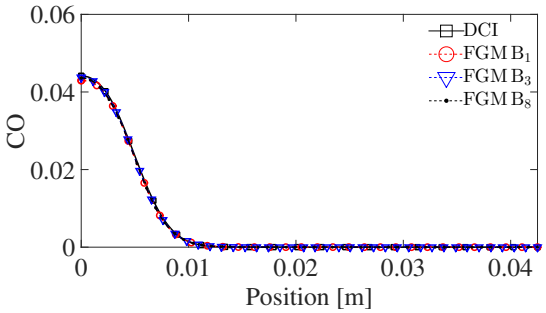

(d) CO profile at 80mm height.

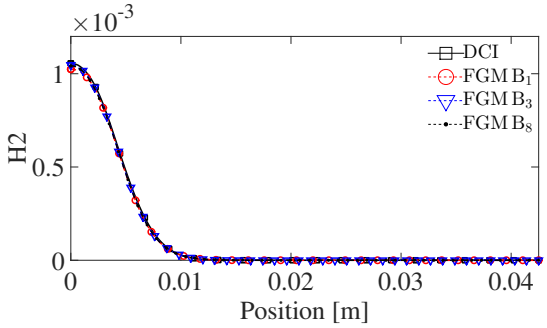

(e) H_2 profile at 80mm height.

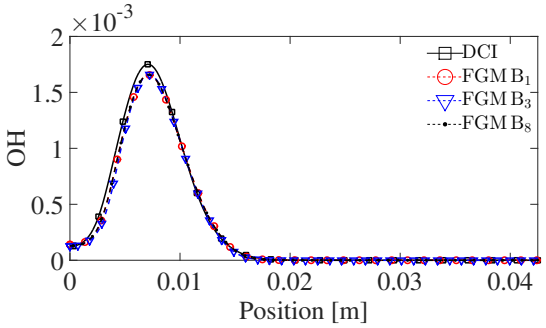

(f) OH profile at 80mm height.

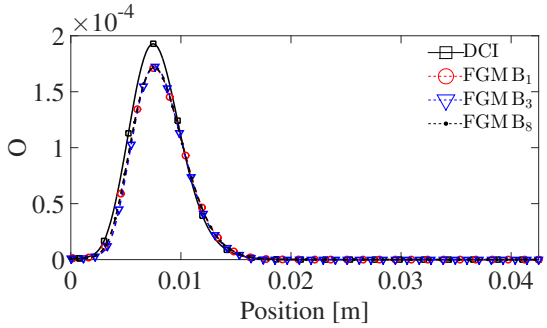

(g) O profile at 80mm height.

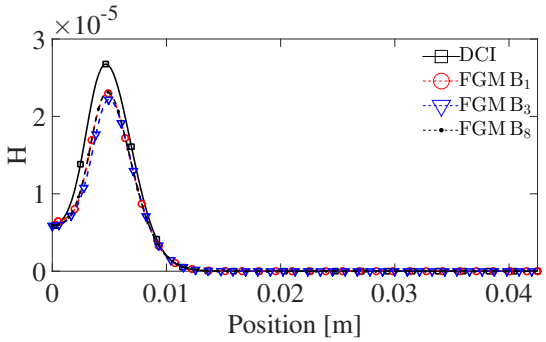

(h) H profile at 80mm height.

Figure A.7 – Radial species mass fraction profiles at 80mm height for methane with 40% CO_2 dilution

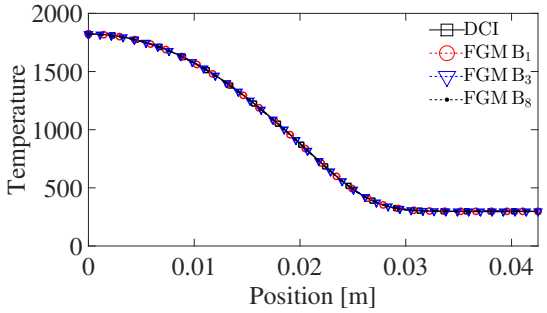

(a) Temperature profile at 120mm height.

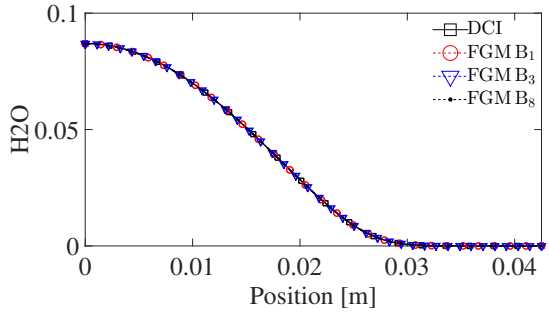

(b) H_2O profile at 120mm height.

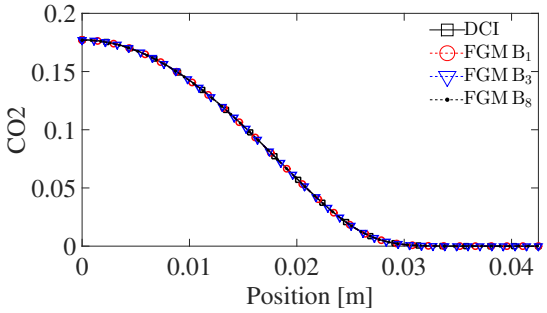

(c) CO_2 profile at 120mm height.

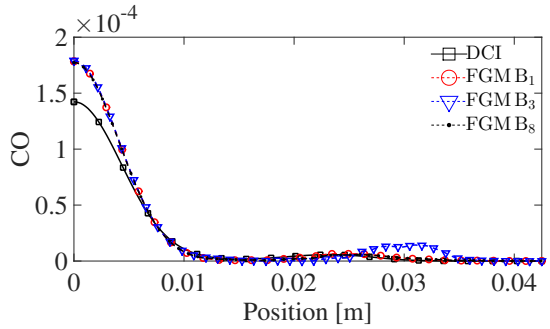

(d) CO profile at 120mm height.

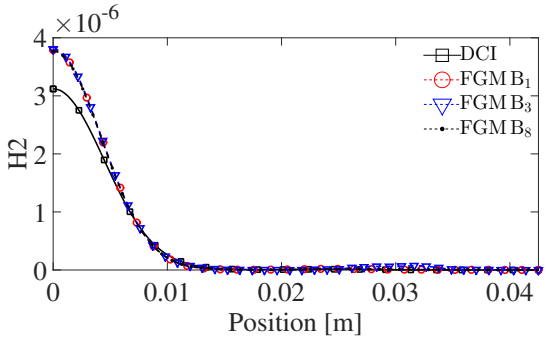

(e) H_2 profile at 120mm height.

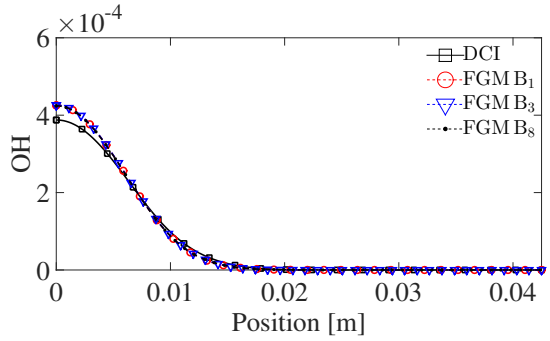

(f) OH profile at 120mm height.

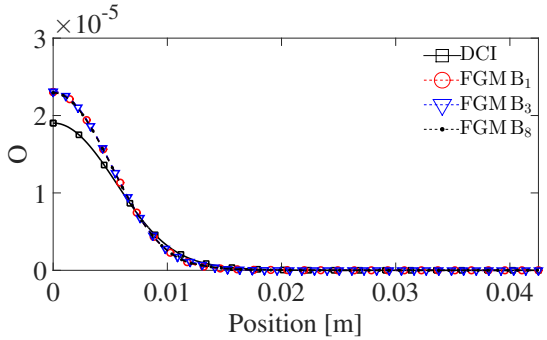

(g) O profile at 120mm height.

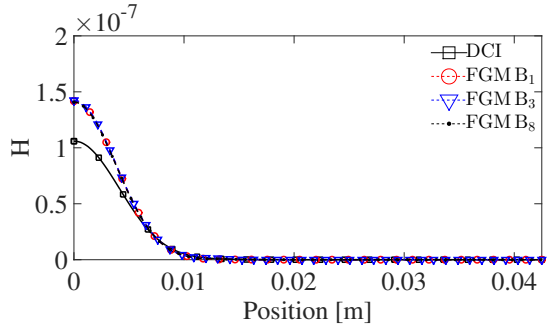

(h) H profile at 120mm height.

Figure A.8 – Radial species mass fraction profiles at 120mm height for methane with 40% CO_2 dilution

100% C_2H_4 two-dimensional results

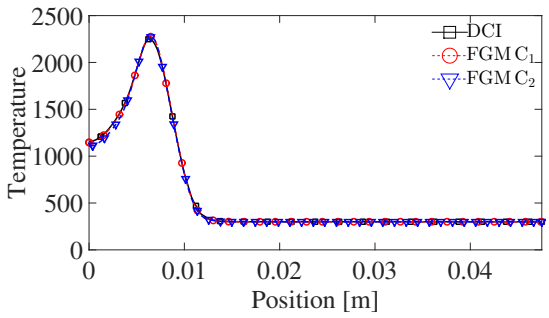

(a) Temperature profile at 10mm height.

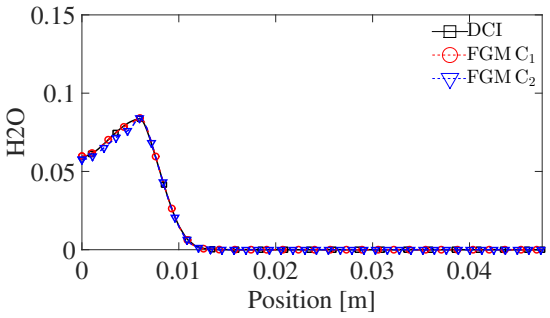

(b) H_2O profile at 10mm height.

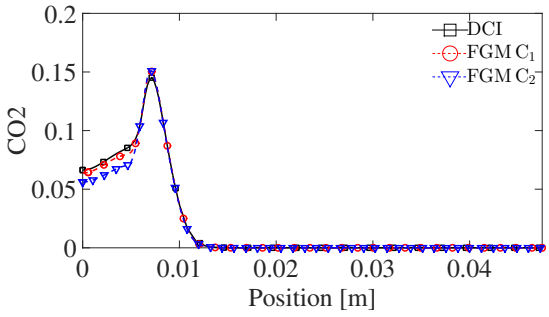

(c) CO_2 profile at 10mm height.

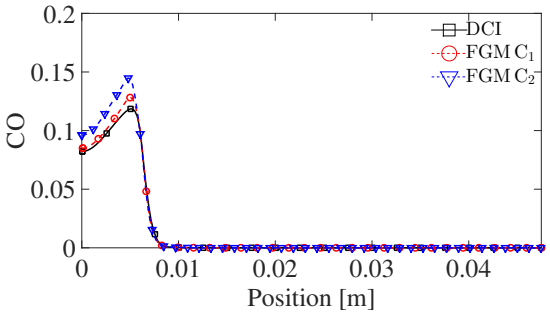

(d) CO profile at 10mm height.

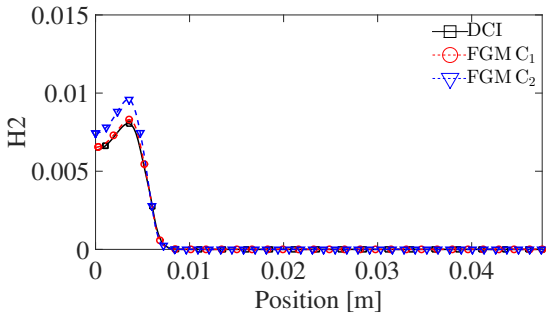

(e) H_2 profile at 10mm height.

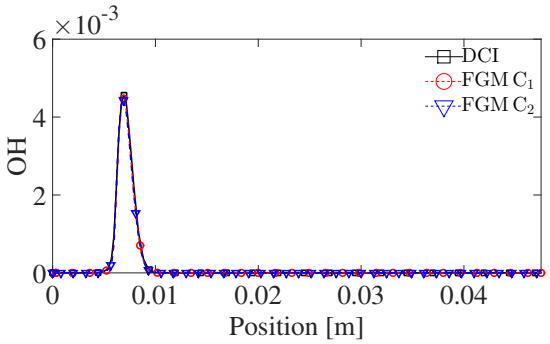

(f) OH profile at 10mm height.

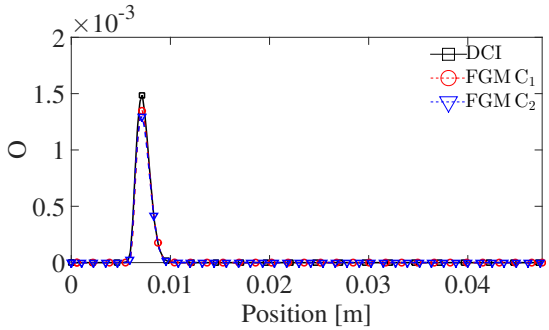

(g) O profile at 10mm height.

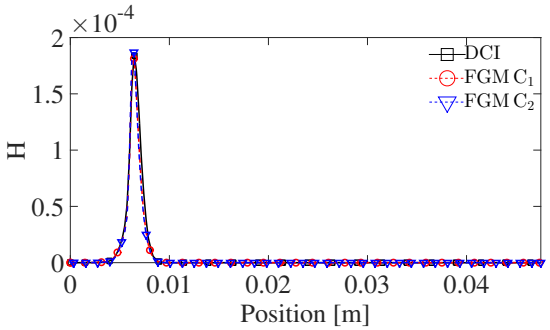

(h) H profile at 10mm height.

Figure A.9 – Radial species mass fraction profiles at 10mm height for 100% C_2H_4

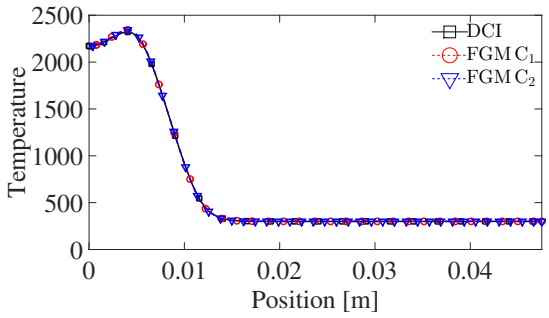

(a) Temperature profile at 40mm height.

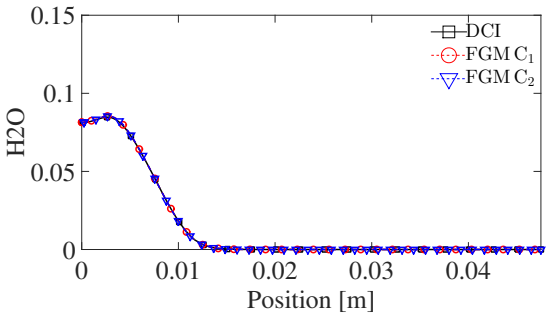

(b) H_2O profile at 40mm height.

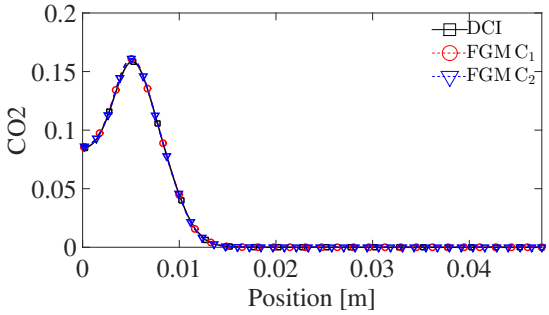

(c) CO_2 profile at 40mm height.

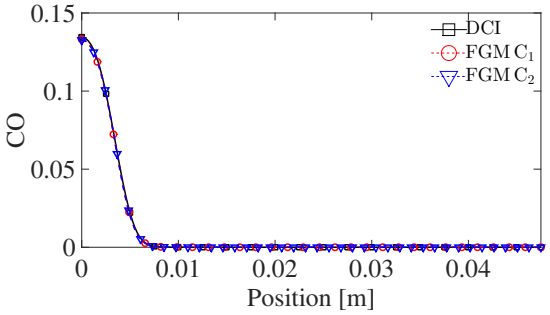

(d) CO profile at 40mm height.

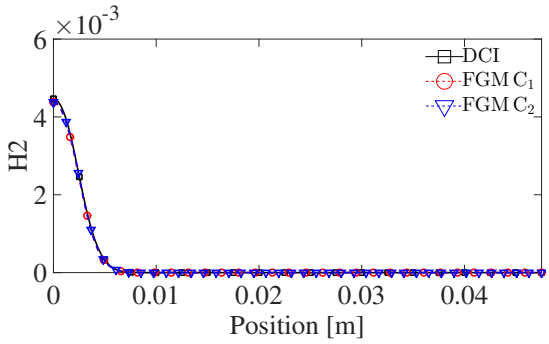

(e) H_2 profile at 40mm height.

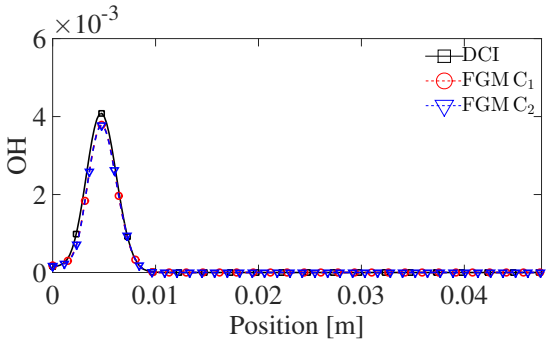

(f) OH profile at 40mm height.

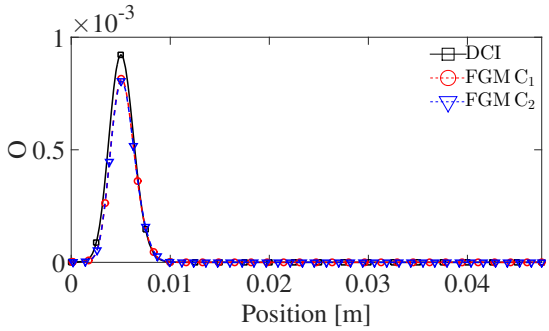

(g) O profile at 40mm height.

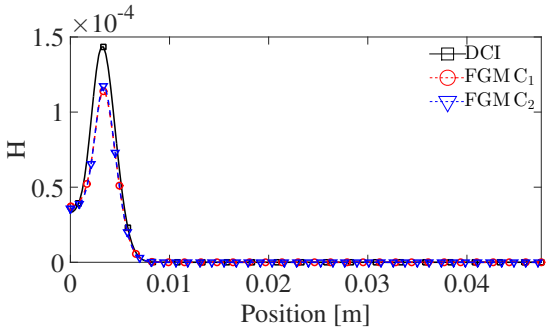

(h) H profile at 40mm height.

Figure A.10 – Radial species mass fraction profiles at 40mm height for 100% C_2H_4

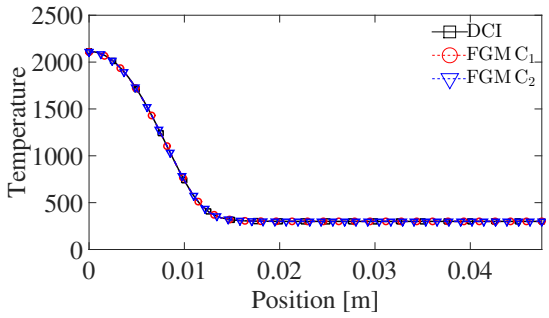

(a) Temperature profile at 80mm height.

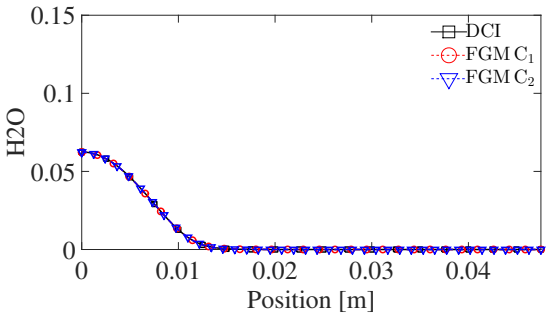

(b) H_2O profile at 80mm height.

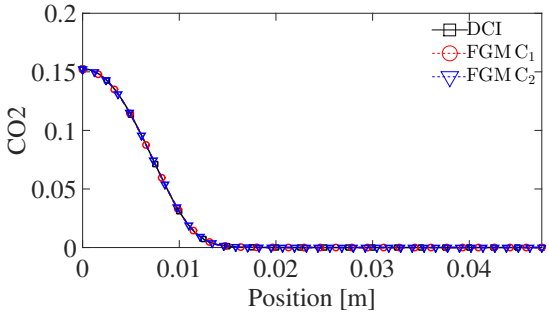

(c) CO_2 profile at 80mm height.

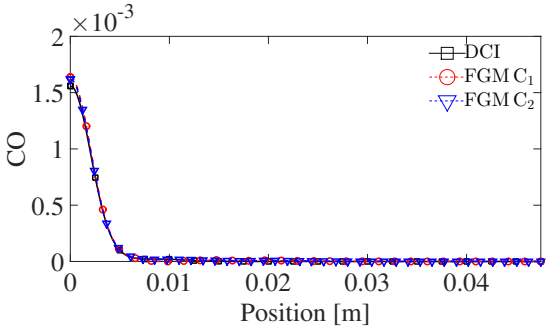

(d) CO profile at 80mm height.

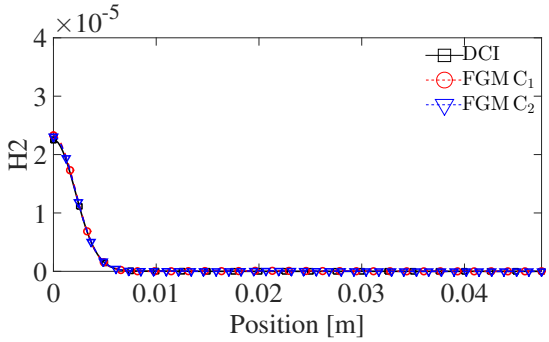

(e) H_2 profile at 80mm height.

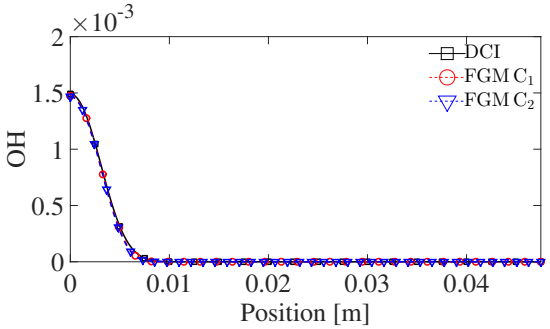

(f) OH profile at 80mm height.

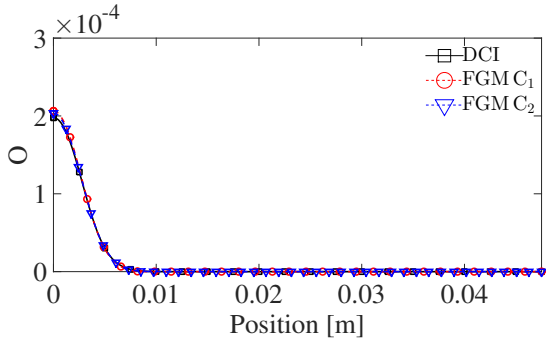

(g) O profile at 80mm height.

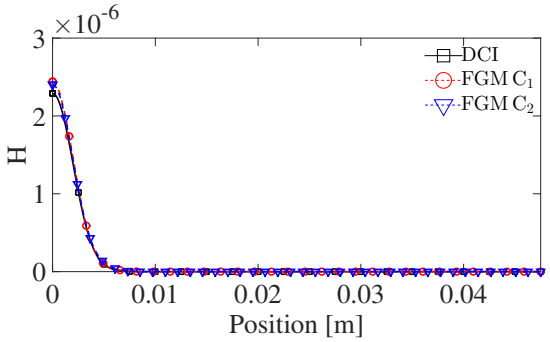

(h) H profile at 80mm height.

Figure A.11 – Radial species mass fraction profiles at 80mm height for 100% C_2H_4

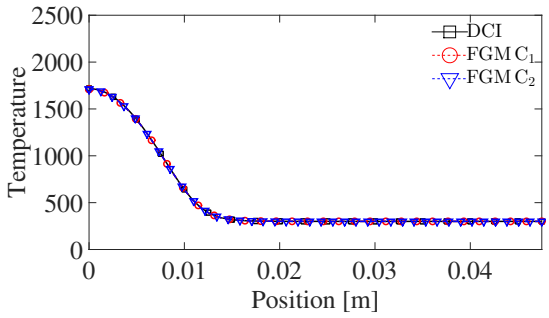

(a) Temperature profile at 120mm height.

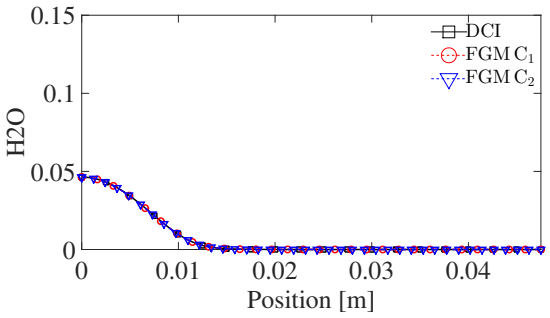

(b) H_2O profile at 120mm height.

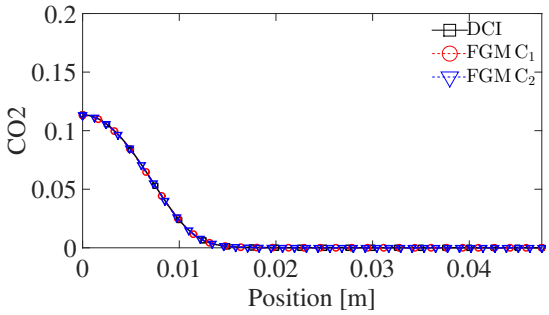

(c) CO_2 profile at 120mm height.

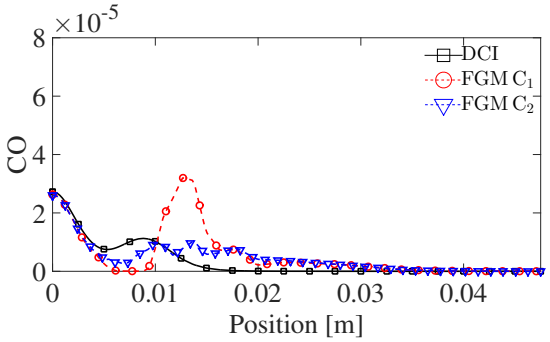

(d) CO profile at 120mm height.

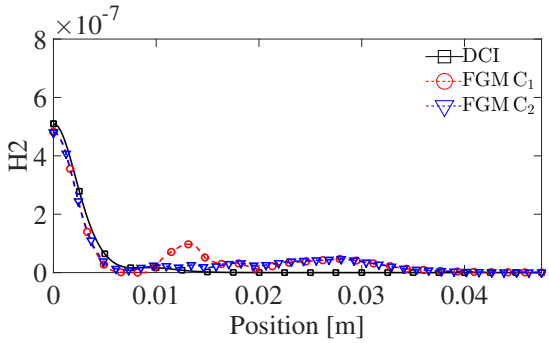

(e) H_2 profile at 120mm height.

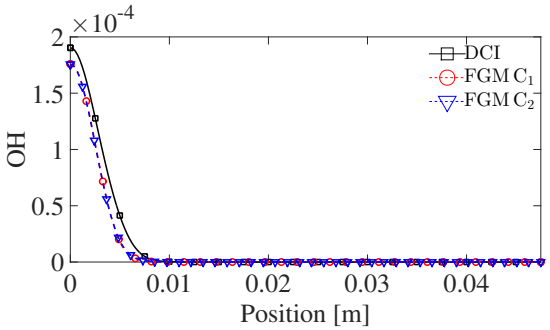

(f) OH profile at 120mm height.

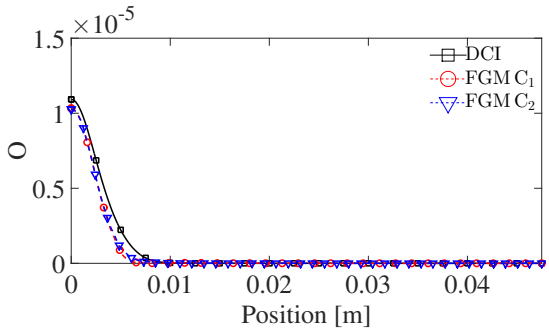

(g) O profile at 120mm height.

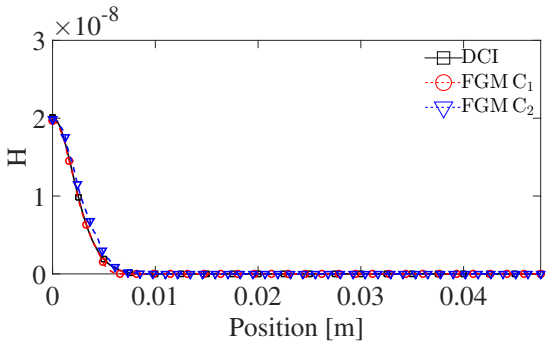

(h) H profile at 120mm height.

Figure A.12 – Radial species mass fraction profiles at 120mm height for 100% C_2H_4